

Generation and propagation
of energetic particles
in relativistic laser-matter interactions

Inaugural-Dissertation

zur

Erlangung des Doktorgrades der
Mathematisch-Naturwissenschaftlichen Fakultät
der Heinrich-Heine-Universität Düsseldorf

vorgelegt von

Oleg Shorokhov
aus Baku

Düsseldorf

2005

Gedruckt mit der Genehmigung der Mathematisch-Naturwissenschaftlichen Fakultät der Heinrich-Heine-Universität Düsseldorf

Referent: Prof. Dr. A. Pukhov

Korreferent: Prof. Dr. K.-H. Spatschek

Tag der mündlichen Prüfung: 20.01.2005

Generation and propagation
of energetic particles
in relativistic laser-matter interactions

Oleg Shorokhov

Dissertation for the degree of Doctor in Philosophy
at the University of Duesseldorf, Germany

Duesseldorf

2005

Printed with permission of the Faculty of Mathematics and Natural Sciences
of Heinrich-Heine University of Duesseldorf

Referee: Prof. Dr. A. Pukhov
Co-referee: Prof. Dr. K.-H. Spatschek

The day of public defense: 20.01.2005

Contents

| | | |
|----------|---|----------|
| 1 | Introduction | 5 |
| 1.1 | Laser plasma interaction physics. Motivation. Historical overview | 5 |
| 1.1.1 | Plasma based accelerators | 5 |
| 1.1.2 | Ultra-short pulses production | 7 |
| 1.2 | Thesis overview | 8 |
| 1.3 | Basic laser plasma interaction theory | 9 |
| 1.3.1 | Ionization | 9 |
| 1.3.2 | Particle motion in electromagnetic wave | 10 |
| | Plane electromagnetic wave | 10 |
| | Free particle motion in an electromagnetic wave | 12 |
| | Relativistic threshold | 13 |
| | Focused laser pulses | 13 |
| 1.3.3 | Basic plasma physics | 14 |
| | Plasma frequency and Debye length | 14 |
| | Plasma kinetic description | 15 |
| | Plasma fluid description | 17 |
| 1.3.4 | Propagation of electromagnetic waves in plasma | 18 |
| 1.3.5 | Relativistic nonlinear optics of plasma | 19 |
| | Relativistic plasma | 19 |
| | Relativistic transparency | 20 |
| | Instabilities | 21 |
| 1.3.6 | Self-focusing | 22 |
| | Self-focusing threshold | 22 |
| 1.3.7 | Relativistic magnetic self-channeling | 23 |
| | Channeling through overdense plasma | 24 |
| 1.3.8 | Electron plasma waves | 24 |
| | Plasma wave phase velocity | 25 |
| | Plasma waves excitation. Wavebreaking | 26 |
| 1.3.9 | Particles acceleration mechanisms | 27 |
| | Direct laser acceleration | 27 |
| | Particles acceleration in plasma wave. Wakefield acceleration | 28 |
| | Bubble regime of electron acceleration | 28 |

Contents

| | | |
|----------|---|-----------|
| 2 | Protons acceleration in a plasma wave | 31 |
| 2.1 | Introduction | 31 |
| 2.2 | Ion relativistic threshold | 32 |
| 2.3 | Ion acceleration at the front surface | 33 |
| 2.4 | Model for ion trapping in a running plasma wave | 34 |
| 2.4.1 | Overview | 34 |
| 2.4.2 | Single particle dynamics in prescribed potential | 34 |
| 2.4.3 | Plasma wave generation | 37 |
| 2.4.4 | Particle motion in laser-generated plasma wave | 39 |
| 2.5 | Numerical Simulations | 42 |
| 3 | Pulse propagation in plasma and relativistic solitons | 47 |
| 3.1 | Introduction | 47 |
| 3.2 | Raman instability overcoming | 47 |
| 3.3 | Analytical theory | 49 |
| 3.3.1 | Pulse evolution investigation using the momentum method | 51 |
| | First momentum | 51 |
| | Second momentum | 51 |
| 3.3.2 | Pulse oscillations | 52 |
| 3.3.3 | Pulse compression | 55 |
| 3.3.4 | Soliton solution | 55 |
| 3.3.5 | 1D model numerical verification | 56 |
| 3.4 | Possibility of 3D-compression | 57 |
| 4 | High harmonics generation from plasma surface | 61 |
| 4.1 | Introduction | 61 |
| 4.1.1 | Motivation | 61 |
| 4.1.2 | Mechanism of harmonics generation from plasma surface | 62 |
| 4.1.3 | Universal spectrum | 62 |
| 4.1.4 | Different focusing regimes. The Coherent Harmonic Focusing | 62 |
| 4.2 | Reflection | 63 |
| 4.2.1 | Laser plasma interaction scalings | 63 |
| 4.2.2 | Oscillating mirror | 64 |
| 4.2.3 | Ideal mirror boundary condition | 64 |
| 4.2.4 | Electrons dynamics near the boundary. Leontovich boundary condition | 65 |
| 4.3 | Pulse reflection | 67 |
| 4.3.1 | Retardation relation | 67 |
| 4.3.2 | Universal spectrum | 68 |
| 4.3.3 | Spectrum modulations | 74 |
| 4.4 | Coherent Harmonics Focusing | 75 |
| 4.4.1 | Intensity scaling of plasma coherent harmonics focusing | 78 |
| 4.4.2 | Schwinger limit | 78 |
| 4.5 | Simulations | 79 |

Contents

| | | |
|----------|--|------------|
| 4.5.1 | Power-law spectra | 79 |
| 4.5.2 | Reflected radiation structure. Ultra-short pulses | 81 |
| 4.6 | Numerical simulations of Coherent Harmonics Focusing | 81 |
| 5 | Summary | 87 |
| 5.1 | Main results | 87 |
| | Appendix | 89 |
| A | Particle-in-cell codes | 90 |
| B | Virtual Laser Plasma Laboratory | 92 |
| | Bibliography | 95 |
| | Acknowledgements | 109 |
| | Erklärung | 111 |

1 Introduction

1.1 Laser plasma interaction physics. Motivation. Historical overview

The major technological breakthrough that gave the impetus for a development of relativistic laser plasma physics was the invention of chirped pulse amplification (CPA) [1]. It gave the opportunity of ultra-short laser pulses production, which in turn resulted in a dramatic increase of achievable powers and focus intensities. The advent of compact table-top terrawatt laser systems [2, 3] has brought the relativistic plasma into university-level laboratories.

This thesis considers relativistic short pulse laser-plasma interactions and important new physical phenomena appearing in this high intensity regime: high gradient acceleration of charged particles, non-linear evolution of the laser pulse itself and high harmonics generation. These new effects are expected to have a great impact on a number of applications in high energy nuclear physics, material science, ultrafast chemistry, molecular biology, etc.

1.1.1 Plasma based accelerators

Due to the recent great leap in the laser technology, intensities up to $\sim 10^{21}$ W/cm² have been achieved at the laser focus [4, 5]. This corresponds to the electric field $E_f \sim 10^3$ GV/cm. This value is much greater than the maximum value of electric fields achievable in conventional radio frequency linear accelerators, where the field is limited to some $E_{rf}^{max} \sim 100$ MV/m due to interaction with the chamber walls. However, using the laser electric field is not straightforward, as the field is fast oscillating and perpendicular to the wave propagation direction [6].

A way to overcome this difficulty is to use *longitudinal* plasma waves excited by laser beams to accelerate electrons, as it was proposed by Tajima and Dawson [7]. When a relativistically intense laser pulse propagates in plasma, its ponderomotive force expels plasma electrons from the regions of the largest intensity. This initiates the plasma oscillations, the so-called wake field. Charged particles can be accelerated by the electric field of this plasma wave.

The main advantage of plasma-based accelerators is that they can sustain extremely large acceleration gradients. Plasma is already an ionized medium and can support very high electric fields. The natural limit for the amplitude of an electron plasma wave is given by wave breaking. The characteristic wavebreaking field has been calculated by Akhiezer and Polovin [8, 9] and is approximately $E_{WB}[\text{V/cm}] \approx 0.96N_e^{1/2}[\text{cm}^{-3}]$,

1. Introduction

where N_e is the background electron density. As the plasma density can be as high as the critical density $n_c \approx 10^{21}[\text{cm}^{-3}]$, we see that the plasma fields are many orders of magnitude higher than those in the conventional linear accelerators (see details and numerical values in [10]). To gain energy from the plasma wave, a highly relativistic particle must move along with the wave at approximately the same speed. Then, the charged particle interacts with this wave for a long time, and can be accelerated to a very high energy. Recently, essentially 3D acceleration mechanisms were proposed, which advantage is a narrow energy spread of accelerated electrons [11].

A number of experiments [12, 13, 14, 15, 16, 17] provided a proof of principle for electron acceleration in plasma waves. Here we list some of the most successful plasma-based acceleration schemes.

- *Laser Wakefield Accelerator* (LWFA)

In the LWFA scheme, the plasma waves are excited by a single ultrashort laser pulse. The condition for the most efficient wakefield excitation (optimum energy transfer from pulse to the plasma wave) is

$$L \sim \lambda_p , \quad (1.1)$$

where L is the pulse length and $\lambda_p = 2\pi c/\omega_p$ is the plasma wavelength and $\omega_p = \sqrt{4\pi N_e e^2/m}$ is the plasma frequency.

The LWFA was proposed by Tajima and Dawson [7]. However its experimental demonstration required high intensity laser systems with subpicosecond pulse lengths. In those days the technology did not satisfy these requirements, and roundabout setups had to be considered (like the PBWA scheme, see below). When at the end of 80s the compact terrawatt laser systems were created, the original LWFA idea [18, 19] was revived.

The first evidences of plasma wave excitation via LWFA mechanism were reported in [20, 21], and the accelerated electrons were first observed in [22].

- *Plasma Beat-Wave Accelerator* (PBWA)

The PBWA was the first method, confirmed in experiment, because it can be done using less powerful lasers, than required in other methods. It was proposed in [7] as the alternative of LWFA in the absence of technologies able to provide ultrashort pulses. In PBWA two long laser pulses with two slightly different frequencies are used. The interference (“beating”) of these laser beams corresponds to a modulation of the electromagnetic wave envelope, which can act resonantly on the plasma.

If one selects the lasers frequencies ω_1 and ω_2 in such a way, that they satisfy the resonance condition

$$\omega_1 - \omega_2 \approx \omega_p , \quad (1.2)$$

where ω_p is the plasma frequency, then a high amplitude plasma wave will be excited.

The first experimental observation of plasma wave generation using PBWA-method was reported by Clayton et al. [23], and the same group was successful in injected particles acceleration from 2 MeV to 30 MeV, which corresponds to 3 GV/m acceleration gradient [24, 15]. Electrons acceleration to 10 MeV without injection (from thermal background) was reported in [25].

- *Self-modulated LWFA* (SM-LWFA)

In the self-modulated LWFA regime, an initially long laser pulse, $L > \lambda_p$, breaks into a series of short pulses [16, 17]. This break is caused by the forward Raman scattering (FRS) and the so-called “sausaging” of the pulse envelope [26, 27, 28, 29].

The FRS instability can grow from noise. The density perturbations cause the group velocity variations, which lead to a longitudinal bunching of the pulse. In that way the pulse is breaking into a train of short pulses, with the characteristic length $\sim \pi c/\omega_p$. Each of these small pulses can be considered as an individual plasma wave driver (and it satisfies resonant condition). Such pulse self-modulation allows to use higher plasma densities, than the standard LWFA.

The first experimental evidence of the self-modulated LWFA has been given in the work [30], where FRS forward scattering and electrons acceleration up to 2 MeV were observed. The possibility of electron acceleration was demonstrated in the series of experiments [16, 17, 31]. In [17] the observation of background electrons acceleration to 30 MeV was reported.

There is a significant physical difference between these three regimes of wake field acceleration. The SM-LWFA relies on an instability (the stimulated forward Raman scattering) for an efficient plasma wave excitation. The PBFA regime also employs a long laser pulse that is subject to Raman instabilities. In the LWFA regime, however, the laser pulse is shorter than the plasma period and thus is free from any Raman instabilities. It is expected that the LWFA regime will finally lead to a practically useful plasma-based accelerator.

However, to use the LWFA regime, one needs a very short and relativistically powerful laser pulse. It appears that relativistic plasma itself can be considered as a nonlinear medium suitable for laser pulse compression and short pulse generation.

1.1.2 Ultra-short pulses production

According to the uncertainty principle, the pulse duration is inversely proportional to the frequency bandwidth occupied by the pulse. Thus, to produce ultra-short laser pulses, one has to increase its bandwidth. This can be done by employing a nonlinear medium, where new frequencies appear due to the non-linear self-interaction. A conventional method is to use atomic non-linearities in a gas medium. However, this method works only for low intensities, below the gas ionization threshold. Plasma may serve as a more advantageous medium, because it allows for much higher laser pulse intensities.

Here we mention two ways of using plasma for pulse compression. The first one is to use the relativistic non-linearity to compress laser pulse in underdense plasmas, see [32, 33]. The second way is harmonics generation at overdense plasma surface [34, 35, 36, 37]. In this thesis we consider both of them in Chapters 3 and Chapter 4 correspondingly.

1.2 Thesis overview

This thesis deals with physical phenomena, which appear in laser-plasma interactions in the wide range of laser intensities $10^{16} - 10^{23}$ W/cm².

The value 10^{16} W/cm² can be considered as the ionization threshold. For intensity $I > 10^{16}$ W/cm², the laser field becomes stronger than the atomic fields. Any material is instantaneously ionized and can be considered as a plasma at these laser intensities. We will consider targets as plasma from the very beginning.

The value 10^{18} W/cm² is the relativistic threshold. Starting with these intensities the electrons move under the influence of laser pulse with velocities close to the speed of light c , and relativistic effects must be taken into account. The physics of laser plasma interaction at such intensities is essentially relativistic and non-linear. Because of this fact, a development of analytical models is very complicated and numerical tools are extremely important. However, in this work we will concentrate on analytical results and use numerical tools mostly to check the analytical results and to support the selection of analytical models.

When relativistic laser pulses propagate through plasma, a number of physical effects appear. Some of them are: particles acceleration, generation of quasistatic fields, pulse compression, front- and back-surface ion acceleration, harmonics generation, X-ray production, extreme pressures generation, and many other effects. Several of them will be considered in this work. Their selection is subjective and was mainly determined by scientific interests of the author.

Below we list the topics, covered in this thesis.

- The first topic of this thesis is the study of particle acceleration mechanisms in laser plasma interaction. This is the mainstream of laser-matter interaction research nowadays. We concentrate our attention on the acceleration of protons, which is a new rapidly developing area of laser plasma interaction physics. This subject will be considered in Chapter 2.
- The second topic of the work deals with the pulse self-interaction in relativistic underdense plasma. During its propagation through plasma, the laser pulse changes optical properties of the plasma, which in its turn influence the pulse itself. Such self-interaction can lead to very complicated pulse dynamics. One of the practical applications is the production of ultra short pulses. Under certain conditions, the laser pulse can compress itself (the self-compression effect). The pulse propagation in plasma and self-compression are considered in Chapter 3.
- The third topic of this work concentrates on the process near a sharp overdense

plasma boundary. Oscillations of particles near the boundary are the point of special interest, because the pulse interaction with the boundary and its reflection can strongly modify the pulse structure. The investigation of excitation of boundary oscillations, pulse reflection, and finally, the reflected pulse structure demonstrates the possibility of extremely short pulses production (with the length of the order of the Bohr radius). Considering the focusing of the reflected radiation, we also demonstrate a possibility to achieve the Schwinger limit of vacuum breakdown intensity using lasers with reasonable energies. All these subjects are considered in Chapter 4.

1.3 Basic laser plasma interaction theory

1.3.1 Ionization

Let us estimate the laser field intensity, starting with which we can consider targets as a plasma. In order to do this, we consider Hydrogen-like atom. The electric field at the first Bohr orbit is

$$E_a = \frac{e}{r_B^2} \approx 5.1 \times 10^9 \text{ V/cm}, \quad (1.3)$$

where the Bohr radius

$$r_B = \frac{\hbar}{m_e e^2} \approx 5 \times 10^{-9} \text{ cm}, \quad (1.4)$$

The laser pulse intensity that corresponds to atomic field E_a is given by formula

$$I_a = \frac{cE_a^2}{8\pi} \approx 3.4 \times 10^{16} \text{ W/cm}^2. \quad (1.5)$$

This value can be considered as the ionization threshold, because for $I \gg I_a$ any target will immediately ionize and we can consider it as plasma.

The particular mechanism of ionization depends on the laser intensity via the dimensionless *Keldysh parameter* [38]

$$\Gamma^2 = \frac{U_i}{2\varepsilon_{os}}, \quad (1.6)$$

where U_i is the atom ionization potential and ε_{os} is the quiver energy of an electron in the laser electromagnetic wave. For a laser with the electric field E and the carrier frequency ω , the quiver energy is given by formula

$$\varepsilon_{os} = \frac{eE(1 + \alpha^2)}{4m_e\omega^2}, \quad (1.7)$$

where the parameter $\alpha = 0$ for linear polarization and $\alpha = 1$ for circular. For $\Gamma \ll 1$, the optical field ionization almost instantly releases electrons from atoms and plasma is formed. In the case $\Gamma \gg 1$, the multi-photon ionization dominates. A simple quasi-classical model of barrier suppression ionization (BSI), which was proposed in [39], gives the threshold

$$I_{BSI} = \frac{4.0 \cdot 10^9 \times U_i^4 [\text{eV}]}{Z^2} \quad [\text{W/cm}^2], \quad (1.8)$$

1. Introduction

where Z is the nucleus charge. The probability of tunnel ionization was calculated in the paper [40] (Ammosov-Delone-Krainov (ADK) model).

1.3.2 Particle motion in electromagnetic wave

Plane electromagnetic wave

A plane electromagnetic wave can be described using the vector potential:

$$\mathbf{A}(\mathbf{r}, t) = \text{Re}(\mathbf{A}_0 \exp i\psi) , \quad (1.9)$$

where \mathbf{A}_0 is the wave amplitude, $\psi = \mathbf{k}\mathbf{r} - \omega t$ is the phase, \mathbf{r} is the space coordinate, t is the time, \mathbf{k} is the wave vector. The dispersion relation in vacuum is

$$\omega = kc , \quad (1.10)$$

where c is the speed of light and $k = |\mathbf{k}|$. Introducing the wavelength $\lambda = cT = 2\pi c/\omega$ we can rewrite Eq. (1.10) as

$$k = \frac{2\pi}{\lambda} . \quad (1.11)$$

Now let us introduce a coordinate system with unit vectors $(\mathbf{e}_x, \mathbf{e}_y, \mathbf{e}_z)$. We are choosing the \mathbf{e}_x -direction in such a way, that it coincides with the wave propagation direction. Then we can write

$$\mathbf{A}_0 = \begin{cases} A_0 \mathbf{e}_y & \text{for linear polarization } (LP) , \\ A_0(\mathbf{e}_y \pm i\mathbf{e}_z) & \text{for circular polarization } (CP) . \end{cases} \quad (1.12)$$

We will use the standard *Coulomb gauge*

$$\text{div } \mathbf{A} = 0 . \quad (1.13)$$

Then, the expressions for electric field \mathbf{E} and magnetic field \mathbf{B} take the form

$$\mathbf{E} = -\frac{1}{c} \frac{\partial \mathbf{A}}{\partial t} , \quad (1.14)$$

$$\mathbf{B} = \text{rot } \mathbf{A} . \quad (1.15)$$

Using the substitution rules for derivatives: $\partial/\partial t \rightarrow -i\omega t$, $\partial/\partial \mathbf{r} \rightarrow i\mathbf{k}$, they can be rewritten as

$$\mathbf{E} = \text{Re} \left\{ \frac{i\omega}{c} \mathbf{A}_0 e^{i\psi} \right\} , \quad (1.16)$$

$$\mathbf{B} = \text{Re} \{ i\mathbf{k} \times \mathbf{A}_0 e^{i\psi} \} . \quad (1.17)$$

With the Poynting vector

$$\mathbf{S} = \frac{c}{4\pi} \mathbf{E} \times \mathbf{B} , \quad (1.18)$$

1.3. Basic laser plasma interaction theory

one obtains the formula for intensity:

$$I(\psi) = |\mathbf{S}| = \frac{\omega k}{8\pi} A_0^2 \times \begin{cases} (1 - \cos 2\psi) & \text{for LP ,} \\ 2 & \text{for CP .} \end{cases} \quad (1.19)$$

When the phase ψ is changed by 2π , the intensity for linear polarization oscillates twice, but it does not depend on the phase for circular polarization. For practical reasons one usually introduces the intensity averaged over phase:

$$I = \frac{1}{2\pi} \int_0^{2\pi} I(\psi) d\psi = \zeta \frac{\omega k}{8\pi} A_0^2 . \quad (1.20)$$

The factor ζ is different for linear polarization and circular polarization:

$$\zeta = \begin{cases} 1 & \text{for LP ,} \\ 2 & \text{for CP .} \end{cases} \quad (1.21)$$

Using Eq. (1.11), Eq. (1.20) can be written as

$$I\lambda^2 = \zeta \frac{\pi}{2} c A_0^2 . \quad (1.22)$$

When we consider the particles of selected species with mass m and charge q , following general methodology we can introduce the *relativistically normalized vector potential*

$$\mathbf{a} = \frac{q\mathbf{A}}{mc^2} . \quad (1.23)$$

The *dimensionless amplitude* is

$$a_0 = |\mathbf{a}_0| = \frac{|q|A_0}{mc^2} . \quad (1.24)$$

Using this notation we can rewrite Eq. (1.22) as:

$$I\lambda^2 = \zeta \frac{\pi}{2} \frac{m^2 c^5}{q^2} a_0^2 . \quad (1.25)$$

The amplitudes of electric and magnetic fields are correspondingly:

$$E_0 = \frac{mc\omega}{|q|} a_0 , \quad B_0 = \frac{mc\omega}{|q|} a_0 . \quad (1.26)$$

Particularly for electrons: $q = -e$, $m = m_e$ and we have:

$$a_0 = \frac{eA_0}{m_e c^2} , \quad (1.27)$$

$$I_0\lambda^2 = \zeta \left[1.37 \times 10^{18} \frac{W}{cm^2} \mu m^2 \right] a_0^2 . \quad (1.28)$$

1. Introduction

Free particle motion in an electromagnetic wave

Let us consider relativistic particle motion in the plane wave. The Lagrange function of particle with mass m and charge q in a prescribed electromagnetic field with potential ϕ and vector-potential \mathbf{A} is

$$L(\mathbf{r}, \mathbf{v}, t) = -mc^2 \sqrt{1 - \frac{v^2}{c^2}} + \frac{q}{c} \mathbf{v} \cdot \mathbf{A} - q\phi . \quad (1.29)$$

Using the Euler-Lagrange equation

$$\frac{d}{dt} \frac{\partial L}{\partial \mathbf{v}} - \frac{\partial L}{\partial \mathbf{r}} = 0 , \quad (1.30)$$

we obtain the relativistic equation of motion for the particle

$$m \frac{d\mathbf{p}}{dt} = q \left(\mathbf{E} + \frac{\mathbf{v}}{c} \times \mathbf{B} \right) , \quad (1.31)$$

where $\mathbf{p} = \gamma m \mathbf{v}$, is the particle momentum and gamma-factor is given by formula

$$\gamma = \frac{1}{\sqrt{1 - v^2/c^2}} . \quad (1.32)$$

Eq. (1.31) can be solved analytically (see the exact solution in [41, 42]). Here we discuss the results, which can be obtained from the analysis of symmetries. Let us introduce the full canonical momentum

$$\mathcal{P} = \frac{\partial L}{\partial \mathbf{v}} = \mathbf{p} + \frac{q}{c} \mathbf{A} = m(\gamma \mathbf{v} + c \mathbf{a}) . \quad (1.33)$$

The first symmetry appears from the plane wave planar symmetry. The conservation of the perpendicular component of the canonical momentum \mathcal{P} follows from the fact that the field does not depend on the transverse coordinate. Thus we have the first invariant

$$\mathcal{P}_\perp = \mathbf{p}_\perp + \frac{q}{c} \mathbf{A}_\perp = \text{const} . \quad (1.34)$$

The second symmetry appears from the fact, that we consider the laser pulse propagation with constant phase velocity v_{ph} (in vacuum $v_{ph} = c$). If we consider an infinite wave $\mathbf{A} = \mathbf{A}(t - x/v_{ph})$, we have the following relation:

$$-\frac{\partial L}{\partial t} = v_{ph} \frac{\partial L}{\partial x} = v_{ph} \frac{d}{dt} \frac{\partial L}{\partial v_\parallel} = v_{ph} \frac{d\mathcal{P}_\parallel}{dt} = v_{ph} \frac{dp_\parallel}{dt} . \quad (1.35)$$

Introducing the Hamilton function $H(\mathbf{r}, \mathbf{p}, t) = E(t)$, we obtain:

$$\frac{dE}{dt} = \frac{dH}{dt} = -\frac{\partial L}{\partial t} . \quad (1.36)$$

1.3. Basic laser plasma interaction theory

Substituting in Eq. (1.35) and taking into account that $A_{\parallel} = 0$ in a plain wave, we obtain the second invariant

$$E - v_{ph}p_{\parallel} = const . \quad (1.37)$$

To exclude the particles rest energy, we will use the kinetic energy

$$E_{kin} = E - mc^2 = (\gamma - 1)mc^2 . \quad (1.38)$$

For the particles which are initially at rest (before the laser pulse reaches them), we have from Eq. (1.34):

$$\mathbf{p}_{\perp} = -\frac{q}{c}\mathbf{A}_{\perp} = -mca_{\perp} . \quad (1.39)$$

Using Eq. (1.37), we obtain:

$$E_{kin} = E - mc^2 = p_{\parallel}c . \quad (1.40)$$

Using relation $E = mc^2\gamma = \sqrt{(mc^2)^2 + p_{\perp}^2c^2 + p_{\parallel}^2c^2}$, we easily obtain the expression for kinetic energy:

$$E_{kin} = \frac{p_{\perp}^2}{2m} = \frac{a^2}{2}mc^2 . \quad (1.41)$$

Relativistic threshold

From Eq. (1.41) we can see, that $E_{kin} \sim mc^2$ for $a_0 \sim 1$. The intensity I_0 which corresponds to $a_0 = 1$ (for specified λ) usually is considered as a relativistic threshold for specified sort of particles. If we consider the motion of electrons, the amplitude $a_0 = 1$ corresponds to laser intensity

$$I_0\lambda^2 = 1.37 \times 10^{18} \text{ W cm}^{-2}\mu\text{m}^2 . \quad (1.42)$$

The physical meaning of this threshold is following: when $|\mathbf{a}| < 1$ and correspondingly $|v_{\perp}| \ll c$, the particle oscillates mainly in the polarization direction with a small ponderomotive drift in the wave propagation direction. On the contrary, in the relativistic regime, when $|\mathbf{a}| > 1$ and $|v_{\perp}| \sim c$, the ponderomotive force $(\mathbf{v} \times \mathbf{B})/c$ pushes the particle forward and the particle motion becomes mainly longitudinal.

Focused laser pulses

As it is well known, if relativistic particle is interacting with infinite electromagnetic wave in vacuum, if one neglects non-linear effect, the total particle acceleration is null (Lawson-Woodward theorem [43, 44]).

In real experiments the laser pulse is not the plane wave. It is focused. But as a first approximation we can use relations obtained above even for a finite laser beam. Using Eq. (1.40), (1.41) we can estimate the scattering angle for a single electron outgoing from the laser focus:

$$\tan \theta = \frac{p_{\perp}}{p_{\parallel}} = \sqrt{\frac{2}{\gamma - 1}} . \quad (1.43)$$

1. Introduction

This result has been verified experimentally in [45].

For the next order of approximation, near the focal plane we can write:

$$\mathbf{A} = \mathbf{A}(\psi_g, \mathbf{r}) \exp(k\psi_{ph}) , \quad (1.44)$$

where

$$\psi_{ph} = z - v_{ph}t , \quad \psi_{gr} = z - v_{gr}t . \quad (1.45)$$

The phase velocity $v_{ph} > c$ and the group velocity $v_{gr} < c$. Using the Coulomb gauge condition Eq. (1.13), we can conclude, that the focused electromagnetic wave has the longitudinal component \mathbf{A}_{\parallel} :

$$\partial_z A_z = -\nabla_{\perp} \mathbf{A}_{\perp} . \quad (1.46)$$

There is no exact analytical theory for particles motion in the focused pulse. But if we suppose that wave amplitude varies slowly with respect to phase, the averaging over fast oscillations can be performed. If we consider the particle momentum $\bar{\mathbf{p}}$, averaged over the laser period, for low intensities $a \ll 1$ the *relativistic ponderomotive force* can be introduced:

$$\mathbf{f}_{pond} = \frac{d\bar{\mathbf{p}}}{dt} = -mc\nabla \frac{\bar{a}^2}{2} , \quad (1.47)$$

(see for details [46]).

From Eq. (1.47) we can see that the particles should be expelled from the region of high intensity. One can also observe that the relativistic ponderomotive force $\propto \nabla \bar{a}^2/2$ and does not depend on the laser polarization. In [47, 48] it was shown that the relativistic ponderomotive force model is still valid even for higher a and Eq. (1.47) takes the form:

$$\frac{d\bar{\mathbf{p}}}{dt} = -\frac{mc^2}{\bar{\gamma}} \nabla \bar{\gamma} . \quad (1.48)$$

In [48] it was shown that the scattering picture depends on dimensionless parameter $\alpha = k\sigma/(1 - v_z/c)$. If $\alpha \ll 1$ the scattering is ponderomotive. If $\alpha > 1$ the particle motion is more complicated and polarization asymmetries appear.

1.3.3 Basic plasma physics

Plasma frequency and Debye length

The main quantity, which defines the time scale for plasma processes is the plasma frequency. The natural oscillation frequency of the electron plasma is the *electron plasma frequency*

$$\omega_{pe} = \sqrt{\frac{4\pi e^2 N_e}{m_e}} , \quad (1.49)$$

where $(-e)$ is the electron charge, m_e is the electron mass, and N_e is the electron density. As the electrons are the lightest particles in the plasma, we will mainly use this frequency and call it sometimes the *plasma frequency* $\omega_p = \omega_{pe}$.

1.3. Basic laser plasma interaction theory

For the ion component, the *ion plasma frequency* can be introduced

$$\omega_{pi} = \sqrt{\frac{4\pi Z^2 e^2 N_e}{m_i}}, \quad (1.50)$$

where Ze is the ion charge, m_i is the ion mass, and N_i is the ions density. Due to the plasma quasi-neutrality $N_e = ZN_i$, and we have:

$$\frac{\omega_{pi}}{\omega_{pe}} = \sqrt{\frac{m_e}{m_i}} \ll 1. \quad (1.51)$$

The other key plasma property is the *Debye length* - the characteristic length which electron, moving with thermal velocity $v_{th} \sim \sqrt{k_B T / m_e}$ overpasses during the time $t \sim \omega_{pe}^{-1}$

$$\lambda_D = \sqrt{\frac{k_B T}{4\pi N_e e^2}}. \quad (1.52)$$

Plasma kinetic description

Let us introduce the six-dimensional phase space (\mathbf{r}, \mathbf{v}) . The most natural way to describe plasma is to consider the motion of a great number of interacting charged particles (electrons, protons, ions). We will use index α to mark the species. Density of one particle in phase space is

$$N_i(\mathbf{r}, \mathbf{v}, t) = \delta(\mathbf{r} - \mathbf{r}_i(t))\delta(\mathbf{v} - \mathbf{v}_i(t)), \quad (1.53)$$

where i is the marker of particle, $\mathbf{r}_i(t)$ and $\mathbf{v}_i(t)$ is correspondingly the position and velocity of particle at moment t , and δ is the Dirac delta function. The density of species α is given by sum over all particles of this specie

$$N_\alpha(\mathbf{r}, \mathbf{v}, t) = \sum_{i \in \{i_\alpha\}} \delta(\mathbf{r} - \mathbf{r}_i(t))\delta(\mathbf{v} - \mathbf{v}_i(t)), \quad (1.54)$$

and the overall density is the sum over all species

$$N(\mathbf{r}, \mathbf{v}, t) = \sum_{\alpha} N_\alpha(\mathbf{r}, \mathbf{v}, t). \quad (1.55)$$

The evolution of this density is described by *Klimontovich equation* [49]

$$\frac{\partial N_\alpha}{\partial t} + \mathbf{v} \cdot \frac{\partial N_\alpha}{\partial \mathbf{r}} + \frac{q_\alpha}{m_\alpha} \left(\mathbf{E}^m + \frac{\mathbf{v}}{c} \times \mathbf{B}^m \right) \cdot \frac{\partial N_\alpha}{\partial \mathbf{v}} = 0. \quad (1.56)$$

Here \mathbf{E}^m and \mathbf{B}^m are the *microscopic fields*. The Maxwell's equations for microscopic fields are

$$\nabla \cdot \mathbf{E}^m(\mathbf{r}, t) = 4\pi \rho^m(\mathbf{r}, t), \quad (1.57)$$

$$\nabla \cdot \mathbf{B}^m(\mathbf{r}, t) = 0, \quad (1.58)$$

$$\nabla \times \mathbf{E}^m(\mathbf{r}, t) = -\frac{1}{c} \frac{\partial \mathbf{B}^m(\mathbf{r}, t)}{\partial t}, \quad (1.59)$$

$$\nabla \times \mathbf{B}^m(\mathbf{r}, t) = \frac{1}{c} \frac{\partial \mathbf{E}^m(\mathbf{r}, t)}{\partial t} + \frac{4\pi}{c} \mathbf{j}^m(\mathbf{r}, t), \quad (1.60)$$

1. Introduction

where the microscopic charge density is

$$\rho^m(\mathbf{r}, t) = \sum_{\alpha} q_{\alpha} \int N_{\alpha}(\mathbf{r}, \mathbf{v}, t) d\mathbf{v} = \sum_{\alpha} q_{\alpha} \sum_{i \in \{i_{\alpha}\}} \delta(\mathbf{r} - \mathbf{r}_i) , \quad (1.61)$$

and the microscopic current is

$$\mathbf{j}^m(\mathbf{r}, t) = \sum_{\alpha} q_{\alpha} \int N_{\alpha}(\mathbf{r}, \mathbf{v}, t) \mathbf{v} d\mathbf{v} = \sum_{\alpha} q_{\alpha} \sum_{i \in \{i_{\alpha}\}} \mathbf{v}_i \delta(\mathbf{r} - \mathbf{r}_i) . \quad (1.62)$$

The Klimontovich equation together with the Maxwell's equations and the definitions for charge and current densities provides a full description of the plasma dynamics. It follows trajectories of all individual particles. However, even using the best modern supercomputers, it is impossible to accomplish this task.

The natural way to reduce Klimontovich equation is to introduce a probability density, associated with ensemble of particles. In such a way we can replace a real plasma by a plasma probabilistic ensemble. Thus for plasma kinetic description in a six-dimensional phase space (\mathbf{r}, \mathbf{v}) one introduces a set of one-particle distribution functions $\{f_{\alpha}(\mathbf{r}, \mathbf{v}, t)\}$ for each species α . The distribution function $\{f_{\alpha}(\mathbf{r}, \mathbf{v}, t)\}$ can be interpreted as the averaged number of particles of species α in a unit phase space volume at the point (\mathbf{r}, \mathbf{v}) at time t .

If we consider the electro-magnetic fields as prescribed by functions $\mathbf{e}(\mathbf{r}, t)$ and $\mathbf{b}(\mathbf{r}, t)$, and ignore the effects of collisions, the kinetic equation can be written as *collisionless Boltzmann equation*:

$$\frac{\partial f_{\alpha}}{\partial t} + \mathbf{v} \cdot \frac{\partial f_{\alpha}}{\partial \mathbf{r}} + \frac{q_{\alpha}}{m_{\alpha}} \left(\mathbf{e} + \frac{\mathbf{v}}{c} \times \mathbf{b} \right) \cdot \frac{\partial f_{\alpha}}{\partial \mathbf{v}} = 0 . \quad (1.63)$$

However in laser plasma interaction problems electro-magnetic fields can not be considered as prescribed and should be determined self-consistently. Using averaged charge and current densities:

$$\rho = \sum_{\alpha} q_{\alpha} \int f_{\alpha} d\mathbf{v} , \quad (1.64)$$

$$\mathbf{j} = \sum_{\alpha} q_{\alpha} \int \mathbf{v} f_{\alpha} d\mathbf{v} , \quad (1.65)$$

we can introduce the mean fields $\mathbf{E} = \langle \mathbf{E}^m(\mathbf{r}, t) \rangle$ and $\mathbf{B} = \langle \mathbf{B}^m(\mathbf{r}, t) \rangle$ which can be defined via the set of macroscopic Maxwell equations

$$\nabla \cdot \mathbf{E} = 4\pi\rho , \quad (\text{Poisson's equation}) \quad (1.66)$$

$$\nabla \cdot \mathbf{B} = 0 , \quad (\text{no magnetic monopoles}) \quad (1.67)$$

$$\nabla \times \mathbf{E} = -\frac{1}{c} \frac{\partial \mathbf{B}}{\partial t} , \quad (\text{Faraday's law}) \quad (1.68)$$

$$\nabla \times \mathbf{B} = \frac{1}{c} \frac{\partial \mathbf{E}}{\partial t} + \frac{4\pi}{c} \mathbf{j} , \quad (\text{Ampere's law}) \quad (1.69)$$

1.3. Basic laser plasma interaction theory

If we neglect the difference between the “exact” fields and the mean fields (*Vlasov approximation*) [50] we can rewrite Eq. (1.63) as a *Vlasov equation*:

$$\frac{\partial f_\alpha}{\partial t} + \mathbf{v} \cdot \frac{\partial f_\alpha}{\partial \mathbf{r}} + \frac{q_\alpha}{m_\alpha} \left(\mathbf{E} + \frac{\mathbf{v}}{c} \times \mathbf{B} \right) \cdot \frac{\partial f_\alpha}{\partial \mathbf{v}} = 0 . \quad (1.70)$$

The set of equations Eq. (1.66) - (1.69) and Eq. (1.70) forms a full *system of Vlasov-Maxwell equations* for collisionless plasma.

If we want to describe collisional effects we should consider the exact fields of point charges in kinetic equations: where summation is performed over all charged particles. Approximately one can take collisions into account by adding a non-zero right-hand side $(\partial f_\alpha / \partial t)_{coll}$ in the Eq. (1.70). In most applications of laser-plasma interactions the plasma can be described in collisionless approximation, so we will not go deeper into discussion of collision effects.

Plasma fluid description

The next step in reduction is to treat plasma as a system of fluids: one fluid for each type of particles. The fluid quantities can be obtained as a velocity momentums of distribution function.

The density is

$$N_\alpha(\mathbf{r}, t) = \int f_\alpha(\mathbf{r}, \mathbf{v}, t) d\mathbf{v} , \quad (1.71)$$

the averaged velocity is

$$v_\alpha(\mathbf{r}, t) = \frac{1}{N_\alpha} \int \mathbf{v} f_\alpha(\mathbf{r}, \mathbf{v}, t) d\mathbf{v} , \quad (1.72)$$

the two-dimensional tensor of pressure is

$$P_\alpha^{ij}(\mathbf{r}, t) = m_\alpha \int (v_i - v_{i\alpha})(v_j - v_{j\alpha}) f_\alpha(\mathbf{r}, \mathbf{v}, t) d\mathbf{v} , \quad (1.73)$$

and the heat flux is

$$\mathbf{q}_\alpha(\mathbf{r}, t) = \frac{1}{2} m_\alpha \int (\mathbf{v} - \mathbf{v}_\alpha)^2 (\mathbf{v} - \mathbf{v}_\alpha) f_\alpha(\mathbf{r}, \mathbf{v}, t) d\mathbf{v} . \quad (1.74)$$

Integrating the kinetic equation one can obtain the continuity equation:

$$\frac{\partial N_\alpha}{\partial t} + \nabla \cdot (N_\alpha \mathbf{v}_\alpha) = 0 . \quad (1.75)$$

The physical meaning of Eq. (1.75) is the conservation of the number of particles of each species. Multiplying by q_i and summarizing over each species one easily obtains the charge conservation law

$$\frac{\partial \rho}{\partial t} + \nabla \cdot \mathbf{j} = 0 . \quad (1.76)$$

1. Introduction

The equation of motion of the particles of species i is

$$\frac{\partial \mathbf{v}_\alpha}{\partial t} + (\mathbf{v}_\alpha \cdot \nabla) \mathbf{v}_\alpha = \frac{q_\alpha}{m_\alpha} \left(\mathbf{E} + \frac{\mathbf{v}}{c} \times \mathbf{B} \right) - \frac{1}{N_\alpha m_\alpha} \nabla \cdot P_\alpha^{ij} . \quad (1.77)$$

As we can see, the equation for the time derivative of the selected momentum always includes the divergence of the higher moment of the distribution function. To truncate the chain of equations one should introduce a closure assumption. We will use the *equation of state* for these purposes.

The simplest equation of state which corresponds to the *cold plasma* approximation is

$$P_\alpha = 0 . \quad (1.78)$$

The other approximation is

$$P_\alpha = N_\alpha^{\gamma_\alpha} . \quad (1.79)$$

For $\gamma_i = 1$ it corresponds to the *isothermal approximation*

$$P_\alpha = N_\alpha k_B T_\alpha . \quad (1.80)$$

For $\gamma = \frac{5}{3}$ it corresponds to the *adiabatic approximation*.

Introducing equation of state, we truncate the chain of the equations. In this way the fluid can be described using the density $N(\mathbf{r}, t)$ and the velocity $\mathbf{v}(\mathbf{r}, t)$. To describe the evolution we will use the equation of motion and the set of Maxwell equations.

1.3.4 Propagation of electromagnetic waves in plasma

Let us consider how a plasma influences on the propagation of electromagnetic waves. We will consider unmagnetized plasma, assuming that there are no large imposed or self-generated magnetic fields. The ions are considered as a stationary background.

Let us examine the cold plasma linear response to an electric field, oscillating at frequency $\omega > \omega_{pe}$:

$$\mathbf{E} = \mathbf{E}(\mathbf{r}) \exp(-i\omega t) . \quad (1.81)$$

Using Eq. (1.77) for the electrons and neglecting terms $\mathbf{v}_e \cdot \nabla \mathbf{v}_e$ and $\mathbf{v}_e \times \mathbf{B}/c$ (as they are proportional to $|\mathbf{E}|^2$) we obtain:

$$\dot{\mathbf{v}}_e = -\frac{e}{m_e} \mathbf{E}(\mathbf{x}) \exp(-i\omega t) . \quad (1.82)$$

If we assume $\mathbf{v}_e = \mathbf{v}_e(\mathbf{r}) \exp(-i\omega t)$, we obtain:

$$\mathbf{v}_e = -\frac{ie}{m_e \omega} \mathbf{E}(\mathbf{r}) , \quad (1.83)$$

and for the density current we have:

$$\mathbf{j} \approx \mathbf{j}_e = -en_e(\mathbf{r}) \mathbf{v}_e(\mathbf{r}) = \frac{ie^2}{m_e \omega} \mathbf{E}(\mathbf{r}) = \frac{i\omega_{pe}^2}{4\pi\omega} \mathbf{E}(\mathbf{r}) , \quad (1.84)$$

1.3. Basic laser plasma interaction theory

where we use the plasma frequency ω_{pe} according to Eq. (1.49). Introducing the conductivity of the plasma σ , we can rewrite Eq. (1.84) as:

$$\mathbf{j} = \sigma \mathbf{E}, \quad \sigma = i \frac{\omega_{pe}^2}{4\pi\omega}. \quad (1.85)$$

Using Eq. (1.85) one can easily obtain the dielectric function of the cold collisionless plasma. As $\omega_{pi} \ll \omega_{pe}$ we can neglect ion contributions, and the dielectric function is the result of electron contributions only

$$\epsilon(\omega) = 1 - \frac{\omega_{pe}^2}{\omega^2}. \quad (1.86)$$

Linearizing the Vlasov equation one can obtain for linear electrostatic waves in unmagnetized plasma dispersion relation

$$\omega^2 = \omega_{pe}^2 + k^2 c^2. \quad (1.87)$$

We can see that for $\omega < \omega_{pe}$ the value $k = \sqrt{\omega^2 - \omega_{pe}^2}/c$ becomes imaginary, so the laser pulse can not propagate in plasma. The condition $\omega = \omega_{pe}$ defines the maximum plasma density through which pulse with specified frequency can penetrate. It is the *critical plasma density*, which is given by the formula

$$N_{cr} = \frac{m_e \omega^2}{4\pi e^2}. \quad (1.88)$$

Using the dispersion relation Eq. (1.87) we can calculate for electromagnetic wave propagating in plasma the phase velocity

$$v_{ph} = \frac{\omega}{k} = \frac{c}{\sqrt{1 - \frac{\omega_{pe}^2}{\omega^2}}}, \quad (1.89)$$

and the group velocity

$$v_{gr} = \frac{\partial\omega}{\partial k} = c \sqrt{1 - \frac{\omega_{pe}^2}{\omega^2}}. \quad (1.90)$$

1.3.5 Relativistic nonlinear optics of plasma

Relativistic plasma

If we consider laser-plasma interaction with $a \geq 1$ relativistic effects should be taken into account. For short-pulse lasers, which are the subject of main interest in laser plasma interaction, the nonlinear optics of plasma involves only electron motion, because the ions can be treated as immobile during the transit time of the laser. Thus the key effect is the relativistic mass increase of plasma electrons. For single electron the so-called relativistic mass can be introduced $m_e^{rel} = \gamma m_e$, where γ is the electron gamma factor

1. Introduction

for this electron. Going to the averaged plasma properties, we will describe plasma with the *relativistic plasma frequency* which is given by the formula:

$$\omega_p^{rel} = \sqrt{\frac{4\pi e^2 N_e}{m_e \langle \gamma \rangle}} , \quad (1.91)$$

where $\langle \gamma \rangle$ is the relativistic γ -factor, averaged locally over many electrons. The dispersion relation for laser light propagation also should be modified and it takes the following form:

$$\omega^2 = (\omega_{pe}^{rel})^2 + k^2 c^2 . \quad (1.92)$$

In that way the Eqs. (1.89), (1.90) and (1.86) should be modified to take into account relativistic corrections, and therefore we have: the phase velocity

$$v_{ph} = \frac{c}{\sqrt{1 - \frac{\omega_{pe}^2}{\omega^2 \langle \gamma \rangle}}} , \quad (1.93)$$

the group velocity

$$v_{gr} = \frac{\partial \omega}{\partial k} = c \sqrt{1 - \frac{\omega_{pe}^2}{\omega^2 \langle \gamma \rangle}} . \quad (1.94)$$

and the dielectric function

$$\varepsilon = 1 - \left(\frac{\omega_{pe}^{rel}}{\omega} \right)^2 = 1 - \frac{\omega_{pe}^2}{\omega^2 \langle \gamma \rangle} . \quad (1.95)$$

Relativistic transparency

Plasma can be considered as a medium with refraction index

$$\eta = \sqrt{\varepsilon} = \sqrt{1 - \frac{N_e}{N_{cr} \langle \gamma \rangle}} , \quad (1.96)$$

where N_{cr} is defined by Eq. (1.88). From Eq. (1.96) we can see that the threshold for plasma non-transparency is $N_e \sim \langle \gamma \rangle N_{cr}$. At relativistic intensities, $\langle \gamma \rangle$ depends on the local intensity I (approximately $\langle \gamma \rangle \sim I^{1/2}$, see below for details), and a bunch of non-linear optics effects appears. This dependence of plasma frequency on γ and through it on the laser radiation intensity has deep consequences for light propagation in plasma.

The condition of electromagnetic wave passing through the plasma is that the length of the wave vector k is a real number. Using Eq. (1.87), it can be rewritten as $\omega > \omega_{pe}^{rel}$.

When an ultra-relativistically intense laser pulse propagates in plasma, we can use for the locally averaged electrons γ -factor the estimation:

$$\langle \gamma \rangle \sim \frac{a_0}{2} , \quad (1.97)$$

1.3. Basic laser plasma interaction theory

(see details in [51]). Using this equation one can easily obtain the condition of relativistic transparency

$$a > 2 \frac{N_e}{N_{cr}} . \quad (1.98)$$

To clarify the physical meaning of this condition, let us consider Eq. (1.69) (the Ampere's law). The condition of electromagnetic wave penetration into the plasma can be written as

$$\frac{4\pi}{c} j \ll \frac{1}{c} \frac{\partial E}{\partial t} . \quad (1.99)$$

Using the estimation from above, $j = N_e e v < N_e e c$, and substituting $A \sim \exp(i\omega t)$, we can rewrite it as:

$$\frac{\omega^2}{c^2} A \gg \frac{4\pi}{c} N_e e c . \quad (1.100)$$

Introducing dimensionless amplitude a , one easily obtains $a \gg N_e/N_{cr}$.

Instabilities

The first results in nonlinear plasma optics were obtained from identification of the so-called parametric instabilities. They were investigated in terms of wave-wave interactions, when an incident electromagnetic wave with frequency ω_0 decays into two sidebands: the Stokes wave with the frequency $\omega_0 - \omega_{mod}$ and the anti-Stokes one with the frequency $\omega_0 + \omega_{mod}$. The frequency ω_{mod} corresponds to the modulations of refraction index. This technique was first applied in the papers [52, 53, 54]. Using this formalism, various instabilities were investigated, including Brillouin and Raman scattering, Compton scattering, filamentation/self-focusing and self-phase modulational instabilities [55, 52, 53, 54, 56, 57].

The most important instabilities for a short laser pulse interaction with plasma are:

FRS Forward Raman scattering ($\omega_{mod} = \omega_{pe}$). Electrostatic plasma wave is generated, with phase velocity $v_{ph} \sim c$. This plasma wave can accelerate electrons to relativistic energies.

SF Relativistic self-focusing / filamentation ($\omega_{mod} \ll \omega_{pe}$).

SPM Relativistic self-phase modulation ($\omega_{mod} \ll \omega_{pe}$).

An alternative formalism to consider the instabilities was proposed in [58, 59, 60]. In these papers, modulations of laser intensity were considered in terms of physical phenomena, which appear from modulations of refraction index. The index of refraction (as well as the group and phase velocities) can be altered by modulations of (i) plasma density N , (ii) laser amplitude a , (iii) laser frequency ω_0 . Therefore, the index of refraction may be expanded on this three perturbations

$$\eta = 1 - \frac{1}{2} \left(1 + \frac{\delta N_e}{N_e} - \frac{\langle a^2 \rangle}{2} - 2 \frac{\delta \omega_0}{\omega_0} \right) , \quad (1.101)$$

1. Introduction

(see for details [51, 61]).

Let us write down the conservation of the photon number

$$\langle a^2 \rangle \omega_0 r^2 L = \text{const} , \quad (1.102)$$

where r is the laser spot size, L is the initial longitudinal pulse length, and $\langle a^2 \rangle$ is the dimensionless amplitude square (the laser intensity), averaged over fast oscillations. From Eq. (1.102), we can see that laser intensity can be modulated by changes in

- L , e.g., due to the longitudinal bunching,
- r , due to the transverse focusing,
- ω_0 , due to the photon acceleration.

1.3.6 Self-focusing

Self-focusing threshold

Let us consider the laser beam propagation in underdense plasma. Two key mechanisms responsible for *relativistic self-focusing* exist. The first one is the *relativistic mass increase* of plasma electrons, which cause plasma frequency decrease according to $\omega_p^{rel} \sim \langle \gamma \rangle^{-1}$. The second mechanism is the *electrons expelling* out of the focal spot by ponderomotive force push. Such electrons expulsion from the pulse region diminishes the local electrons density N_e and therefore the local plasma frequency. As a result of such local decrease of plasma frequency we have the plasma refraction index increasing, and the plasma acts as a positive lens. The process of relativistic self-focusing was investigated theoretically in [53, 62, 63, 64] and experimentally in [65, 66].

Let us first consider $a < 1$. If we investigate low-intensity laser beam $a \ll 1$, the plasma density can be considered as undisturbed $N_e \approx N_0$, and electrons can be treated as non-relativistic particles with $\gamma \approx 1$. As the amplitude increases, first gamma-nonlinearity appears, $\gamma \approx 1 + a^2/4$, while the density perturbations contribute in the higher order. Then the wave equation in envelope approximation can be used

$$\left(\nabla_{\perp}^2 + 2ik \frac{\partial}{\partial x} \right) a = -\frac{\omega_p^2}{c^2} \frac{|a|^2}{4} a . \quad (1.103)$$

The term $\nabla_{\perp}^2 a$ disperses the beam, the term $\omega_p^2 |a|^2 a / (4c^2)$ compresses it and at the threshold intensity they should balance each other. For Gaussian envelope approximation $a(r, z) \sim a_0(z) \exp(-r^2/R^2(z))$ the critical power is given by formula

$$P_{cr} = 2 \left(\frac{\omega}{\omega_p} \right)^2 P_0 , \quad (1.104)$$

where the power unit is

$$P_0 = \frac{m_e^2 c^5}{e^2} = 8.7 \text{ GW} . \quad (1.105)$$

1.3. Basic laser plasma interaction theory

One should note, that then the power approaches to P_{cr} , contraction of the beam leads to the increase of light intensity on the axis and ponderomotive expulsion of the electrons. This leads to plasma channel formation with reduced electron density. Numerical investigations performed in paper [62] give approximately the same value for self-focusing threshold

$$P_{cr} \approx 17 \left(\frac{\omega}{\omega_p} \right)^2 \text{ GW} . \quad (1.106)$$

From this value the laser pulse becomes relativistically focused. An analysis in envelope approximation, which was performed in [67], shows that the picture of self-focusing depends on laser pulse and plasma parameters. The first possibility is that the self-focusing of the whole laser pulse leads to single channel production. But if the laser power exceeds the value P_{cr} by a few order of magnitude, instead of single channel, the multiple channels can be produced. This effect is known as the relativistic filamentation, (see for details [67]).

1.3.7 Relativistic magnetic self-channeling

The analytical theory of self-focusing was developed in weakly relativistic approximation $a \leq 1$. If the laser intensity overcomes the relativistic threshold, given by Eq. (1.42), the new physical effects can be expected.

As it was discussed above, at $a > 1$, the Lorentz force $(e/c)\mathbf{v} \times \mathbf{B}$ drives the electrons forward in the pulse propagation direction. In this regime the radiation drives currents of relativistic electrons in the direction of pulse propagation. These currents create a strong magnetic field, which significantly change the picture of pulse interaction with plasma.

Let us consider a simplified model of this process. Each filament carries a strong current, which can be estimated as $-feN_e c$, where $f \leq 1$ and N_e is the background density. This currents magnetize the plasma. Quasi-static magnetic field, generated by such current at the distance r from the axis is $B_\phi^s = 2\pi r(feN_e)$. Under certain conditions, this field can reach the value of the light magnetic field $B_l = aB_0$, $B_0 = m_e c \omega / e \approx 107 \text{ MG}$. The ratio of these fields can be rewritten as

$$\frac{B^s}{B^l} = \frac{1}{a} \frac{f N_e \pi r}{N_{cr} \lambda} , \quad (1.107)$$

where λ is the laser wavelength, $N_{cr} = \pi m_e c^2 / (e\lambda)^2$.

This very complex situation was investigated in 2D and 3D PIC simulations in papers [68, 69]. It was shown, that the quasistatic magnetic field is strong enough to pitch the electrons, and therefore to direct the light deflection. As a result the current and light filaments can merge into the single channel, which contains a significant part of incident laser power. The physical reason of this merging is the attraction of electric currents inside the filaments. In 3D PIC simulation [69] it was shown, that the incident beam first propagates through an unstable filamentary stage and then collapses into the single channel with a width $(1 - 2)\lambda$.

Channeling through overdense plasma

The problem of laser hole boring into overdense plasma is the subject of great interest in connection with inertial confinement fusion (ICF). The laser can generate the relativistic electrons, which will heat the ignitor spot in the precompressed fuel core [70].

The ICF target at ignition time consists of a core, surrounded by ablated plasma. The plasma density is falling from $\sim 10^5 N_{cr}$ to N_{cr} over a distance $\sim 100 \mu m$. The pulse should drill a channel through this plasma towards the core. During this process, the maximum mean currents cannot exceed the Alfvén limit $J_A = mc^3\gamma/e$. This current would correspond to the power transport of only $P_0 = J_A^2/c = \gamma^2 \times 9 \text{ GW}$. Fortunately, the forward current J in plasma is partially neutralized by return current J_{ret} , so that the maximum transportable power is increased by the factor $f = J/(J - J_{ret})$. Also, the energy transport through regions close to the critical surface is exposed to strong magnetic fields influence. The corresponding 2D and 3D PIC simulations were performed in [71, 72].

The recent review of fast ignition of ICF targets can be found in [73, 74].

1.3.8 Electron plasma waves

In this Section, we will consider plasma in one-fluid approximation, i.e. as electron fluid. In that way we will use electrons density $N(\mathbf{r}, t)$ and velocity $\mathbf{v}(\mathbf{r}, t)$ to describe plasma. The equation of motion and the set of Maxwell equations will be used to follow plasma evolution (see details in Section 1.3.3).

To investigate electron density oscillations we will consider the Poisson's equation:

$$\nabla \cdot \mathbf{E} = -4\pi e(N - N_0) , \quad (1.108)$$

together with the equation of motion:

$$m_e \frac{d\mathbf{v}}{dt} = -e\mathbf{E} - \frac{1}{N} \nabla P , \quad (1.109)$$

and continuity equation:

$$\frac{\partial N}{\partial t} + \nabla \cdot (N\mathbf{v}) = 0 . \quad (1.110)$$

We will use isothermal approximation, so $P = Nk_B T$ is the thermal pressure.

Let us designate is the uniform background density as N_0 . We will consider small density perturbations $|N - N_0| \ll N_0$. Then one can write

$$N(x, t) = N_0 + N_1(x, t) , \quad (1.111)$$

$$\mathbf{v}(x, t) = v_1(x, t) \mathbf{e}_x , \quad (1.112)$$

$$\mathbf{E}(x, t) = E_1(x, t) \mathbf{e}_x , \quad (1.113)$$

$$P(x, t) = P_0 + P_1(x, t) . \quad (1.114)$$

We will search for the plane wave solutions for which

$$\{n_1, v_1, E_1, P_1\} \propto e^{i(kx - \omega t)} . \quad (1.115)$$

1.3. Basic laser plasma interaction theory

So in Eq. (1.111)-(1.114) we can substitute $\partial_t \rightarrow -i\omega$, $\partial_x \rightarrow ik$.

Let us first consider *cold* plasma with $P \equiv 0$. When we have a set of algebraic equations

$$\begin{cases} ikE_1 = -4\pi eN_1, \\ -i\omega m_e v_1 = -eE_1, \\ -i\omega N_1 + ikN_0 v_1 = 0. \end{cases} \quad (1.116)$$

This system has a non-trivial solution if

$$\omega^2 = \frac{4\pi e^2 N_0}{m_e} \equiv \omega_p^2. \quad (1.117)$$

Now lets consider *warm* plasma. Using the adiabatic relation $P/P_0 = (N/N_0)^3$, we obtain dispersion relation for propagating plasma waves:

$$\omega^2 = \omega_p^2 + 3k^2 v_{th}^2, \quad (1.118)$$

where $v_{th}^2 = k_B T$.

Plasma wave phase velocity

The phase velocity of plasma wave is determined by its “driver”. If we consider plasma wave excited by short laser pulse (laser-driven wakefield), we can postulate

$$v_{ph} \approx v_{gr}^{las}. \quad (1.119)$$

Therefore in linear 1D regime we have the plasma wave phase velocity

$$v_{ph} = c \sqrt{1 - \frac{\omega_p^2}{\omega^2}}, \quad (1.120)$$

and the plasma wave gamma-factor

$$\gamma_p = \frac{1}{\sqrt{1 - v_{ph}^2/c^2}} = \frac{\omega}{\omega_p} = \sqrt{\frac{N_{cr}}{N_0}}. \quad (1.121)$$

Taking into account nonlinear corrections (see [51, 61]), we have for the case $\omega \gg \omega_p$

$$v_{ph} = v_{gr}^{las} = c \sqrt{1 - \frac{\omega_p^2}{\omega^2 \langle \gamma \rangle}}, \quad (1.122)$$

where $\langle \gamma \rangle = (1 + a_0^2/2)^{1/2}$.

The group velocity of laser pulse can be reduced by 3D effects. In 3D case, there are finite angular distribution of wave vectors \mathbf{k} . If R is the transverse size of the pulse, the perpendicular component of wave vector k_\perp can be estimated as $k_\perp \simeq 1/R$, and the characteristic angle θ of this distribution is $\theta \simeq k_\perp/k \simeq 1/(kR)$. Therefore the pulse axial group velocity is reduced $v_{gr}^{las} \simeq c \cos \theta \simeq c/(kR)$. Due to finite angular

1. Introduction

distribution of wave vectors the relativistic gamma-factor of the pulse can be estimated as

$$\gamma \simeq kR, \quad k = \frac{\omega}{c} \sqrt{1 - \frac{\omega_p^2}{\omega^2}}. \quad (1.123)$$

For real laser pulse the corrections given by Eq. (1.122) and Eq. (1.123) take place simultaneously. The concrete pulse parameters define the dominating mechanism.

In this discussion we neglect the pulse shape modification, which takes place after pulse propagation in plasma for a finite time. The plasma wave can distort the pulse profile, which in turn leads to plasma wave phase velocity reduction [75].

Plasma waves excitation. Wavebreaking

In the linear regime the electric field in plasma wave can be described as

$$E_z = E_0 \exp \left[\omega_p \left(\frac{z}{v_{ph}} - t \right) \right], \quad (1.124)$$

where E_0 is the field amplitude and v_{ph} is the wave phase velocity. The maximum amplitude of plasma wave E_{max} can be estimated using the assumption, that *all* plasma electrons oscillate with wavenumber $k_p = \omega_p/c$. Then using Poisson Eq. (1.66) we have

$$\nabla \cdot \mathbf{E}_{max} = k_p E_{max} = 4\pi e N_e \quad (1.125)$$

and

$$E_{WB} = \frac{cm_e \omega_p}{e}. \quad (1.126)$$

This value is known as *nonrelativistic wavebreaking* field [9]. Using 1D relativistic cold fluid equations it is possible to show, that maximum accessible amplitude of plasma wave is

$$E_{RWB} = \sqrt{2(\gamma_p - 1)} \frac{cm_e \omega_p}{e}, \quad (1.127)$$

where $\gamma_p = (1 - v_{ph}^2/c^2)^{-\frac{1}{2}}$. This value is called *relativistic wavebreaking* field, and it was first derived in [8].

Let us clarify the physical meaning of this value. The fluid equations can be used to describe plasma wave as long as the electron fluid velocity satisfies the condition $v_e < v_{ph}$. When the wave amplitude increases, the v_e also increases, and at the limit $v_e \rightarrow v_{ph}$ plasma density becomes singular, and we call it “wavebreaking”.

These values were derived using cold plasma approximation. Thermal effects can reduce the wavebreaking limit. Wavebreaking limit, $E_{th} < E_{RWB}$, was obtained in papers [76, 77] using relativistic fluid equations.

The similarity theory, developed for 3D case in [78], shows that in 3D case the wavebreaking looks rather like a thermalization, with characteristic “wavebreaking” time t_d . As concerning the electric field, there is no limit analogous to Eq. (1.126), (1.127) in 3D case. In that way 3D geometry allows regular wake field existing with arbitrary amplitudes.

For $E_0 \ll E_{WB}$, the plasma wave exists in linear regime and can be described as a sinusoidal oscillation with frequency equals to plasma frequency ω_p and phase speed v_{ph} , defined by driver velocity.

When $E_{WB} < E_0 < E_{RWB}$, the plasma wave is strongly nonlinear. Electric field take so-called, “saw-tooth” form. The period of such wave increases with the amplitude. See for details [8, 79, 80, 81].

1.3.9 Particles acceleration mechanisms

Direct laser acceleration

The mechanism of *direct laser acceleration* (DLA) was proposed in [82]. This mechanism works only for the linearly polarized laser pulses. The basic physical idea of this mechanism, is that the electrons propagating in plasma channel, can interact resonantly with the light traveling in the same direction. The ponderomotive pressure expelles the electrons from the channel and creates a radial electrostatic field. At the same time, the light propagating in channel, accelerates the electrons in forward direction, producing a current, which generates the azimuthal magnetic field.

If we roughly approximate laser plasma channel as a cylinder with uniform electron density $N_e = fN_0$ ($0 \leq f \leq 1$) we can write the radial electric field:

$$-eE_r = (1 - f) \frac{m\omega_{pe}^2}{2} r . \quad (1.128)$$

The current $-efN_0c$ produces the azimuthal magnetic field:

$$-eB_\phi = f \frac{m\omega_{pe}^2}{2} r . \quad (1.129)$$

Therefore the equation of radial motion for electron in such idealized channel can be written as:

$$m\gamma \frac{d^2r}{dt^2} = -eE_r - eB_\phi , \quad (1.130)$$

and we can find the oscillation (betatron frequency)

$$\omega_\beta = \frac{\omega_{pe}}{\sqrt{2}\gamma} . \quad (1.131)$$

In this model the fields cooperate in such a way, that the electrons are moving mainly in the direction of the channel axis, and in the radial direction the channel works as a potential well. The electrons are trapped in this well and oscillate radially with frequency $\approx \omega_\beta$. One should note, that betatron frequency does not depend on the degree of channel cavitation.

As the electrons are moving in channel axial direction with velocity v_z , they observe a strongly downshifted optical frequency. The conditions can be selected in such a way, that the transverse betatron oscillations are in resonance with laser. Then a fraction of electrons, can be resonantly driven by the laser field.

1. Introduction

The electron oscillations are directed along the laser polarization, so the electron can gain energy two times for the laser period (energy coupling). Because of that, the transverse velocity v_{\perp} oscillates according to the laser period, and longitudinal velocity v_{\parallel} oscillates twice during the period. This leads to the electron bunching in space two times per laser wavelength.

For more details of DLA-mechanism see [82, 83].

Particles acceleration in plasma wave. Wakefield acceleration

In this Section we describe briefly laser wakefield acceleration (LWFA). This acceleration mechanism uses laser-driven plasma waves and their longitudinal electric fields to accelerate particles.

When a laser pulse propagates through underdense plasma, it excites a running plasma wave oscillating at the plasma frequency ω_p . The wave phase velocity is defined by the laser pulse group velocity: $v_{ph}^{wave} = v_{gr}^{laser} = c\sqrt{1 - \omega_p^2/\omega_0^2}$, where ω_0 is the laser frequency. The electric field of this plasma wave is longitudinal, i.e. it points into the propagation direction. Under certain circumstances an electron can be put in this plasma wave and can be accelerated.

The laser pulse can excite the plasma wave in a different ways. For $a_0 \gg 1$ this process cannot be described by the linear plasma theory. One should note, that the pattern of wake field excitation depends significantly on the laser pulse length L in comparison with the plasma wavelength λ_p , (see LWFA and SM-LWFA mentioned above).

The energy which electron trapped in wakefield can gain can be estimated as

$$eW \approx eE_m L_d , \quad (1.132)$$

where E_m is the maximum electric field, L_d - dephasing length, i.e. the length of part, over which electron experiences accelerating field. It can be defined from this estimation

$$\omega_p \left(\frac{L_d}{v_p} - t_d \right) \sim \pi , \quad (1.133)$$

where $t_d = L_d/c$.

Bubble regime of electron acceleration

If one considers the 3D geometry of short laser pulse propagation, a new regime appears, in which the laser wave takes the shape of a solitary plasma cavity: the so-called ‘‘bubble regime’’. It was discovered in numerical simulations [11].

When the intensity of the laser pulse is ultra-relativistic and the pulse duration is shorter than the relativistic plasma period, then the wake field takes the form of a single cavity: the bubble. Background plasma electrons can be trapped and accelerated inside the bubble. Such trapping is a continuing process. With the increase of the number of trapped electrons, the bubble elongates. The effective bubble velocity decreases, and electrons start to dephase with respect to the accelerating field. This causes electron

1.3. Basic laser plasma interaction theory

self-bunching in the phase space, which results in the monoenergetic peak in the energy spectrum. An extremely collimated and quasi-monoenergetic electron beam was recently observed in the experiment [84], which is in a good agreement with “bubble” picture.

The theoretical investigation of this regime is very complicated, because the problem should be described with the system of non-linear kinetic equations, and contains a number of parameters. The significant progress was done in paper [78], where the similarity theory for laser-plasma interaction in the ultra-relativistic limit was developed. It was shown that the optimal configuration for the high energy electron acceleration is the following one: the focal spot radius

$$R \approx \frac{\sqrt{a_0}}{k_p}, \quad (1.134)$$

and the pulse duration

$$\tau \leq \frac{R}{c}, \quad (1.135)$$

where a_0 is the pulse dimensionless amplitude, $k_p = \omega_p/c$. This configuration corresponds to the “bubble” regime.

Using the similarity theory for the regime $c\tau < R$, several scalings were obtained in [78]. The maximum energy of monoenergetic peak in the electron spectrum is given by formula

$$E_{mono} \approx 0.65 m_e c^2 \sqrt{\frac{P}{P_{rel}} \frac{c\tau}{\lambda}}, \quad (1.136)$$

there P is the pulse power and $P_{rel} = m_e^2 c^5 / e^2 \approx 8.5$ GW. The number of accelerated electrons in monoenergetic peak is

$$N_{mono} \approx \frac{1.8}{k_0 r_e} \sqrt{\frac{P}{P_{rel}}}, \quad (1.137)$$

where $r_e = e^2 / m_e c^2$, $k_0 = 2\pi / \lambda$. One should note that from Eq. (1.136), (1.137), that efficiency of laser energy conversion into monoenergetic electrons is a universal constant

$$\eta = \frac{N_{mono} E_{mono}}{P\tau} \approx 20\%. \quad (1.138)$$

The parametric dependencies in the scalings Eq. (1.136)-(1.137) follow from the analytical theory while the numerical pre-factors have been obtained from direct 3D particle-in-cell simulations.

2 Protons acceleration in a plasma wave

2.1 Introduction

Till now electron acceleration in laser fields was the main point of interest. Electrons are the lightest charged particles in plasma. That is the reason, why they absorb the most of laser pulse energy and accelerate first. However the acceleration of heavy charged particles (protons and ions) to high energies is one of the most promising aspects for applications of intense short laser pulses. The possible applications of proton beams, produced by laser-solid interactions are:

- The imaging of electromagnetic fields in overdense plasmas (see [85]).
- Fast ignition of targets in Inertial Confinement Fusion (ICF) (see [86]).
- Medical applications (see [87, 88]).

A number of recent experiments have demonstrated that protons [89, 90, 91, 92, 93, 94, 95, 96] and even heavier ions [97] can be efficiently accelerated in laser-plasma experiments. Different acceleration mechanisms have been proposed for explanation of the experimental results.

In underdense plasma channels (see [89]) the mechanism of ion acceleration is the Coulomb explosion of the electron-cavitated region near laser channel axis.

Laser interactions with overdense targets was investigated in details in the experiments with solid foils. In most of these experiments, very powerful lasers have been used with the pulse energies 100 – 1000 J and powers of 100 – 1000 TW and protons with energies of the order \sim MeV and higher have been observed. They originate from water and hydrocarbon molecules always covering the target surface. The presence of water and pump oil vapor is practically inevitable in current experimental setups.

To explain the observed MeV protons two reasonable acceleration scenario were proposed. The first explanation [90, 91, 98] suggests that the protons come from the *front surface* of the target. Their appearance deals with the direct ponderomotive push at the front surface. This push leads to a double-layer formation and the ion acceleration.

The second explanation [94, 97, 99] suggests that the protons come from the *rear surface* of the target. In this case, the proposed reason of protons acceleration is the so-called Target Normal Sheath Acceleration (TNSA). The TNSA suggests that the laser pulse produces hot electrons at the front surface. Then these electrons propagate through the foil and generate a space charge sheath at the rear surface of the target.

2. Protons acceleration in a plasma wave

The electrostatic field of this space charge pulls the ions sitting on the rear surface and accelerates them to high energies.

According to multi-dimensional particle-in-cell simulations [100, 101], the both mechanisms can co-exist, which finds confirmation in recent experiments [102, 92]. In the paper [103], the influence of laser prepulse on the protons acceleration in thin-foil experiments was investigated. The authors show that prepulse duration has a profound effect on the maximum proton energy and found optimal thickness of the target, which depends on the prepulse duration. At the optimal thickness, the rear side mechanism produces the highest proton energies, while in the case when protons are primarily accelerated at the front side, lower cutoff energies were observed.

Particularly, very interesting is the possibility of proton acceleration to the energies 300 – 600 MeV using the lowest possible laser pulse energy. One of the practical reasons for this study is that the protons at this energy range might be used for cancer therapy in medicine [87, 88]. To achieve these energy using the TNSA mechanism, very high laser intensities are required to heat electrons to the necessary energies. The pulse duration should be also long enough, because the electric fields in the Debye sheath represent only a small fraction of the laser ones. Therefore, for these purpose, short and intense lasers which are applied to the front surface can be more suitable for ion acceleration with high repetition rate.

In this Chapter we are discussing in detail the ion acceleration at the front surface of the plasma layer. Our aim is to understand what is the scaling of the maximum attainable ion energy as a function of the laser intensity. We also discuss the possibility of protons acceleration in an electron plasma wave, which is possible in the case of a two-ion components plasma mixture.

2.2 Ion relativistic threshold

The direct coupling of the laser energy to the ions begins at very high laser intensities. Considering protons we can find using Eq. (1.25) and (1.28) the proton relativistic threshold:

$$I_p = \left(\frac{m_p}{m_e} \right)^2 I_0 \approx \frac{4.6 \cdot 10^{24} [\text{W cm}^{-2}]}{\lambda[\mu\text{m}]^2}, \quad (2.1)$$

where I_0 is the electron relativistic threshold given by Eq. (1.42) and λ is the laser wavelength. In terms of the dimensionless amplitude we can rewrite this criterion as

$$a_0 = \frac{eA_0}{m_e c^2} > \frac{m_p}{m_e} \approx 1836. \quad (2.2)$$

For intensities $I > I_p$, the protons motion becomes essentially relativistic. Presently, such intensities are unattainable, but new technologies, such as optical parametric amplification (OPA-CPA) probably will make them feasible [104].

In this Chapter we will study intensities still well below I_p , and investigate the possibility of reducing $a \sim m_p/m_e$ scaling to $\sqrt{m_p/m_e} \approx 43$ which looks much more suitable for nowadays technology. We will show analytically and numerically that plasma fields

induced with laser intensities $a \leq 100$ may be sufficient to accomplish the proton acceleration to nearly-relativistic energies.

2.3 Ion acceleration at the front surface

Let us consider which processes take place when laser pulse strikes the overdense plasma. At the first stage of interaction the plasma is accelerated due to radiation pressure. This implies that we may consider the pulse as sufficiently wide, so that the one-dimensional geometry of interaction may be considered. If the laser pulse dimensionless amplitude $a \gg 1$, then electrons are quickly accelerated by the transverse electric field \mathbf{E} , which acts on the electrons with the force $e\mathbf{E}$ and accelerates them to velocities $v_e \sim c$. The Lorentz force push them forward. Because $v_{e\perp} \sim c$, the Lorentz force can be estimated as $|e\mathbf{v}_e \times \mathbf{B}/c| \sim eE$. We assume that at the first stage of boring into the plasma, laser pulse displaces *all* electrons, until the electric field, created by the charge separation becomes equal the Lorentz force.

At the second stage, due to the longitudinal electric field, created by the charge separation, the radiation momentum is transferred to the ions. As the electrons and the ions move with the same velocity and $m_e \ll m_i$, we can approximate that the momentum is transported only by ions.

The energy of accelerated ions can be easily estimated if the plasma contains only one ion species and is overdense for the laser pulse [105]. Then one can use the momentum conservation law. The laser light pressure can be considered as a momentum flux:

$$P_l = \frac{I}{c} = N_{cr} m_e c^2 \frac{a^2}{2}, \quad (2.3)$$

where $a = eA/m_e c^2$ is the dimensionless amplitude of the laser vector potential, and $N_{cr} = m_e \omega^2 / 4\pi e^2$ is the critical density. The momentum flux which is transported by the ions can be defined by formula:

$$P_i = N_i \frac{p_i^2}{m_i \gamma_i}, \quad (2.4)$$

where N_i is the ion density, m_i is the ion mass, p_i is the mean ion momentum, and $\gamma_i = \sqrt{1 + (p_i/m_i c)^2}$ is the relativistic γ -factor.

Using the absorption rate $0 \leq \eta \leq 1$ we can write relation between incident light momentum and momentum, absorbed by ions

$$P_i = (2 - \eta) P_l. \quad (2.5)$$

To make clear the physical sense of Eq. (2.5) let us consider the limiting cases. If the laser pulse is completely absorbed, we must set $\eta = 1$ and in this way obtain $P_i = P_l$. If the laser pulse is completely back reflected, then $\eta = 0$ and $P_i = 2P_l$.

Using Eq. (2.5) we can obtain the ion energy estimation:

$$E_i = \frac{p_i^2}{(1 + \gamma_i) m_i} = (2 - \eta) \frac{N_{cr}}{N_i} \frac{a^2}{2} m_e c^2. \quad (2.6)$$

2. Protons acceleration in a plasma wave

The plasma layer remains overdense for a relativistically intense laser pulse only if $N_e/N_{cr} > a/2$ (see Eq. (1.98)), where $N_e = ZN_i$ is the electron density and Z is the ion charge. At higher intensities, the plasma is relativistically transparent. Setting the laser amplitude at the boundary of relativistic transparency, $a \approx 2ZN_i/N_{cr}$, we can estimate the maximum ion energy as:

$$E_i^{max} \approx (2 - \eta)Zam_e c^2 . \quad (2.7)$$

The estimations given by Eq. (2.6) and Eq. (2.7) are based on the fundamental law of momentum conservation. They are insensitive to the particular interaction physics. The only assumption we used to receive this conclusion is that *all the plasma ions are equivalent, i.e., a single species plasma is considered.*

As it was mentioned above, the experiments show that whatever material is irradiated by the laser, usually the protons are accelerated first. Let us consider plasma, which is a mixture of different species. If the plasma contains a small portion of ions with a large charge-to-mass ratio, then these ions can be accelerated to higher energies than the simple limits Eq. (2.6) and (2.7) predict. In this case, the particular mechanism of acceleration is very important.

In particular experiments hydrogen-helium mixture can be used, which charge-to-mass ratios differ by the factor 2.

2.4 Model for ion trapping in a running plasma wave

2.4.1 Overview

We propose here the so-called "*ion wakefield acceleration*" mechanism. This mechanism works when some energetic ions get trapped into an electrostatic plasma wave. Let us assume that the plasma wave is running with the phase velocity v_p , i.e., all the density perturbations and the potential are functions of $\xi = x - v_p t$. If the background ions are oscillating in the field of this wave, they get the velocities which are comparable with the wave phase velocity, $v_i \sim v_p$, then they are trapped and may be accelerated further to very high energies. This mechanism is analogous to the well-known electron trapping in plasma waves [106]. Below using simple analytical model we will estimate the laser intensity and plasma parameters needed for such type of ion trapping, and check it using a number of one-dimensional (1D) particle-in-cell (PIC) simulations for different range of parameters.

2.4.2 Single particle dynamics in prescribed potential

Let us consider the particle motion in the prescribed external electrostatic potential Φ . And we will postulate, that it is moving with constant velocity v_p , so $\Phi = \Phi(x - v_p t)$. The Hamiltonian of particle with mass m and charge q is

$$H = \gamma m c^2 + q\Phi(x - v_p t) = m c^2(\gamma + \phi) , \quad (2.8)$$

2.4. Model for ion trapping in a running plasma wave

where γ is the relativistic gamma-factor and

$$\phi = \frac{q}{mc^2} \Phi , \quad (2.9)$$

is the dimensionless potential. The equations of motion for this particle can be described using Hamilton equations:

$$\frac{dx}{dt} = \frac{\partial H}{\partial p} , \quad (2.10)$$

$$\frac{dp}{dt} = -\frac{\partial H}{\partial x} , \quad (2.11)$$

$$(2.12)$$

(see [107] for details). Let us introduce dimensionless velocities $\beta = v/c$, $\beta_p = v_p/c$ and dimensionless coordinates

$$\hat{x} = k_p x , \quad (2.13)$$

$$\psi = k_p (x - v_p t) , \quad (2.14)$$

where $k_p = 2\pi/\lambda_p$ and λ_p is the distance between nearest maximums of ϕ . If the potential ϕ is the consequence of excited plasma wave, the relation between v_p and k_p is defined by dispersion relation. We not concretize it here.

Using Eq. (2.8)-(2.14) and taking into account that particle momentum $p = mc\beta\gamma$, we will rewrite the differential form as

$$pdx - Hdt = \frac{mc^2}{k_p v_p} \left\{ (\gamma\beta\beta_p - (\gamma + \phi)) d\hat{x} + \gamma d\psi \right\} + \frac{mc^2}{k_p v_p} \phi(\psi) d\psi . \quad (2.15)$$

It is easy to see, that last item is an exact differential dF , where

$$F(\psi) = \frac{mc^2}{k_p v_p} \int_0^\psi \Phi(\zeta) d\zeta . \quad (2.16)$$

So we have

$$pdx - Hdt = \lambda(\gamma d\psi - h d\hat{x}) + dF , \quad (2.17)$$

where $\lambda = mc^2/(k_p v_p) = const$, dF is the exact differential. The dimensionless Hamiltonian is given by formula

$$h(\gamma, \psi) = \gamma(1 - \beta\beta_p) + \phi(\psi) , \quad (2.18)$$

where

$$\beta(\gamma) = \sqrt{1 - \frac{1}{\gamma^2}} . \quad (2.19)$$

2. Protons acceleration in a plasma wave

In such a way we can rewrite Eq. (2.10), (2.11) as

$$\frac{d\psi}{d\hat{x}} = \frac{\partial h}{\partial \gamma} = 1 - \frac{\beta}{\beta_p}, \quad (2.20)$$

$$\frac{d\gamma}{d\hat{x}} = -\frac{\partial h}{\partial \psi} = -\frac{\partial \phi}{\partial \psi}. \quad (2.21)$$

The phase space particle trajectory (orbit) $\gamma(\psi)$ can be found as the solution of equation

$$h(\gamma, \psi) = \text{const}. \quad (2.22)$$

The fixed points can be found from equations

$$\frac{d\psi}{d\hat{x}} = \frac{d\gamma}{d\hat{x}} = 0. \quad (2.23)$$

Stable ‘‘O’’ points:

$$\begin{aligned} \gamma &= \gamma_p, \\ \psi &= \psi_{min} + nk_p\lambda_p, n \in \mathbb{Z}, \end{aligned} \quad (2.24)$$

unstable ‘‘X’’ points:

$$\begin{aligned} \gamma &= \gamma_p, \\ \psi &= \psi_{max} + nk_p\lambda_p, n \in \mathbb{Z}. \end{aligned} \quad (2.25)$$

The phases ψ_{min} and ψ_{max} correspond to potential minimum and maximum

$$\phi(\psi_{min}) = \phi_{min}, \quad \phi(\psi_{max}) = \phi_{max} \quad (2.26)$$

$$\psi_{max} - \psi_{min} = \frac{1}{2}k_p\lambda_p. \quad (2.27)$$

The separatrix $\gamma_s(\psi)$ which separates the close orbits from the open orbits can be found from equation:

$$h(\gamma_s, \psi) = h(\gamma_p, \psi_{min}). \quad (2.28)$$

The close orbits correspond to trapped particles, and the open orbits correspond to untrapped particles.

Using this formalism, we can find the maximum energy gain. It takes place for trapped particles, with orbits tending to the separatrix from the inside. So

$$\Delta E_{max} = mc^2(\gamma_{max} - \gamma_{min}). \quad (2.29)$$

For separatrix $\gamma_s(\psi)$ we have:

$$h(\gamma_m, \psi_{max}) = h(\gamma_p, \psi_{min}), \quad (2.30)$$

where $\gamma_m = \{\gamma_{min}, \gamma_{max}\}$. Eq. (2.30) can be rewritten as quadratic equation

$$\gamma_m^2 - 2\gamma_m\gamma_p(1 + \gamma_p\Delta\phi) + \beta_p^2\gamma_p^2 + (1 + \gamma_p\Delta\psi)^2 = 0, \quad (2.31)$$

and its roots are given by formula

$$\gamma_m = \gamma_p(1 + \gamma_p\Delta\phi) \pm \gamma_p\beta_p\sqrt{(1 + \gamma_p\Delta\phi)^2 - 1}, \quad (2.32)$$

where ‘‘+’’ corresponds to γ_{max} and ‘‘-’’ corresponds to γ_{min} .

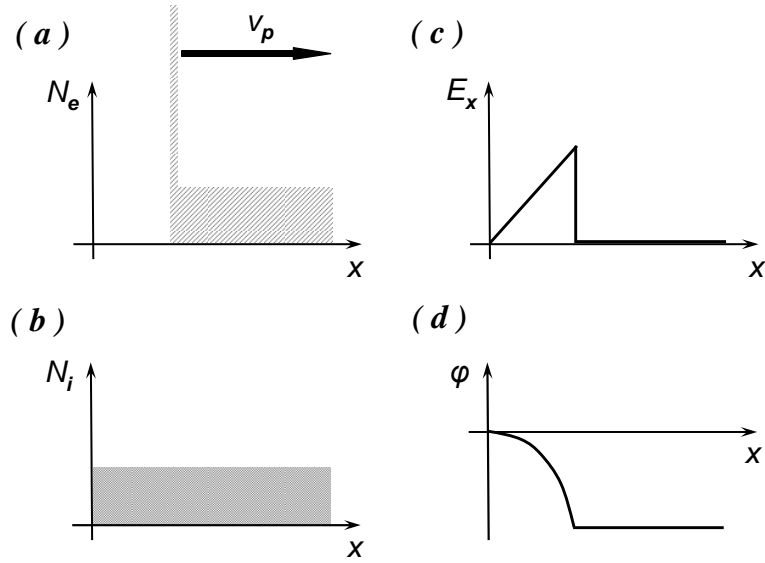


Figure 2.1: Snow plow model

2.4.3 Plasma wave generation

We will consider the plasma slab which initially has a uniform density distribution with a sharp boundary:

$$N(x) = \begin{cases} 0 & \text{for } x < 0, \\ N & \text{for } x \geq 0. \end{cases} \quad (2.33)$$

Let us introduce

- The laboratory system of reference (K), in which the plasma slab is motionless.
- The reference system co-moving with the plasma wave (K'). In laboratory system (K), the system (K') is moving with the plasma wave phase velocity v_p .

We will assume that the ponderomotive pressure of the laser pulse works as a “snow plough” [108] and sweeps forward the background electrons until an electrostatic field develops, which counterbalances the light pressure. In the laboratory system of reference (K), the “snow plough” moves with the plasma wave phase velocity v_p and creates a non-compensated charge density Ne behind the shock-wave (see Figure (2.1)).

In the (K') we have region with charge density eN' which creates behind the shock-wave. Using Poisson Eq. (1.66) we obtain for the electrostatic field in K' :

$$\frac{dE'_x}{dx'} = \begin{cases} 4\pi N'e & \text{for } 0 \leq x' \leq d, \\ 0 & \text{for } x' > d, \end{cases} \quad (2.34)$$

where

$$d = \frac{E'_{max}}{4\pi N'e}. \quad (2.35)$$

2. Protons acceleration in a plasma wave

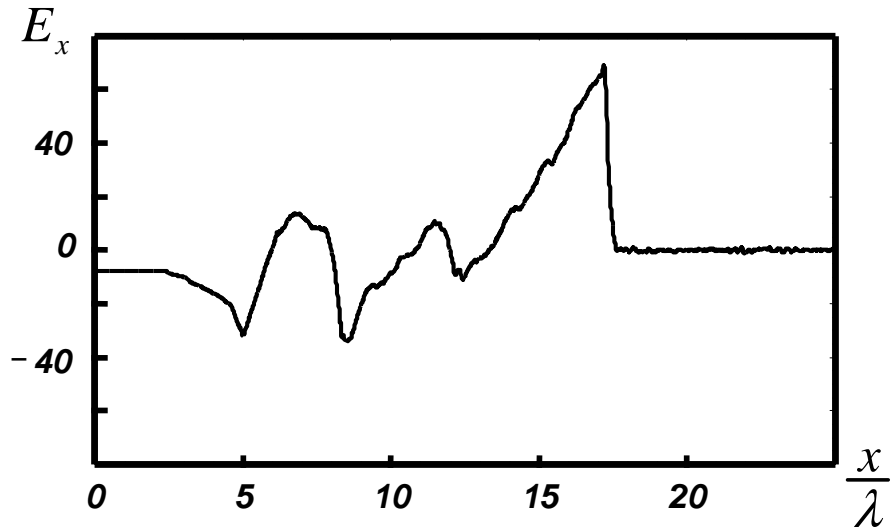


Figure 2.2: Plasma wave obtained in the PIC simulation. The laser amplitude $a = 60$, the plasma density $N = 10N_{cr}$. The maximum electric field is close to the laser amplitude.

Because of the plasma quasi-neutrality, the wave of compression is followed by the wave of rarefaction and the electric field E'_x and potential ϕ' obtain a quasi-symmetric form:

$$E'_x(x) = \begin{cases} 4\pi N' e x' & \text{for } |x'| \leq d, \\ 0 & \text{for } |x'| > d, \end{cases} \quad (2.36)$$

$$\phi'(x') = - \int_0^{x'} E'_x(\xi) d\xi = \begin{cases} -2\pi N' e x'^2 & \text{for } |x'| \leq d, \\ -\frac{E_{max}'^2}{8\pi N' e} & \text{for } |x'| > d. \end{cases} \quad (2.37)$$

We choose the integration constant in such a way to have $\phi'(0) = 0$. In that case the condition of particle trapping is

$$H' < 0, \quad (2.38)$$

where H' is the particles Hamiltonian. If one choose the other standard condition $\phi'(\infty) = 0$, the trapping condition will be $H' < \phi'_0 = \phi'(0)$.

In the reference system K' , the charge density and the electric field form a stationary periodic structure with the period $2d$. In laboratory system K this structure moves behind the laser pulse with the phase velocity v_p . A typical structure of such a wave obtained from one-dimensional PIC simulation is shown in Figure 2.2.

The electric field E_{max} can be found from the condition of equilibrium with the laser ponderomotive pressure at the front of the wave. Doing this, we obtain the estimation $E_{max} \approx E_0$, where E_0 is the amplitude of the laser pulse electric field. Making a transition from K to K' and taking into account that Lorentz transformation does not change longitudinal components of fields, we obtain:

$$E'_{max} = E'_x(x' = d) \approx E_0 = \frac{m_e \omega c}{e} a_0, \quad (2.39)$$

2.4. Model for ion trapping in a running plasma wave

where

$$x' = \frac{x - v_p t}{\sqrt{1 - \frac{v_p^2}{c^2}}} . \quad (2.40)$$

The ω and $a_0 = eA/m_e c^2$ are the laser frequency and dimensionless vector potential correspondingly. Calculating the integral in Eq. (2.37) we obtain the potential difference over the half plasma wavelength $\Delta\Phi = \phi(d) - \phi(0)$:

$$e|\Delta\Phi| = m_e c^2 \left(\frac{N_{cr}}{N'} \right) \frac{a_0^2}{2} . \quad (2.41)$$

Since the plasma wave is driven by the laser pulse and the plasma is relativistically transparent, we can postulate with a good accuracy that the wave phase velocity v_p is equal to the laser group v_{gr}^{las} velocity:

$$v_p = v_{gr}^{las} \approx \sqrt{1 - \frac{\omega_p^2}{\omega_0^2 \langle \gamma \rangle}} , \quad (2.42)$$

where $\langle \gamma \rangle$ is an averaged relativistic gamma-factor of plasma electrons. The calculation of gamma-factor for an ultra-relativistically intense laser pulse, propagating in plasma is complicated and not completely resolved theoretical problem (see for details [51]). We will use the estimation

$$\langle \gamma \rangle \sim \frac{a_0}{2} , \quad (2.43)$$

which is in a good agreement with the recent paper [109]. Substituting this estimation for γ in Eq. (2.42) we obtain:

$$\frac{v_p}{c} \approx \sqrt{1 - \frac{N}{N_{cr}} \frac{2}{a_0}} , \quad (2.44)$$

$$\gamma_p = \frac{1}{\sqrt{1 - \frac{v_p^2}{c^2}}} = \sqrt{\frac{N_{cr} a_0}{N} \frac{2}{a_0}} , \text{ for } a_0 \geq \frac{2N}{N_{cr}} . \quad (2.45)$$

2.4.4 Particle motion in laser-generated plasma wave

To describe the ion motion in the laser-generated wave, following Section 2.4.2 we introduce the ions Hamilton function $H(x, p, t)$. In the moving system of reference K' , the plasma wave can be considered as quasi-stationary and the Hamiltonian has the form

$$H'(x', p') = E'_i + q\phi'(x') , \quad (2.46)$$

where E'_i is the ion kinetic energy in K' .

As we can see, Eq. (2.46) is similar to to Eq. (2.8), so we will use the separatrix method, described in details in Section 2.4.2.

2. Protons acceleration in a plasma wave

The energy conservation along an ion trajectory provides the equation for the trajectories $H'(x', p') = E' = \text{const}$. Using Eq. (2.40) and expressing the particle energy through the momentum p_i in the laboratory frame we will obtain

$$H'(x, p_i) = \frac{\sqrt{p_i^2 c^2 + m_i^2 c^4} - v_p p_i}{\sqrt{1 - \frac{v_p^2}{c^2}}} + e\phi' \left(\frac{x - v_p t}{\sqrt{1 - \frac{v_p^2}{c^2}}} \right). \quad (2.47)$$

Introducing the new dimensionless variables:

$$\frac{v}{c} \rightarrow v, \quad \frac{p_i}{m_i c} \rightarrow p_i, \quad \frac{N}{N_{cr}} \rightarrow N, \quad y = \frac{x - v_p t}{d\sqrt{1 - \frac{v_p^2}{c^2}}}, \quad (2.48)$$

we obtain:

$$h'(x, p_i) = \frac{H'}{m_i c^2} = \frac{\sqrt{1 + p_i^2} - v_p p_i}{\sqrt{1 - v_p^2}} + \frac{q}{m_i c^2} \phi' \left(\frac{x - v_p t}{\sqrt{1 - v_p^2}} \right). \quad (2.49)$$

Now we will substitute the particular form of the potential given by Eq. (2.37), taking into account that the electron density in N in K is expressed through the density N' in K' by relation $N = N'/\sqrt{1 - v_p^2}$. Finally we obtain

$$h'(y, p_i) = \frac{\sqrt{1 + p_i^2} - v_p p_i}{\sqrt{1 - v_p^2}} - \frac{m_e}{m_i} \frac{1}{n\sqrt{1 - v_p^2}} \frac{a^2}{2} y^2. \quad (2.50)$$

The equation

$$h'(y, p_i) = 1 \quad (2.51)$$

gives us the separatrix in phase space (y, p_i) . It separates the trapped ions with $h' < 1$ from the passing ions with $h' > 1$. The ion trajectories and the separatrix for different laser amplitudes are shown in Figure (2.3).

The ions which are initially at rest can be trapped in the wave, when the separatrix touches the axis $p = 0$. This condition can be written as

$$1 - \frac{m_e}{m_i} \frac{a_{tr}^2}{2N} = \frac{1}{\gamma_p}. \quad (2.52)$$

There are two different regions of parameters, when the ions can be trapped into the plasma wave. The first one corresponds to low laser group velocities, when the laser is just at the verge of the relativistic transparency: $a \geq 2N$, $\gamma_p \approx 1$. In this case, the plasma wave is very slow and it is easy to fulfill the ion trapping condition $v_i \approx v_p$. The phase portrait in Figure (2.3 a) corresponds to this case.

When the laser amplitude increases, the lower bound of the separatrix rises and the ions at rest cannot be trapped anymore, Figure (2.3 b).

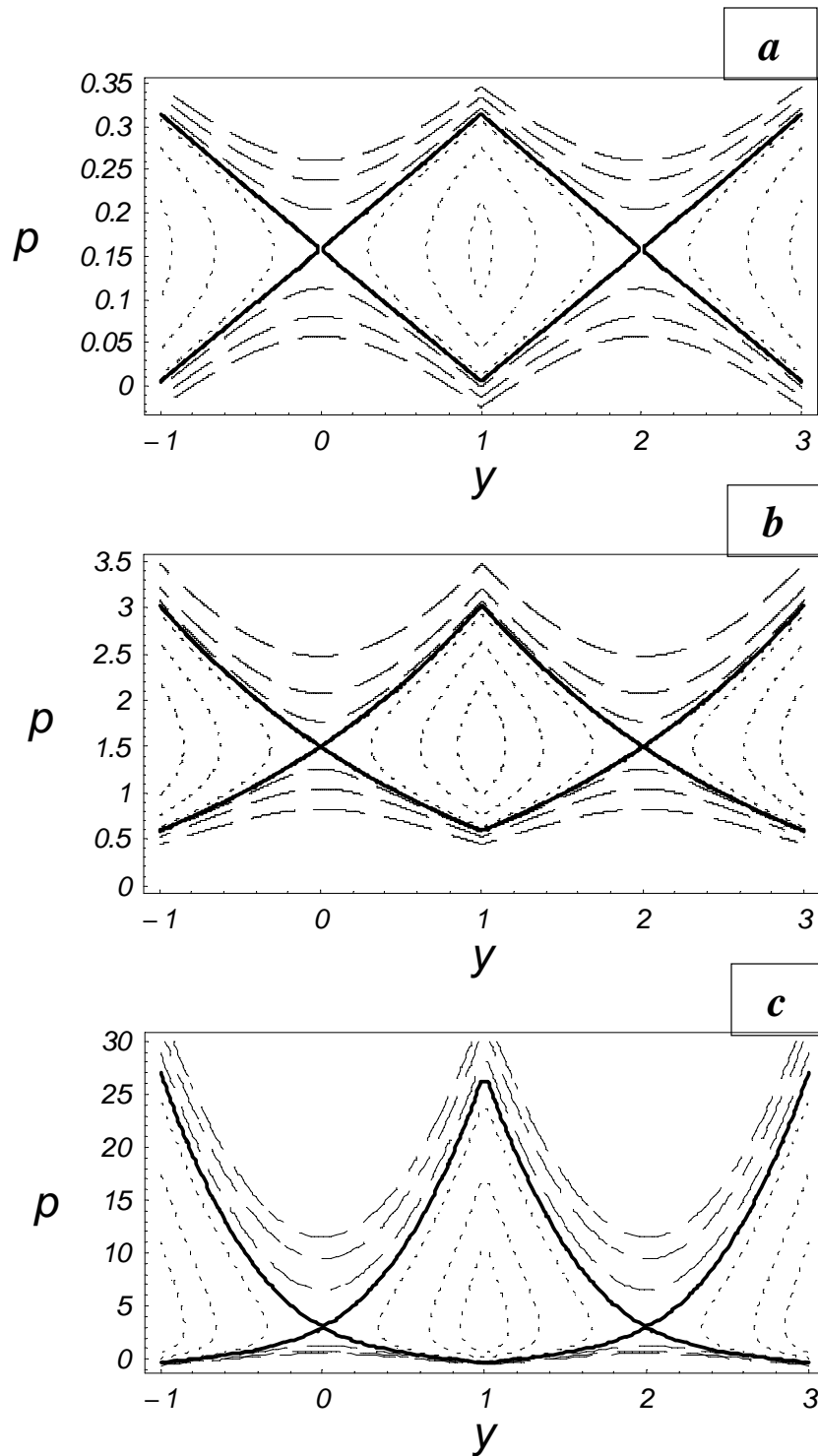


Figure 2.3: Trajectories of protons in the (y, p) phase space. The plasma density is assumed to be $N = 10N_{cr}$. The dimensionless laser amplitude for the panel (a) is $a = 20.5$, (b) - $a = 65$, (c) - $a = 200$.

2. Protons acceleration in a plasma wave

Another region of parameters, where the separatrix goes down to the axis $p = 0$ corresponds to $\gamma_p \gg 1$. Here we have a very simple estimation for the threshold laser amplitude:

$$a_{tr} \approx \sqrt{2 \frac{m_i}{m_e} N} . \quad (2.53)$$

This case is shown in Figure (2.3 c). The laser intensity corresponding to this threshold amplitude Eq. (2.53) can be 1 – 2 orders of magnitude lower than the proton relativistic intensity I_p . Yet, pretty large. On the other hand, laser pulses that allow for the relativistic transparency of overdense plasmas can become available in the nearest future. We have seen, Figure (2.3 a), that already at the relativistic transparency threshold the protons can be trapped in the plasma wave.

2.5 Numerical Simulations

In order to investigate the ion acceleration near the front surface and the propagation through the plasma we use one-dimensional particle-in-cell simulations. The laser pulse is emitted at the left side of the simulation domain. It first propagates through a vacuum region and then interacts with a slab of overdense plasma. The plasma slab has constant density n with a sharp boundary. For the simulations we use the one-dimensional version of the code VLPL, described in Appendix B.

The simulation box is 50λ long, where $\lambda = 2\pi c/\omega_0$ is the laser wavelength. We use absorbing boundary conditions: particles which achieve the boundaries are removed from the simulation box, fields are absorbed completely on the boundaries. The laser pulse has a cosine intensity profile: $a = a_0 \cos(\pi t/\tau) \cos(\omega_0 t)$ with $\tau = 10T_\omega$, where $T_\omega = 2\pi/\omega_0$ is the laser period. The laser is circularly polarized.

We perform a parametric study of the ion acceleration by varying the laser pulse amplitude a_0 in the range from $a = 1$ till $a = 100$ and the plasma density n from $5N_{cr}$ till $10N_{cr}$.

In general, we consider plasma consisting of three types of particles: electrons, heavy ions and protons. We model heavy ions presence using either infinitely heavy "nailed" ions or ions with deuteron charge-to-mass ratio. Thus, we have for the ion concentration:

$$N_i = N_p + N_h , \quad (2.54)$$

where N_p is the proton concentration, and N_h is the heavy ion concentration.

Figure (2.4) shows the maximum proton energy obtained in our simulation for laser-plasma interaction with pure hydrogen (the solid curve), with 10% hydrogen – 90% deuterium mixture (the dotted line), and 10% hydrogen – 90% heavy "nailed" ions mixture (the dashed line).

One sees from Figure 2.4 that the maximum proton energy scales quadratically with the laser amplitude, for all types of considered plasmas at moderate intensities

$$E_p^{max} \propto a^2 . \quad (2.55)$$

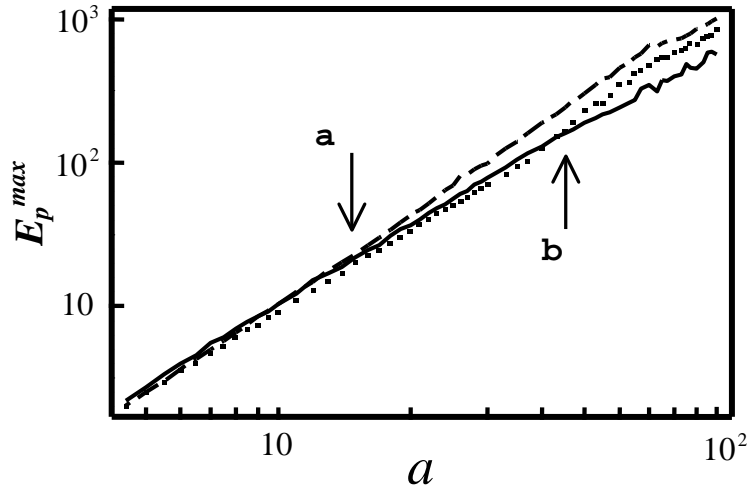


Figure 2.4: The maximum proton energy observed in the simulation as a function of the laser pulse amplitude in double-logarithmic scales. The pulse length $\tau = 10\lambda$. The electron density $N = 10N_{cr}$. The simulation is done for the cases of pure hydrogen (the solid curve); 10% hydrogen – 90% deuterium mixture (the dotted line); 10% hydrogen – 90% heavy “nailed” ions mixture (the dashed line).

As we can see from Figure (2.4), for the pure hydrogen plasma the energy keeps the same dependence in the full scanned range of laser amplitudes. But in the case of mixed plasmas, we observe a change in the scaling after some critical amplitude is reached. This is seen as branching points in Figure (2.4) (pointed by arrows). The first branching point (a) is observed for the mixture of a small amount of protons in a background of “nailed” ions. This first break in the scaling approximately corresponds to amplitude, when plasma becomes relativistic transparent. This results in a generation of the plasma wave, which traps the lightest ions, protons, and accelerates them.

Of course, the plasma wave can be generated in a purely hydrogenic plasma as well. In this case, however, it is destroyed very fast, because all the plasma ions get trapped simultaneously. In addition, the ponderomotive scaling given by Eq. (2.7) obtained for the momentum conservation must be valid for the single-species plasma. The scaling break in the proton-deuteron mixture happens at much larger laser amplitudes (point (b)) than for the proton – immobile ions mixture. The reason is that the charge to mass ratio between the protons and deuterons is not very large and at the low laser amplitudes, the deuterons also start to move and disturb significantly the plasma wave structure.

Figure (2.5) presents more details of the laser pulse interaction with plasma. The two types of the interaction can be clearly distinguished in this picture: the “light pressure regime” (column *I*) and the “wake field regime” (column *II*). The frame (b) in the column *I* shows that the electrostatic plasma field does not change its sign. It corresponds to the double layer produced at the plasma boundary by the ponderomotive pressure of the laser. The frame (b) in the column *II* clearly corresponds to a decaying plasma wave. The wave decay is due to the particle acceleration in the wave. In the

2. Protons acceleration in a plasma wave

second case, the plasma becomes relativistically transparent for the laser pulse.

Using the estimation for the plasma refraction index:

$$n_R = \sqrt{1 - \frac{N_e}{N_{cr}\langle\gamma\rangle}}, \quad (2.56)$$

and taking into account Eq. (2.43) we find that for this particular density, $N = 10N_{cr}$, the plasma becomes transparent for $a_0 \geq 20$. The plasma wave generation and the form of the proton longitudinal phase space (frames (a) in Figure (2.5), make the proton acceleration mechanism evident).

We mention that the trapping condition given by Eq. (2.53) for protons at rest is not fulfilled. Yet, the protons get trapped. This can be explained by the fact that when the head of the laser pulse reaches the plasma boundary, the plasma is changing from the overdense reflection to relativistic transparency. As it is seen from Figure (2.3 a), the protons can be trapped and pre-accelerated in this regime. Later, when the laser intensity continues to grow, these pre-accelerated protons get trapped into the plasma wave and the acceleration continues.

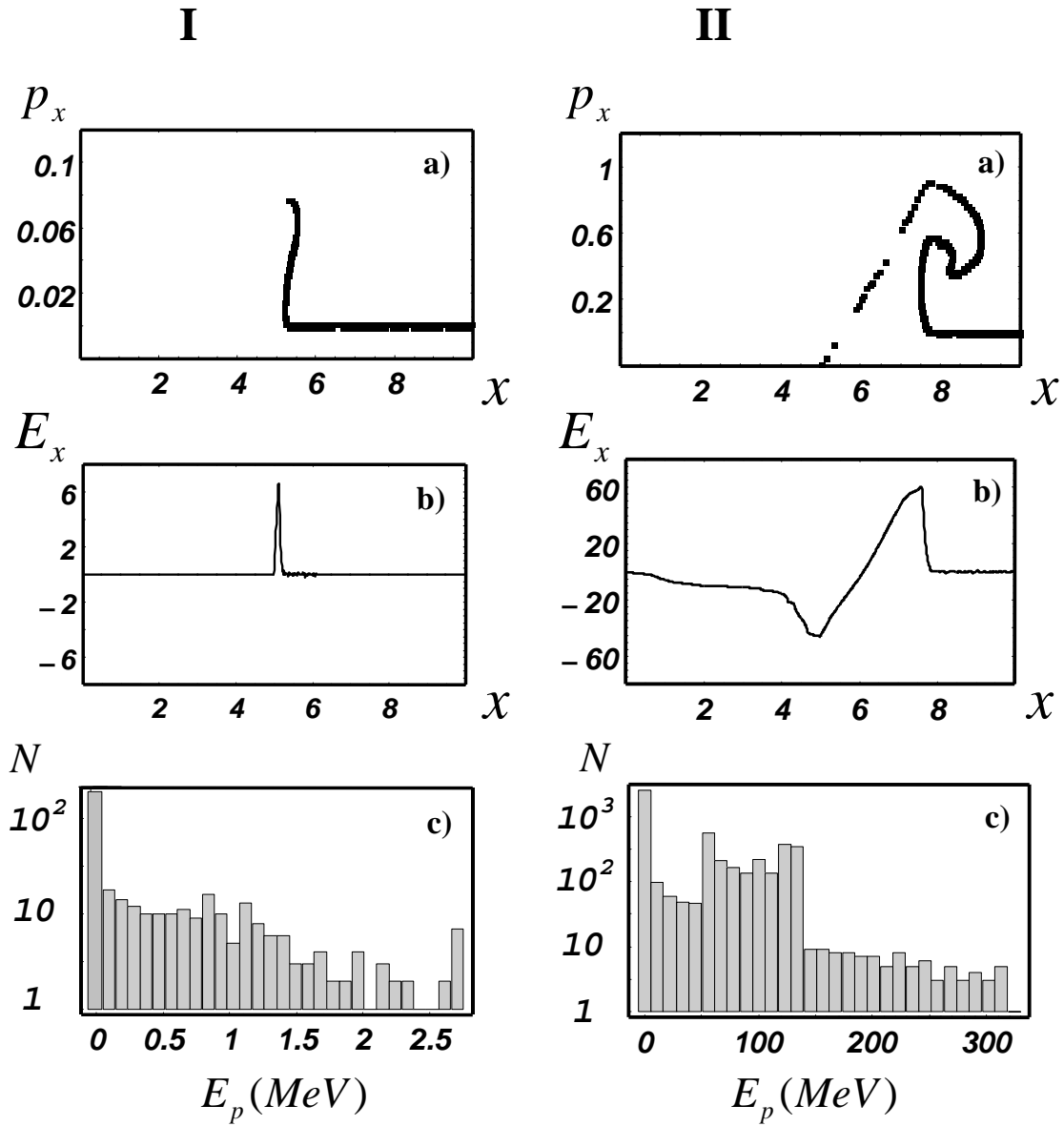


Figure 2.5: Results of the PIC simulation. The laser pulse is 10λ long. The plasma electron density $N = 10N_{cr}$. The plasma consists of a mixture of protons and heavy “nailed” ions, $N_h/N_p = 9$. The column *I* and *II* correspond to the laser pulse amplitudes $a = 5$ and $a = 50$ correspondingly. The snapshots are taken when the pulse maximum reaches the plasma boundary. The frames (a) show the phase space of the protons (x, p_x); the frames (b) give the longitudinal electric field; the frames (c) show the proton energy spectra.

3 Pulse propagation in plasma and relativistic solitons

3.1 Introduction

In this Chapter we investigate the propagation of laser pulses in underdense plasmas. The laser pulse dynamics can be approximated by the non-linear Schrödinger equation, whose properties are well-known [110]. This equation has a family of solutions, but we are particularly interesting in the self-similar solution in the solitonic form. One-dimensional soliton solutions for weakly relativistic laser pulses propagating in underdense plasmas have been proposed by many authors [111, 112, 113, 114]. The plasma dispersion is compensated by the relativistic nonlinearity and the soliton runs through the plasma with nearly light velocity maintaining its shape.

The well-known fact from the soliton theory is, that if one starts with a pulse slightly different from the soliton shape (e.g., with a wider pulse), then the pulse width oscillates around the equilibrium value. This effect can be exploited to compress an initially wide laser pulse to a shorter one.

In spite of the simplicity of the analytical model, the previous direct particle-in-cell (PIC) simulations of this effect failed to demonstrate a significant pulse compression. The PIC simulations reported in [32] show merely a pulse modulation in the longitudinal direction and a transverse filamentation rather than a smooth self-compression.

In this Chapter we present direct one- and three-dimensional PIC simulations of a successful pulse self-compression in underdense plasma. We show that the self-compression effectively works only for a narrow range of plasma densities.

3.2 Raman instability overcoming

The fastest instability which leads to pulse erosion is the simulated Raman scattering (SRS) instability [46]. SRS is the result of scattering electromagnetic pump wave (ω_0, \mathbf{k}_0) by a plasma wave (ω_e, \mathbf{k}_e) . Let us designate scattered wave as (ω_1, \mathbf{k}_1) . Using conservation laws of energy and momentum we can write:

$$\omega_0 = \omega_1 + \omega_e , \tag{3.1}$$

$$\mathbf{k}_0 = \mathbf{k}_1 + \mathbf{k}_e . \tag{3.2}$$

The case when the vectors \mathbf{k}_1 and \mathbf{k}_0 are nearly parallel, corresponds to *stimulated*

3. Pulse propagation in plasma and relativistic solitons

forward Raman scattering (SFRS). For this case we can write

$$\mathbf{k}_1 \approx \mathbf{k}_0 , \quad (3.3)$$

$$k_e \approx k_p = \omega_p/c \ll k_0 . \quad (3.4)$$

This leads to self-modulation of the laser pulse [28, 115]. Modulation length

$$l_{mod} = \frac{2\pi}{k_p} \approx \frac{2\pi c}{\omega_p} = \lambda_p . \quad (3.5)$$

The case when vectors \mathbf{k}_1 and \mathbf{k}_0 are antiparallel, corresponds to *stimulated backward Raman scattering* (SBRs). For that case we can write

$$\mathbf{k}_1 \approx -\mathbf{k}_0 , \quad (3.6)$$

$$\mathbf{k}_e \approx 2\mathbf{k}_0 . \quad (3.7)$$

SBRs leads to erosion of the pulse profile [116]. For ultrashort laser pulses this instability develops first.

Let us find the plasma density, then the stimulated Raman instability can take place. For electron plasma wave (ω_e, \mathbf{k}_e) we have

$$\omega_e > \omega_p , \quad (3.8)$$

as it should satisfy the dispersion relation for electrostatic wave. And for scattered electromagnetic wave (ω_1, \mathbf{k}_1) we have

$$\omega_1 > \omega_p , \quad (3.9)$$

as it should satisfy the dispersion relation for electromagnetic wave. Substituting into Eq. (3.1) we have

$$\omega_0 > 2\omega_{pe} . \quad (3.10)$$

So as one can see, the stimulated Raman instability is taking place only if the electron plasma density satisfies the following condition

$$N_e < \frac{1}{4}N_{cr} , \quad (3.11)$$

where N_{cr} is the critical plasma density, which is given by Eq. (1.88).

In order to overcome pulse profile destruction by stimulated Raman instability, we will use plasma with density

$$\frac{1}{4}N_{cr} < N_e < N_{cr} . \quad (3.12)$$

In this density region, slightly below critical density N_{cr} , the plasma is still transparent, but the Raman instability that otherwise destroys the pulse, is prohibited.

3.3 Analytical theory

We will consider the simplified analytical model, which takes into account only the relativistic nonlinearity and neglects electron density perturbations. Taking plasma density in region, given by Eq. (3.12) we exclude Raman, hosing and other instabilities [46, 117, 118]. We will consider long laser pulses, which initial length T satisfies the condition

$$cT \gg \lambda_p , \quad (3.13)$$

where λ_p is the plasma wavelength.

Let us select coordinate system in such a way, that z -direction coincides with the pulse propagation direction. According to [119] to describe the pulse propagation we will write the wave equation

$$\frac{\partial^2 \mathbf{A}}{\partial z^2} - \frac{1}{c^2} \frac{\partial^2 \mathbf{A}}{\partial t^2} = -\frac{4\pi}{c} \mathbf{j}, \quad (3.14)$$

where \mathbf{A} is the vector potential and \mathbf{j} is the current. Strictly speaking the current is the sum of electrons and ions currents

$$\mathbf{j} = \mathbf{j}_e + \mathbf{j}_i . \quad (3.15)$$

In this Chapter we consider the ions as immobile particles and we will use one-fluid approximation. Then one can write for the current:

$$\mathbf{j} \approx \mathbf{j}_e = -N e \mathbf{v} , \quad (3.16)$$

where $N(z, t)$ is the local electrons density and $\mathbf{v}(z, t)$ is the local electrons speed.

Using invariant defined in Eq. (1.34)

$$\mathcal{P}_\perp = \mathbf{p}_\perp - \frac{e}{c} \mathbf{A}_\perp = const , \quad (3.17)$$

(generalized momentum perpendicular component conservation) we can express \mathbf{p}_\perp as a function of \mathbf{A}_\perp . We will select the initial conditions as:

$$\mathbf{p}_\perp = 0, \quad \mathbf{A}_\perp = 0 \quad \text{at } t = 0 . \quad (3.18)$$

The physical meaning of this condition, is that the electrons are initially at rest and there is no field. Then, substituting Eq. (3.18) in Eq. (3.17) we obtain that at any moment $t > 0$:

$$\mathbf{p}_\perp = \mathbf{A}_\perp . \quad (3.19)$$

Using the Eq. (3.19) we can rewrite (see [112, 120]) Eq. (3.14) as:

$$\frac{\partial^2 \mathbf{A}_\perp}{\partial z^2} - \frac{1}{c^2} \frac{\partial^2 \mathbf{A}_\perp}{\partial t^2} = \frac{1}{\gamma} \frac{\omega_p^2}{c^2} \frac{N}{N_0} \mathbf{A}_\perp , \quad (3.20)$$

3. Pulse propagation in plasma and relativistic solitons

where N_0 is the background plasma density, N is the current electron density, $\omega_p = \sqrt{4\pi e^2 N_0/m_e}$ is the background plasma frequency and γ is the Lorentz factor of the plasma electrons.

Let us consider a circularly polarized laser pulse propagating in the z -direction:

$$\mathbf{A}(z, t) = \frac{1}{2}A(z, t)(\mathbf{e}_x + i\mathbf{e}_y) \exp(-i\omega t + ikz) + \text{c.c.} \quad (3.21)$$

By substituting (3.21) in Eq. (3.20) we obtain equation for the amplitude $A(z, t)$

$$\frac{\partial^2 A}{\partial z^2} - \frac{1}{c^2} \frac{\partial^2 A}{\partial t^2} - \left(k^2 - \frac{\omega^2}{c^2}\right) A + 2i \left(k \frac{\partial A}{\partial z} + \frac{\omega}{c^2} \frac{\partial A}{\partial t}\right) = \frac{1}{\gamma} \frac{\omega_p^2}{c^2} \frac{N}{N_0} A. \quad (3.22)$$

The pulse propagates with the group velocity

$$v_{gr} = c \frac{ck}{\omega}, \quad (3.23)$$

where $k = 2\pi/\lambda$ is the wave number given by the plasma dispersion relation $c^2 k^2 = \omega^2 - \omega_p^2$. Introducing the dimensionless amplitude $a = eA/mc^2$ and taking into account Eq. (3.23) we have

$$\frac{\partial^2 a}{\partial z^2} - \frac{1}{c^2} \frac{\partial^2 a}{\partial t^2} + \frac{\omega^2}{c^2} \left(1 - \frac{v_{gr}^2}{c^2}\right) a + 2i \frac{\omega}{c^2} \left(v_{gr} \frac{\partial a}{\partial z} + \frac{\partial a}{\partial t}\right) = \frac{1}{\gamma} \frac{\omega_p^2}{c^2} \frac{N}{N_0} a. \quad (3.24)$$

In order to study the pulse shape evolution we will turn to the reference system co-moving with pulse. We introduce the new dimensionless variables:

$$z' = \omega z/c, \quad (3.25)$$

$$\psi = \omega(z/v_{gr} - t). \quad (3.26)$$

(We will omit the prime later on).

We will work in the *quasi-static approximation*, i.e., we suppose that the pulse envelope changes significantly only after the laser pulse has propagated through the distance much larger than its own length

$$\frac{1}{v_{gr}} \frac{\partial}{\partial \psi} \gg \frac{1}{c} \frac{\partial}{\partial z'}. \quad (3.27)$$

Using this approximation and taking into account that $\gamma_p^2 = N_{cr}/N$ (see Eq. (1.121)), we have in the new coordinates equation which describes the pulse shape evolution

$$\frac{\partial^2 a}{\partial \psi^2} + 2i\beta^3 \gamma_p^2 \frac{\partial a}{\partial z'} = \beta^2 a \left(\frac{1}{\gamma} - 1\right). \quad (3.28)$$

For a weakly relativistic circularly polarized pulse, $|a| \ll 1$, the electron γ -factor can be expanded as

$$\gamma = \sqrt{1 + |\mathbf{a}|^2} \approx 1 + |\mathbf{a}|^2/2. \quad (3.29)$$

Now Eq. (3.28) takes the form of the well-known nonlinear Schrödinger equation [112, 32, 120]

$$2i\beta^3 \gamma_p^2 \frac{\partial a}{\partial z} = -\frac{\partial^2 a}{\partial \psi^2} - \frac{1}{2} \beta^2 |a|^2 a, \quad (3.30)$$

where $\beta = v_{gr}/c$, $\gamma_p^2 = (1 - \beta^2)^{-1} = N_{cr}/N$.

3.3. Analytical theory

3.3.1 Pulse evolution investigation using the momentum method

We consider evolution of a finite laser pulse,

$$a(\psi = \pm\infty) = 0 , \quad (3.31)$$

$$\frac{da}{d\psi}(\psi = \pm\infty) = 0 . \quad (3.32)$$

First momentum

Multiplying Eq. (3.30) with a^* , we obtain

$$2i\beta^3\gamma_p^2 a^* \frac{\partial a}{\partial z} + a^* \frac{\partial^2 a}{\partial \psi^2} = -\frac{1}{2}\beta^2 |a|^4 . \quad (3.33)$$

Subtracting the complex conjugated expression, and taking into account, that

$$a^* \frac{\partial a}{\partial z} + a \frac{\partial a^*}{\partial z} = \frac{\partial |a|^2}{\partial z} , \quad (3.34)$$

we have

$$2i\beta^3\gamma_p^2 \frac{\partial |a|^2}{\partial z} + \left(a^* \frac{\partial^2 a}{\partial \psi^2} - a \frac{\partial^2 a^*}{\partial \psi^2} \right) = 0 . \quad (3.35)$$

Integrating Eq. (3.35) along ψ , and taking into account, that

$$\int_{-\infty}^{+\infty} \left(a^* \frac{\partial^2 a}{\partial \psi^2} - a \frac{\partial^2 a^*}{\partial \psi^2} \right) d\psi = \left(a^* \frac{\partial a}{\partial \psi} - a \frac{\partial a^*}{\partial \psi} \right) \Big|_{-\infty}^{+\infty} = 0 \quad (3.36)$$

one obtains conservation of the first momentum:

$$J_1 = \int_{-\infty}^{+\infty} |a|^2 d\psi , \quad \frac{dJ_1}{dz} = 0 . \quad (3.37)$$

This equation can be easily interpreted as the pulse energy conservation.

Second momentum

Multiplying Eq. (3.30) with $\partial a^*/\partial z$, we obtain

$$2i\beta^3\gamma_p^2 \frac{\partial a}{\partial z} \frac{\partial a^*}{\partial z} + \frac{\partial^2 a}{\partial \psi^2} \frac{\partial a^*}{\partial z} = -\frac{1}{2}\beta^2 |a|^2 a \frac{\partial a^*}{\partial z} . \quad (3.38)$$

Adding the complex conjugated expression one obtains

$$\frac{\partial^2 a}{\partial \psi^2} \frac{\partial a^*}{\partial z} + \frac{\partial^2 a^*}{\partial \psi^2} \frac{\partial a}{\partial z} = -\frac{1}{2}\beta^2 |a|^2 \left(a \frac{\partial a^*}{\partial z} + a^* \frac{\partial a}{\partial z} \right) . \quad (3.39)$$

3. Pulse propagation in plasma and relativistic solitons

Let us integrate Eq. (3.39) along ψ . For left-hand term we have

$$lht = \int_{-\infty}^{+\infty} \left(\frac{\partial^2 a}{\partial \psi^2} \frac{\partial a^*}{\partial z} + \frac{\partial^2 a^*}{\partial \psi^2} \frac{\partial a}{\partial z} \right) d\psi = \quad (3.40)$$

$$= \left(\frac{\partial a}{\partial \psi} \frac{\partial a^*}{\partial z} + \frac{\partial a^*}{\partial \psi} \frac{\partial a}{\partial z} \right) \Big|_{-\infty}^{+\infty} - \int_{-\infty}^{+\infty} \left(\frac{\partial a}{\partial \psi} \frac{\partial^2 a^*}{\partial z \partial \psi} + \frac{\partial a^*}{\partial \psi} \frac{\partial^2 a}{\partial z \partial \psi} \right) d\psi . \quad (3.41)$$

As we can see from Eq. (3.32)

$$\left(\frac{\partial a}{\partial \psi} \frac{\partial a^*}{\partial z} + \frac{\partial a^*}{\partial \psi} \frac{\partial a}{\partial z} \right) \Big|_{-\infty}^{+\infty} = 0 , \quad (3.42)$$

and thus we have

$$lht = -\frac{\partial}{\partial z} \int_{-\infty}^{+\infty} \frac{\partial a}{\partial \psi} \frac{\partial a^*}{\partial \psi} d\psi = -\frac{\partial}{\partial z} \int_{-\infty}^{+\infty} \frac{\partial a}{\partial \psi} \frac{\partial a^*}{\partial \psi} d\psi = -\frac{\partial}{\partial z} \int_{-\infty}^{+\infty} \left| \frac{\partial a}{\partial \psi} \right|^2 d\psi . \quad (3.43)$$

For the right-hand term (rht) in Eq (3.39) we have

$$rht = -\frac{1}{2} \beta^2 \int_{-\infty}^{+\infty} |a|^2 \frac{\partial |a|^2}{\partial z} d\psi = -\frac{1}{4} \beta^2 \frac{\partial}{\partial z} \int_{-\infty}^{+\infty} |a|^4 d\psi . \quad (3.44)$$

Combining Eq. (3.43) and (3.44) together, we obtain the second momentum conservation:

$$J_2 = \int_{-\infty}^{+\infty} \left(\left| \frac{\partial a}{\partial \psi} \right|^2 - \frac{\beta^2}{4} |a|^4 \right) d\psi, \quad \frac{dJ_2}{dz} = 0 . \quad (3.45)$$

3.3.2 Pulse oscillations

Let us consider an incident laser pulse with the Gaussian envelope

$$a_0 \exp \left(-\frac{t^2}{T_0^2} \right) . \quad (3.46)$$

Below we use dimensionless time $t' = \omega t$. We will look for a solution in the form:

$$a(z, \psi) = a_0 \sqrt{\frac{T_0}{T}} \exp \left(-\frac{\psi^2}{T^2} - \frac{i\beta^3 \gamma_p^2 \psi^2}{2T} \frac{dT}{dz} \right) . \quad (3.47)$$

Here $T = T(z)$ is the width of the pulse envelope (measured in ω^{-1}); $T(0) = T_0$ is the initial width of the pulse. Choosing initial conditions at $z = 0$

$$T(0) = T_0 , \quad (3.48)$$

$$\frac{dT}{dz}(0) = 0 . \quad (3.49)$$

3.3. Analytical theory

we can rewrite

$$J_2 = J_2(z = 0) \quad (3.50)$$

an equation, which describes pulse length evolution. Let us calculate $J_2(z)$ for Gaussian pulse given by Eq. (3.47):

$$|a|^4 = a_0^4 \left(\frac{T_0}{T} \right)^2 (-2\psi) \exp \left(-\frac{4\psi^2}{T^2} \right), \quad (3.51)$$

$$\left| \frac{\partial a}{\partial \psi} \right|^2 = a_0^2 \frac{T_0}{T} \left(\frac{1}{T^4} + \frac{\beta^6 \gamma_p^4}{4T^2} \left(\frac{dT}{dz} \right)^2 (4\psi^2) \exp \left(-\frac{2\psi^2}{T^2} \right) \right). \quad (3.52)$$

Integrating over ψ we obtain second momentum as function of z

$$J_2(z) = \sqrt{\frac{\pi}{2}} a_0^2 \frac{T_0}{T^2} \left(1 + \frac{\beta^6 \gamma_p^4}{4} T^2 \left(\frac{dT}{dz} \right)^2 \right) - \frac{\sqrt{\pi}}{8} a_0^4 \beta^2 \frac{T_0^2}{T}, \quad (3.53)$$

and particular value at $z = 0$

$$J_2(0) = \sqrt{\frac{\pi}{2}} a_0^2 \frac{1}{T_0} - \frac{\sqrt{\pi}}{8} a_0^4 \beta^2 T_0, \quad (3.54)$$

Expressing dT/dz we have:

$$\left(\frac{dT}{dz} \right)^2 = \frac{4}{\beta^6 \gamma_p^4} \left(\frac{1}{T} - \frac{1}{T_0} \right) \left(\frac{\beta^2 a_0^2 T_0^2}{4\sqrt{2}} - \frac{1}{T} - \frac{1}{T_0} \right). \quad (3.55)$$

Taking into account Eq. (1.121), we can rewrite the equation describing the pulse length changes as

$$\left(\frac{dT}{dz} \right)^2 = \frac{4n^2}{\beta^6 N_{cr}^2} \left(\frac{1}{T} - \frac{1}{T_0} \right) \left(\frac{1}{T_m} - \frac{1}{T} \right), \quad (3.56)$$

where

$$T_m = \frac{T_0}{\delta - 1}, \quad \delta = \frac{a_0^2 T_0^2 \beta^2}{4\sqrt{2}}, \quad (3.57)$$

$$\beta = \sqrt{1 - \frac{N}{N_{cr}}}. \quad (3.58)$$

Let us analyze the solutions behavior of Eq. (3.56) qualitatively. In order to do this we can note, that right side of Eq. (3.56) is proportional to function

$$f(T) = \left(1 - \frac{T}{T_0} \right) \left(\frac{T}{T_0/(\delta - 1)} - 1 \right). \quad (3.59)$$

The solution $T(z)$ should satisfy the condition

$$f(T) \geq 0. \quad (3.60)$$

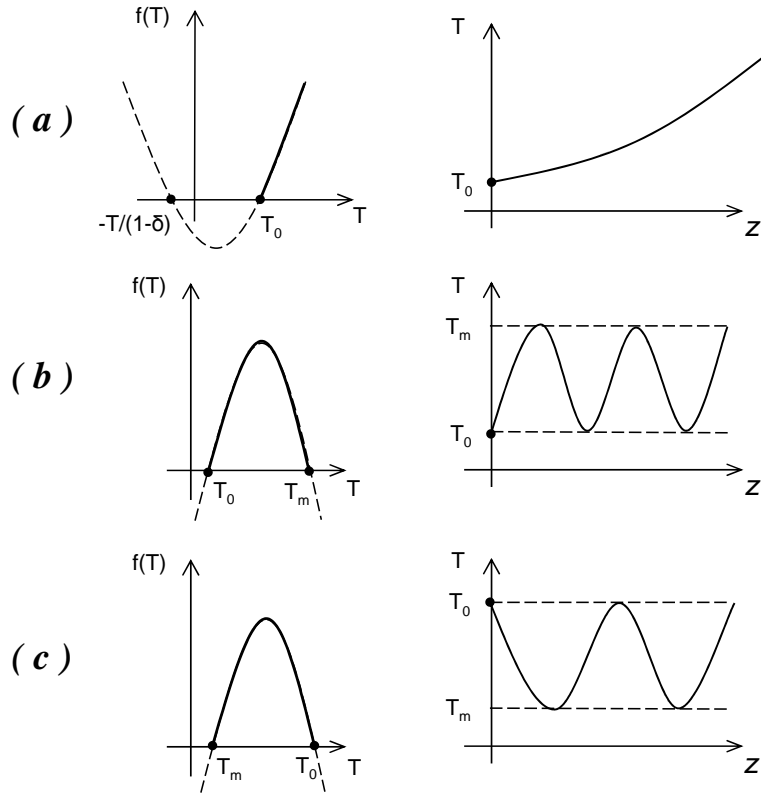


Figure 3.1: Pulse behavior in plasma. In case (a) $0 < \delta < 1$ pulse width T monotonically grows; in case (b) $1 < \delta < 2$ and case (c) $\delta > 2$ pulse width oscillates between T_0 and T_m .

If we rewrite Eq. (3.59) as

$$f(T) = (1 - \delta) \left(\frac{T}{T_0} + \frac{1}{1 - \delta} \right) \left(\frac{T}{T_0} - 1 \right). \quad (3.61)$$

We can see that there are three modes of solution behavior, with initial condition $T(z = 0) = T_0 > 0$, (see Figure (3.1) for illustration). In case $0 < \delta < 1$ we can see that on an interval $z \in [0, \infty)$ function $T(z)$ monotonically grows $T(z) \in [T_0, +\infty)$ (Figure (3.1 a)). When $1 < \delta < 2$ we have $T_0 < T_m = T_0/(\delta - 1)$, and function $T(z)$ oscillates in the range $T(z) \in [T_0, T_m]$ (Figure (3.1 b)). And in case $\delta > 2$ we have $T_0 > T_m = T_0/(\delta - 1)$ and function $T(z)$ oscillates in the range $T(z) \in [T_m, T_0]$ (Figure (3.1 c)).

It is also clear from Eq. (3.56) that the both oscillatory regimes $1 < \delta < 2$ and $\delta > 2$ have the same period of oscillations.

Let us consider physical meaning of such $T(z)$ behavior. If we consider dispersion-nonlinearity competition, we can see that there are three regimes of the pulse behavior after it enters into the plasma:

Case $0 < \delta < 1$: The plasma dispersion dominates, and the pulse length increases monotonically.

Case $1 < \delta < 2$: After the entrance into the plasma, the pulse extends first to the width $T_{max} = T_m$ and then oscillates.

3.3. Analytical theory

Case $\delta > 2$: After the entrance into the plasma, the pulse compresses to $T_{min} = T_m$ and then oscillates.

3.3.3 Pulse compression

For practical reasons we are mostly interested in pulse compression, so let us consider the regime ($\delta > 2$) in detail. Taking a root in Eq. (3.56) we have

$$\frac{dT}{dz} = -\frac{2N}{\beta^3 N_{cr}} \frac{\sqrt{T_0 - T} \sqrt{T - T_m}}{T \sqrt{T_0 T_m}} . \quad (3.62)$$

One should note that we take a negative branch of a square root in order to satisfy condition

$$\frac{dT}{dz} (z = 0+) < 0 . \quad (3.63)$$

Integrating Eq. (3.62) we obtain the exact analytical solution

$$\begin{aligned} \frac{z}{D} = & \frac{1}{4} + \frac{\sqrt{\delta - 1}}{\pi \delta} \sqrt{1 - \frac{T}{T_0}} \sqrt{\frac{T}{T_m} - 1} \\ & - \frac{1}{2\pi} \arctan \left(\frac{1}{2} \sqrt{\frac{T - T_m}{T_0 - T}} - \frac{1}{2} \sqrt{\frac{T_0 - T}{T - T_m}} \right), \end{aligned} \quad (3.64)$$

where

$$D = \frac{\pi T_0^2 N_{cr}}{2} \frac{\beta^3 \delta}{N (\delta - 1)^{3/2}} \quad (3.65)$$

is the period of the pulse envelope oscillation (in ω^{-1}).

3.3.4 Soliton solution

We will look for soliton solution in a form

$$a = a_s \exp(i\kappa z) / \cosh(\psi/T_s) , \quad (3.66)$$

where κ and ψ are the constants. We have

$$\frac{\partial a}{\partial z} = i\kappa \frac{a_s e^{i\kappa z'}}{\cosh(\psi/T_s)} , \quad (3.67)$$

$$\frac{\partial^2 a}{\partial \psi^2} = \frac{a_s \cosh^2(\psi/T_s) - 2}{T_s^2 \cosh^3(\psi/T_s)} e^{i\kappa z'} . \quad (3.68)$$

Substituting in Eq. (3.30), we can see that non-linear Schrödinger equation has the soliton solution

$$a = \frac{a_s e^{i\kappa z}}{\cosh(\psi/T_s)} , \quad (3.69)$$

where a_s , κ and T_s are connected by the relations

$$\kappa = \frac{1}{2\gamma_p^2 \beta^3 T_s^2}, \quad a_s T_s \beta = 2. \quad (3.70)$$

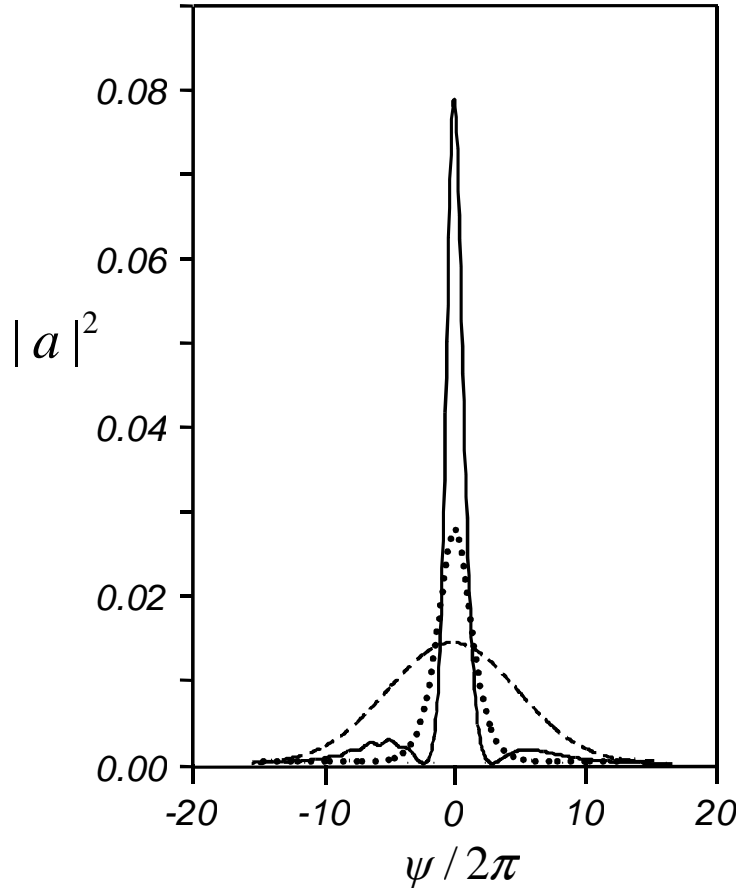


Figure 3.2: 1D PIC simulation of pulse compression. The initial pulse has amplitude $a_0 = 0.1$ and duration $T_0/2\pi = 30$. Plasma density is $N = 0.3N_{cr}$. The laser pulse intensity, $|a|^2$ vs. ψ , is given in the pulse co-moving frame at the different times: dashed line at $t = 0$; dotted line at $t = 290\lambda/c$; solid line at $t = 890\lambda/c$.

3.3.5 1D model numerical verification

In order to check the validity of our simplified model, we have performed 1D PIC simulations using VLPL, see Appendix B for details.

An initially Gaussian pulse, $a = a_0 \exp(-t^2/T_0^2)$ with the duration $T_0/2\pi = 10$ and the amplitude $a_0 = 0.12$ propagates through a slab of uniform plasma of density $n = 0.3n_c$. Figure (3.2) shows how shape of the pulse changes during its propagation in plasma in the pulse co-moving reference system. We observe a compression by more than 5 times, and this process is energetically efficient.

We find that the theoretically predicted soliton-like solution can be observed numerically with parameters $T_s/2\pi = 2.15$ and $a_s = 0.16$ which are close to our theoretical values. ($a_s T_s \beta \sim 1.8$ in comparison with 2 from the simplified model.)

Figure (3.3) demonstrates how the pulse intensity changes in time for pulses with different initial parameters. Two Gaussian pulses with the same initial length $T_0/2\pi = 10$, but different initial amplitudes $a_0 = 0.1$ (line A) and $a = 0.12$ (line C) demonstrate

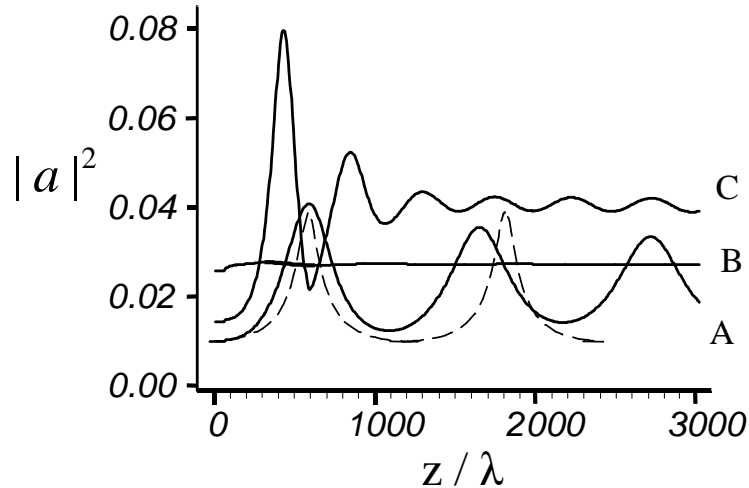


Figure 3.3: Pulse oscillations during its propagation in plasma: maximum pulse intensity $|a|^2$ vs the propagated distance z/λ . Plasma density is $N = 0.3N_{cr}$. Solid lines correspond to the results of 1D PIC simulation: lines A, C are Gaussian pulses with initial amplitudes $a_0 = 0.1$ and $a_0 = 0.12$ correspondingly and duration $T_0/2\pi = 10$. B is the soliton pulse with $a_s = 0.16$ and $T_s/2\pi = 2.15$. The dashed line is the analytical prediction for a Gaussian pulse with the initial parameters $a_0 = 0.1$, $T_0/2\pi = 10$

periodic oscillations of the amplitude. (It should be noted that for this initial amplitude, when the compression rate becomes rather high, the solution given by Eq. (3.64) does not accurately describes the pulse compression and plasma nonlinearity determined by the ponderomotive force must be taken into account.) Otherwise, the soliton pulse with parameters $a_s = 0.16$ and $T_s/2\pi = 2.15$ (line B) propagates stably over at least 3000λ .

3.4 Possibility of 3D-compression

The PIC simulations mentioned above are one-dimensional and thus exclude the pulse transverse dynamics. On the other hand, the pulse compression works only at relatively high plasma densities, close to the critical one, and sub-relativistic intensities. In this parameter region, the laser pulse power easily overcomes the relativistic self-focusing/filamentation threshold [121]. If we consider the filamentary instability of an infinite plane wave, then the maximum growth rate is $\gamma = (\omega_p^2/8\omega_0)a^2$ [53]. This is comparable with the inverse self-compression time of the laser pulse. Thus, the transverse filamentary instability can significantly deteriorate the self-compression process and the full pulse compression can hardly be accomplished in a single stage.

A similar problem of pulse transverse dynamics is successfully solved in the conventional lasers. The amplification is split into many stages, and after each stage a telescope system cleans the amplified pulse from parasitic transverse modes [122]. Of course, a similar technology could be applied also for pulse self-compression in plasma. However, we suggest a different approach.

3. Pulse propagation in plasma and relativistic solitons

Let us consider the pulse self-compression in a periodic plasma-vacuum structure. Each plasma layer must be shorter than the characteristic filamentation time of the laser pulse, so that passing it the laser pulse is slightly compressed longitudinally and not significantly modulated transversely. In the vacuum region, we use the fact that the parasitic transverse modes propagate under the angle k_{\perp}/k and thus are slower than the compressed pulse. When reaching the next plasma layer, the transverse modes lag behind the main pulse.

To check the feasibility of the pulse compression in the periodic plasma-vacuum structure, we do explicit 3D PIC simulations using the code VLPL, see Appendix B. We send a transversely super-Gaussian laser pulse $a = a_0 \exp(-(r_{\perp}/\sigma)^4 - (t/T)^2)$ onto a periodic plasma-vacuum structure. The initial laser amplitude was $a_0 = 0.14$, the duration $T/2\pi = 11$ and the focal spot $\sigma = 100 \lambda$. The initial pulse power is thus 26 TW, for the wavelength $\lambda = 800$ nm. The plasma layers with $N = 0.6 N_{cr}$ were 10λ long with 100λ vacuum regions in between.

The simulation results are shown in Figure (3.4). The frames (a) and (c) give the on-axis intensity distribution, the frames (b) and (d) show the (ZX) cuts of the pulse intensity before and after the compression. In Figure (3.4 c), and Figure (3.4 d) the pulse has passed four plasma layers. The pulse is compressed by more than 5 times. The FWHM of the compressed pulse is about 5 fs, and the peak power exceeds 100 TW. The compression efficiency is thus about 80%. No significant parasitic transverse modulation is seen in the main part of the pulse and the compression is quasi-1D. However, one observes a post-pulse formation, where the transverse modes have been piled up.

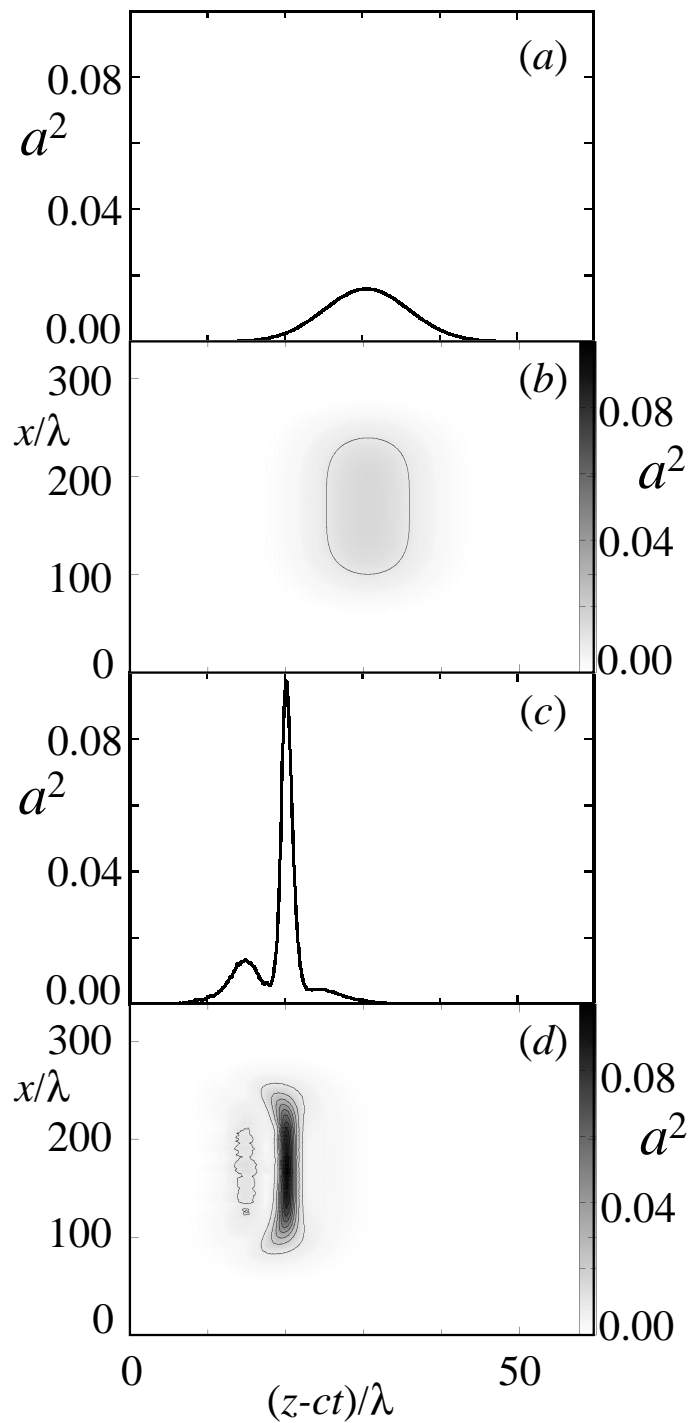


Figure 3.4: 3D PIC simulation results of pulse compression in periodic plasma-vacuum structure. (a) On-axis intensity a^2 of the initial laser pulse; (b) (ZX) -section of the initial pulse intensity; (c) on-axis intensity of the compressed pulse; (d) (ZX) -section of the compressed pulse intensity. The initial pulse amplitude $a_0 = 0.14$, duration $T/2\pi = 11$, and the power 26 TW. The compressed pulse is 5 fs long and has the peak power of more than 100 TW.

3. Pulse propagation in plasma and relativistic solitons

In conclusion, we have discussed here the possibility of self-compression of multi-TW laser pulses in plasma. The self-compression works only in nearly critical plasmas with electron density above $0.25 n_c$, where Raman instabilities are prohibited. Pulses consisting of just 1-2 oscillations can be produced in this way. We have studied the realistic three-dimensional geometry and found that the usage of periodic plasma-vacuum structures stabilizes the parasitic transverse filamentation of the pulse.

We also mention that at ultra-relativistic amplitudes, $a \gg 1$, another compression mechanism can be active. Because the intense center of the laser pulse propagates faster than the lower intensity head, the energy is accumulated at the pulse front and an optical shock is created [11]. Experimentally this is observed as the pulse spectral broadening [123]. Simultaneously, a large-amplitude plasma wave is excited and background electrons are accelerated to relativistic energies [11, 123].

The self-compression in the weakly relativistic regime, as it was discussed in this paper, is free from energy losses, because no plasma wave is generated behind the laser pulse. The losses in this case are mainly connected with the aberrations. When one wants to achieve a large compression ratio, then the compressed pulse is not exactly Gaussian and side wings appear. Still, as we have seen above, efficiencies of the order of 80% are achievable with the laser compression by a factor 5.

4 High harmonics generation from plasma surface

4.1 Introduction

4.1.1 Motivation

Recently, a tremendous progress was achieved in the field of attosecond pulses production [124, 125, 126, 127]. This stimulates researchers to look for mechanisms, which allow us to produce even shorter pulses: subattosecond i.e. zeptosecond (zepto = 10^{-21}) pulses. To produce such pulses, the idea of high order harmonics generation was proposed.

It is well known that a single electron placed in a relativistically strong laser pulse emits high harmonics [128]. The harmonics generation due to atomic electrons nonlinear response in gases when laser field approaches to the ionization limit was investigated experimentally and harmonics up to number $n \sim 300$ were observed in experiments with helium gas jets [129]. Unfortunately these harmonics disappear if we consider not a single electron, but an electron cloud. The reason is that all electrons in the cloud radiate at different phases and the harmonics are canceled by the destructive interference. The harmonics emission is then incoherent [130, 131].

Thus if we are interesting in intensities, which exceed ionization limit, given by Eq. (1.5), another collective-mechanisms of harmonics generation should be considered. Recently was proposed mechanism, which is based on the usage of the petawatt laser beam focused on a subwavelength-size solid particle or thin wire. According to theoretical estimations presented in paper [132] zeptosecond pulse can be produced in this way (“lasetron”).

In this Chapter we propose the mechanism of harmonics generation not from single electrons, but from an electron fluid. The principal point for the mechanism under consideration is the approximation of *step-like plasma density gradient*. The usage of ultra-short laser pulses (femtosecond or shorter) allows to create such step-like gradients, because there is not enough time for noticeable plasma expansion. Adjusting this to solid targets, a thin plasma layer where plasma density drops from solid density to zero, can be created.

Harmonics in radiation reflected from solid surfaces were considered in [133, 134, 135]. In these papers harmonics up to $n \sim (10-100)$ were observed. Therefore, the theoretical investigation of possibility of harmonics generation from plasma boundary is the point of great interest.

4.1.2 Mechanism of harmonics generation from plasma surface

The problem of laser interaction with overdense plasma and the high-harmonics generation was investigated via simulations in [136, 105, 34, 137, 138] and in recent experiments [139, 140]. The possibility of harmonic generation via reflection from a laser-driven oscillating plasma boundary was emphasized in papers [35, 36].

In the *moving mirror model* harmonics are generated by reflecting from the oscillating mirror - the critical surface - where electrons density $N = N_{cr}$, (N_{cr} is the critical density, given by Eq. (1.88)). This conception is extremely useful for understanding basic physics of high order harmonic generation from oscillating plasma boundary (see below Section 4.2.2).

The detailed numerical simulation of collective electron dynamics, which was performed in [35], has shown a good agreement with model, in which harmonics can be interpreted as an anharmonic distortion of the laser field due to reflection from the oscillating surface. The importance of retardation effects for efficient harmonics generation was pointed in [36].

In [141] it was realized that plasma as an oscillating mirror gives an opportunity to produce short pulses. The possibility of a single attosecond pulse isolation, when a laser pulse, focused down to the λ^3 volume, is reflected from a plasma surface, was investigated in [142] (λ^3 regime).

4.1.3 Universal spectrum

Gordienko et al. [37] first pointed at the applicability of Leontovich boundary condition for laser pulse interaction with plasma surface. Using it we show the existence of universal harmonics spectrum (it will be considered below in details).

In this work we concentrate on the basic physics of laser interaction with plasma surface. Using simple physical model, which nevertheless expresses the essential properties of the plasma surface motion, and its influence on the pulse, we discover the harmonics spectrum universality and investigate the properties of this spectrum. We also check the validity of analytical theory using PIC simulation.

4.1.4 Different focusing regimes. The Coherent Harmonic Focusing

The basic idea of harmonic focusing is to take an initial laser pulse with the wavelength λ , send it through a nonlinear medium, generate n high harmonics with the wavelengths $\lambda_n = \lambda/n$ and then focus them down to a spot size $\sim \lambda_n$.

But one should distinguish the coherent and the incoherent harmonics focusing. If the harmonics are incoherent, then the harmonics *intensities* are to be summarized. Since the dimension of the focal spot scales as $1/n$, the field at the incoherent focus is boosted only if the harmonic spectrum decays slower than $1/n^2$.

In the case of a *Coherent Harmonic Focusing* (CHF), which we introduced in [143], the high harmonics are generated coherently. They are focusing in such a way, that

4.2. Reflection

the *fields* of all harmonics interfere constructively within the focal volume. In order to boost the intensity by means of the CHF mechanism, the harmonic spectrum must decay slower than $1/n^4$ (see below for details).

It also will be shown below, that such spectra do exist. The high harmonics spectrum produced in the laser interaction with a sharp plasma boundary is a universal one and it decays as $1/\omega^{5/2}$. In [37] was also shown, that under certain conditions even ω^{-3} spectrum can be observed. It is also important that the laser-plasma surface harmonics are coherent and appear in the form of (sub-)attosecond pulses [142, 37].

Experimentally, the plasma surface harmonics are produced by irradiating the surface of a solid material by a relativistically intense laser pulse [139]. Being exposed to the laser, the surface becomes a plasma with the solid state density. Shaping the target surface appropriately, one can focus the harmonics.

4.2 Reflection

4.2.1 Laser plasma interaction scalings

In this Section we will present an analytical scaling for laser plasma interaction.

Let us consider the electron distribution function $f(t, \mathbf{r}, \mathbf{p})$. To describe laser plasma interactions we have to solve the Vlasov equation

$$\frac{\partial f}{\partial t} + \mathbf{v} \frac{\partial f}{\partial \mathbf{r}} - e \left(\mathbf{E} + \frac{\mathbf{v}}{c} \times \mathbf{B} \right) \frac{\partial f}{\partial \mathbf{v}} = 0 \quad (4.1)$$

together with the Maxwell equations on the electric \mathbf{E} and magnetic \mathbf{B} fields. A dimensional analysis [144] gives

$$f = \frac{N_e}{(m_e c)^3} F \left(\omega_0 t, \frac{\mathbf{p}}{m_e c}, \frac{\omega_0 \mathbf{r}}{c}, \frac{N_c}{N_e}, a_0, \omega_0 \tau \right), \quad (4.2)$$

where F is an unknown universal function. Eq. (4.2) contains three dimensionless parameters. However, in the ultra-relativistic limit their number can be reduced. In the ultra-relativistic limit we can set

$$\mathbf{v} = c\mathbf{n}, \quad \mathbf{n} = \frac{\mathbf{p}}{|\mathbf{p}|} \quad (4.3)$$

and re-write the Vlasov equation as

$$[\partial_t + c\mathbf{n}\partial_{\mathbf{r}} - e(\mathbf{E} + \mathbf{n} \times \mathbf{B})\partial_{\mathbf{v}}] f = 0. \quad (4.4)$$

Introducing dimensionless variables

$$\hat{t} = \omega_0 t, \quad (4.5)$$

$$\hat{\mathbf{p}} = \frac{\mathbf{p}}{mca_0}, \quad (4.6)$$

$$\hat{\mathbf{r}} = \frac{\omega_0 \mathbf{r}}{c}, \quad (4.7)$$

$$\hat{\mathbf{E}} = \frac{c\mathbf{E}}{\omega_0 A_0}, \quad (4.8)$$

4. High harmonics generation from plasma surface

we can re-write Eq. (4.4) together with the Maxwell equations in the dimensionless form

$$\begin{aligned} \left[\partial_{\hat{t}} + \mathbf{n} \partial_{\hat{\mathbf{r}}} - e \left(\hat{\mathbf{E}} + \mathbf{n} \times \hat{\mathbf{B}} \right) \partial_{\hat{\mathbf{p}}} \right] \hat{f} &= 0, \\ \nabla_{\hat{\mathbf{r}}} \cdot \hat{\mathbf{E}} &= (1 - \hat{\rho})/\Gamma, \quad \nabla_{\hat{\mathbf{r}}} \cdot \hat{\mathbf{B}} = 0, \\ \nabla_{\hat{\mathbf{r}}} \times \hat{\mathbf{B}} &= \hat{\mathbf{j}}/\Gamma + \partial_{\hat{t}} \hat{\mathbf{E}}, \quad \nabla_{\hat{\mathbf{r}}} \times \hat{\mathbf{E}} = -\partial_{\hat{t}} \hat{\mathbf{B}}, \end{aligned} \quad (4.9)$$

where $\hat{\rho} = \int \hat{f} d\hat{\mathbf{p}}$, $\hat{\mathbf{j}} = \int \mathbf{n} \hat{f} d\hat{\mathbf{p}}$. Eqs. (4.9) contain the only one dimensionless parameter

$$\Gamma = a_0 \frac{N_{cr}}{N_e} \quad (4.10)$$

and the unknown universal function

$$\hat{f}(\hat{t}, \hat{\mathbf{p}}, \hat{\mathbf{r}}) = \frac{m_e^3 c^3 a_0^3}{N_e} f(t, \mathbf{p}, \mathbf{r}). \quad (4.11)$$

Now we can re-write the distribution function from Eq. (4.2) as

$$f = \frac{N_e}{(m_e c a_0)^3} \hat{f} \left(\omega_0 t, \frac{\mathbf{p}}{m_e c a_0}, \frac{\omega_0 \mathbf{r}}{c}, \Gamma, \omega_0 \tau \right). \quad (4.12)$$

4.2.2 Oscillating mirror

In this Section we consider the process of laser interaction with plasma boundary and pulse reflection. The plasma layer is considered as preionized and steeply bounded. We use index *in* to denote values related to *incident* radiation, and index *rf* for *reflected* radiation.

Let us consider an incident monochromatic laser wave, propagating in a direction opposite to the *x*-axis. This wave can be described by the vector potential

$$\mathbf{A}_{in}(t, x) = \text{Re} \{ \mathbf{A}_0 \exp(-i\omega t - i\omega x/c) \}. \quad (4.13)$$

This wave is reflected by a *sharp* plasma surface positioned at $X(t')$ at the time t' .

We are interesting in reflection from the overdense plasma, with background density $N_e \gg N_{cr}$, where $N_{cr} = \omega^2 m_e / 4\pi e^2$ is the critical density (see Eq. (1.88)). Following the analysis presented above, we assume that the condition

$$\Gamma = a_0 \frac{N_{cr}}{N_e} \ll 1 \quad (4.14)$$

is satisfied, where a_0 is the dimensionless amplitude of incident pulse (see Eq. (4.10)).

4.2.3 Ideal mirror boundary condition

First of all, we must decide what boundary conditions should be used. The standard “*ideal mirror*” *boundary condition* implies zero tangential components of the vector potential at the mirror surface. Let us consider a laser pulse with electric field E_{in} and

4.2. Reflection

duration τ_{in} , and consider a situation, when the ideal mirror moves with relativistic gamma-factor $\gamma \gg 1$ towards the laser pulse. A direct consequence of such a choice of boundary condition is that the reflected pulse acquires the electric field

$$E_{rf} \propto \gamma^2 E_{in} . \quad (4.15)$$

As the mirror moves toward the pulse with $v \sim c$ the duration

$$\tau_{rf} \approx \frac{(c-v)}{2c} \tau_{in} \propto \frac{\tau_{in}}{\gamma^2} . \quad (4.16)$$

Consequently, the energy of the reflected pulse $\propto E_{rf}^2 \tau_r$ must be γ^2 times higher than that of the incident one. As we assume, that the plasma surface is driven by the same laser pulse, this scaling is energetically prohibited. So one can see that the plasma cannot serve as an ‘‘ideal mirror’’.

If we consider the process in detail, we can see, that the ‘‘ideal mirror’’ must support a current. The value of that surface current J_s can be estimated using Eq. (1.69) in integral form:

$$J_s \propto \frac{m_e \omega c^2}{e} a_0 \gamma \propto e N_{cr} c^2 \frac{\gamma a_0}{\omega} . \quad (4.17)$$

This current is growing with the gamma-factor. A realistic plasma surface has no mechanism to provide such a current, so the boundary condition must be changed.

4.2.4 Electrons dynamics near the boundary. Leontovich boundary condition

Let us consider the tangential component of vector potential of laser pulse normally incident onto an overdense plasma slab. We choose $-x$ as a pulse propagation direction. To describe its evolution, we will use a wave equation (see [119])

$$\frac{1}{c^2} \frac{\partial^2 \mathbf{A}(t, x)}{\partial t^2} - \frac{\partial^2 \mathbf{A}(t, x)}{\partial x^2} = \frac{4\pi}{c} \mathbf{j}(t, x) , \quad (4.18)$$

where \mathbf{j} is the tangential component of plasma current density. We will look for solution of Eq. (4.18) which will satisfy the boundary condition:

$$\mathbf{A}(t, x = -\infty) = 0 . \quad (4.19)$$

Physically this boundary condition means, that the wave does not penetrate deep into the plasma.

Let us consider the vector potential

$$\mathbf{A}(t, x) = 2\pi \int_{-\infty}^{+\infty} \mathbf{J}(t, x, t', x') dt' dx' , \quad (4.20)$$

4. High harmonics generation from plasma surface

where

$$\mathbf{J}(t, x, t', x') = \mathbf{j}(t', x') (\Theta_- - \Theta_+) , \quad (4.21)$$

$$\Theta_- = \Theta \left(t - t' - \frac{|x - x'|}{c} \right) , \quad (4.22)$$

$$\Theta_+ = \Theta \left(t - t' + \frac{|x - x'|}{c} \right) , \quad (4.23)$$

and $\Theta(t)$ is the Heaviside step-function. This vector potential satisfies both Eq. (4.18) and the boundary condition given by Eq. (4.19) since $\mathbf{J}(t, x = -\infty, t', x') = 0$.

The tangential electric field is

$$\mathbf{E}_t = -\frac{1}{c} \frac{\partial \mathbf{A}(t, x)}{\partial t} . \quad (4.24)$$

So at the electron fluid surface $X(t)$ we have

$$\mathbf{E}_t(t, X(t)) = \frac{2\pi}{c} \sum_{\alpha=-1}^{\alpha=+1} \alpha \int_0^{-\infty} \mathbf{j}(t + \alpha\xi/c, X(t) + \xi) d\xi , \quad (4.25)$$

where $\xi = x' - X(t)$.

To simplify this formula we should consider the electrons movement near the boundary in details. The pressure of incident electromagnetic wave on the electrons is

$$P_{in} = \frac{E_{in}^2}{4\pi} . \quad (4.26)$$

If the laser moves electrons on the distance d from the boundary (of immobile ions), the electric field created by uncompensated ions charge is

$$E_d = \frac{eN_e d}{4\pi} = \frac{e\sigma}{4\pi} , \quad (4.27)$$

where $\sigma = N_e d$ is the number of displaced electrons on a unit area. Therefore, the force acting on a unit surface area by the ions is

$$P_d = E_d \sigma e = \frac{e^2 N_e^2 d^2}{4\pi} . \quad (4.28)$$

From the condition $P_{in} = P_d$ one can easily find the distance of electron indentation

$$d = \frac{E_{in}}{eN_e} . \quad (4.29)$$

Let us investigate how the characteristic time of the skin layer evolution τ and the plasma skin depth δ correspond with each other. The time for which parameters of the skin layer are changing, can be estimated as $\tau \sim \omega^{-1}$ and the thickness on which the

4.3. Pulse reflection

field penetrates into plasma $\delta \sim d$ from Eq. (4.29). Thus, using Eq. (1.26), (1.88) we have:

$$\frac{\delta}{c\tau} \approx \frac{d\omega_p}{c} = \frac{E_{in}\omega_p}{eN_e c} = a_0 \frac{m_e \omega^2 / e^2}{N_e} \propto a_0 \frac{N_{cr}}{N_e} . \quad (4.30)$$

Since we assume that the condition given by Eq. (4.14) is valid, it follows from Eq. (4.30) that

$$\tau c \gg \delta . \quad (4.31)$$

Taking into account Eq. (4.31) we can Taylor-expand:

$$\mathbf{j}(t \pm \xi/c, x' = X(t) + \xi) \approx \mathbf{j}(t, x') \pm \epsilon , \quad (4.32)$$

where

$$\epsilon = (\xi/c) \partial_t \mathbf{j}(t, x') . \quad (4.33)$$

We substitute this expression into Eq. (4.25). The zero order terms cancel each other and we get

$$\mathbf{E}_t(t, X(t)) \propto J_s(\delta/c\tau) , \quad (4.34)$$

where J_s is the plasma surface current. As the electrons can not move with a speed higher than the speed of light c , the above estimation for the surface current is

$$J_s < ceN_e d = cE_{in} , \quad (4.35)$$

and one obtains that

$$E_t(t, X(t)) \ll E_{in} \frac{\delta}{c\tau} . \quad (4.36)$$

Thus, as long as the skin-layer is thin and the plasma surface current is limited, we can use the *Leontovich boundary condition* [145]

$$\mathbf{E}_t(t, X(t)) = 0. \quad (4.37)$$

The same boundary condition was postulated *ad hoc* in [141] to interpret PIC simulation results. Here we give the physical reasons why the boundary condition should be given by Eq. (4.37). Using this boundary condition we will derive very general properties of the reflected radiation.

4.3 Pulse reflection

4.3.1 Retardation relation

The incident laser field at the reflection time t' is

$$\mathbf{E}_{in}(t', X(t')) = -\frac{1}{c} \frac{\mathbf{A}_{in}(t', X(t'))}{\partial t'} . \quad (4.38)$$

According to Eq. (4.37), the reflected wave electric field at the plasma surface is

$$\mathbf{E}_{rf}(t', X(t')) = -\mathbf{E}_{in}(t', X(t')) . \quad (4.39)$$

4. High harmonics generation from plasma surface

As the one-dimensional wave equation simply translates a signal in vacuum, we can write for the reflected wave field at the observer position x and the time t

$$\mathbf{E}_{rf}(t, x) = -\mathbf{E}_{in}(t', X(t')). \quad (4.40)$$

Let us choose $x = 0$ as the observer position. The time which is needed for the reflected radiation to propagate from the reflection from the surface (at the coordinate $X(t')$) to the observer (located at $x = 0$) is $-X(t')/c$. Therefore, we have the *retardation relation*

$$t' - X(t')/c = t. \quad (4.41)$$

Differentiating this equation on t

$$\frac{dt'}{dt} = 1 + \frac{1}{c} \frac{dX}{dt} = 1 + \frac{1}{c} \frac{dX}{dt'} \frac{dt'}{dt} \quad (4.42)$$

and expressing dt'/dt we obtain a relation between the time difference on the surface dt' and the time difference, observed by observer dt

$$\frac{dt'}{dt} = \left(1 - \frac{1}{c} \frac{dX}{dt'}\right)^{-1}. \quad (4.43)$$

The value dX/dt' has a clear physical sense: it is the velocity of oscillating plasma surface at the time t'

$$\beta = \frac{1}{c} \frac{dX}{dt'}. \quad (4.44)$$

We also need the surface gamma-factor $\gamma = 1/\sqrt{1 - \beta^2}$. Using Eq. (4.44) we can rewrite Eq. (4.43) as

$$\frac{dt'}{dt} = \frac{1}{1 - \beta}, \quad (4.45)$$

and for the ultra-relativistic surface motion with $\gamma \gg 1$ one can approximate

$$dt = \frac{1}{2\gamma^2} dt'. \quad (4.46)$$

The Eq. (4.46) demonstrates that we have $1/\gamma^2$ pulse Doppler compression.

4.3.2 Universal spectrum

Substituting retardation relation in Eq. (4.40), one can find that the Fourier spectrum of the electric field $\mathbf{E}_{rf}(t, x = 0)$ coincides with the spectrum of

$$F(t) = \frac{A_0\omega}{c} \cos(2\omega t' - \omega t). \quad (4.47)$$

The fine structure of the spectrum of $F(t)$ depends on a particular surface motion $X(t)$, which is defined by complex laser-plasma interactions at the plasma surface. Attempts

4.3. Pulse reflection

to approximate the function $X(t)$ were done in the previous theoretical works concerning harmonic generation from plasma surfaces [35, 141].

It appears, however, that a universal spectrum scaling can be obtained without an exact knowledge of the function $X(t)$. Being interested in universal results we avoid the calculation of $X(t)$, and this makes our approach very different from the previous ones. We will only suppose for a moment that the boundary motion is periodic

$$X(t + T_{osc}) = X(t) , \quad (4.48)$$

where T_{osc} is the period of plasma surface oscillations.

If the laser pulse is linearly polarized (LP), then the ponderomotive pressure $P_{pond} \sim \nabla a^2/2$, which acts on the plasma surface, contains a term oscillating at twice the laser frequency $P_{osc} \sim a_0^2 \cos 2\omega_0 t$, (the pressure gets its maximum value two times in one laser period $T_\omega = 2\pi/\omega$ of the basic wave). This makes the plasma surface to oscillate at the same frequency $2\omega_0$. So for linearly polarized laser pulse we have

$$T_{osc}^{LP} = \frac{\pi}{\omega} . \quad (4.49)$$

Here we consider monochromatic incident laser pulses, but using the Fourier integral, this restriction can be bypassed, and even non-monochromatic laser pulses can be considered. Only non-monotonous dependence of the surface gamma-factor of time is important for the overall spectrum scalings, (see for details [37]).

Let us consider the Fourier spectrum of $F(t)$:

$$\begin{aligned} \hat{F}_n &= \int_{-T_{osc}/2}^{+T_{osc}/2} F(t) e^{-i\omega n t} dt = \frac{A_0 \omega}{2c} \int_{-T_{osc}/2}^{+T_{osc}/2} \cos(2\omega t' - \omega t) e^{-i\omega n t} dt = \\ &= \frac{A_0 \omega}{2c} \int_{-T_{osc}/2}^{+T_{osc}/2} (\cos(2\omega t') e^{-i\omega t(n-1)} + \cos(2\omega t') e^{-i\omega t(n+1)} \\ &\quad - i \sin(2\omega t') e^{-i\omega t(n-1)} + i \sin(2\omega t') e^{-i\omega t(n+1)}) dt . \end{aligned} \quad (4.50)$$

$$(4.51)$$

As we can see, the Fourier spectrum of $F(t)$ can be represented in the form:

$$\hat{F}_n = \frac{A_0 \omega}{2c} \left[\hat{C}_{n+1} + \hat{C}_{n-1} + i(\hat{S}_{n+1} - \hat{S}_{n-1}) \right] , \quad (4.52)$$

where \hat{C}_n and \hat{S}_n are the n -th harmonics of

$$C(t) = \cos(2\omega t') , \quad (4.53)$$

$$S(t) = \sin(2\omega t') , \quad (4.54)$$

and t' is the retarded time from Eq. (4.41).

4. High harmonics generation from plasma surface

We examine only the spectrum of $C(t)$, because the spectrum of $S(t)$ can be worked out analogously. Using Eq. (4.53) and retardation relation Eq. (4.41), one can express t' through t :

$$t' = t + \frac{1}{c}X \left(\frac{1}{2\omega} \arccos C(t) \right) . \quad (4.55)$$

It is easy to see that the function $C(t)$ has a period π/ω . Thus, its spectrum

$$\hat{C}_n = \int_{-T_{osc}/2}^{+T_{osc}/2} \cos(2\omega t') e^{-in\omega t} dt \quad (4.56)$$

contains only even laser harmonics

$$n = 2m . \quad (4.57)$$

Making simple arithmetic, we easily obtain:

$$\hat{C}_{n=2m} = \frac{1}{2} \int_{-T_{osc}/2}^{+T_{osc}/2} (e^{i\Phi_1(t)} + e^{i\Phi_2(t)}) dt , \quad (4.58)$$

where

$$\Phi_1(t) = 2(1 - m)\omega t + 2\Phi_r(t) , \quad (4.59)$$

$$\Phi_2(t) = -2(1 + m)\omega t - 2\Phi_r(t) , \quad (4.60)$$

$$\Phi_r(t) = \frac{\omega}{c}X(t') = \frac{\omega}{c}X \left(\frac{1}{2\omega} \arccos C(t) \right) . \quad (4.61)$$

The definition of the retarded phase $\Phi_r(t)$ is recurrent, because $C(t)$ itself is defined through X .

To calculate the spectrum Eq. (4.58), we will use the saddle point technique. The saddle points $\{t_n\}_1$ and $\{t_n\}_2$ can be obtained correspondingly from the equations

$$\frac{d\Phi_1(t_n)}{dt} = 0 , \quad (4.62)$$

$$\frac{d\Phi_2(t_n)}{dt} = 0 . \quad (4.63)$$

Taking a derivative, we can rewrite them as

$$2\omega(1 - m) + 2\frac{\omega}{c} \frac{dX}{dt'} \frac{dt'}{dt} = 0 , \quad (4.64)$$

$$-2\omega(1 + m) - 2\frac{\omega}{c} \frac{dX}{dt'} \frac{dt'}{dt} = 0 . \quad (4.65)$$

4.3. Pulse reflection

And using Eq. (4.45) we can rewrite saddle point conditions as

$$\frac{\beta}{1-\beta} = m-1, \quad (4.66)$$

$$\frac{\beta}{1-\beta} = -(m+1). \quad (4.67)$$

Now it is seen that the first saddle-point equation has a non-empty set of solutions and the second saddle-point equation has no real solutions

$$\{t_n\}_1 = t_n, \quad (4.68)$$

$$\{t_n\}_2 = \emptyset. \quad (4.69)$$

Let us introduce the notation

$$t'(t_n) = T_n. \quad (4.70)$$

The Eq. (4.66) can be rewritten as

$$\beta_n = \beta(t_n) = 1 - \frac{2}{n}. \quad (4.71)$$

Using the surface gamma-factor $\gamma_n = 1/\sqrt{1-\beta_n^2}$, we can rewrite Eq. (4.71) for $n \gg 1$ as

$$n \approx 4\gamma_n^2. \quad (4.72)$$

This equation has a clear physical meaning. The reflected radiation frequency is multiplied by the factor $4\gamma^2$, because of the relativistic Doppler effect, where γ is the relativistic factor of the plasma surface. If the plasma surface oscillates non-relativistically, so that $\beta \ll 1$, then Eq. (4.66) has no real solutions for $n > 1$, and the spectrum of $C(t)$ exponentially decays. When $\beta \sim 1$, then there is a real solution for any $n < n_c \approx 4\gamma_{\max}^2$. The stationary points $\{t_n\}$ corresponding to $\beta(t_n) = \beta_n = 1 - 2/n$ are responsible for the generation of n -th harmonic. The maximum harmonic number n_c is defined by the maximum surface velocity β_{\max} , see illustration on Figure (4.1).

We will calculate the spectrum for

$$1 \ll n \ll n_c. \quad (4.73)$$

Using the obtained saddle-points, we can rewrite the integral in Eq. (4.58)

$$\begin{aligned} \hat{C}_n &= \frac{1}{2} \int_{-\pi/\omega}^{\pi/\omega} \exp \left\{ i \left(\Phi_1(t_n) + \frac{1}{2} \Phi_1''(t_n)(t-t_n)^2 \right) \right\} d\tau \\ &\approx \frac{1}{2} \exp \left(i\Phi_1(t_n) \pm \frac{\pi}{4} \right) \int_{-\infty}^{+\infty} \exp \left(\frac{1}{2} \Phi_1''(t_n)(t-t_n)^2 \right), \end{aligned} \quad (4.74)$$

and taking into account

$$|d_t^2 \Phi_1(t_n)| = 2|d_t^2 \Phi_r(t_n)|, \quad (4.75)$$

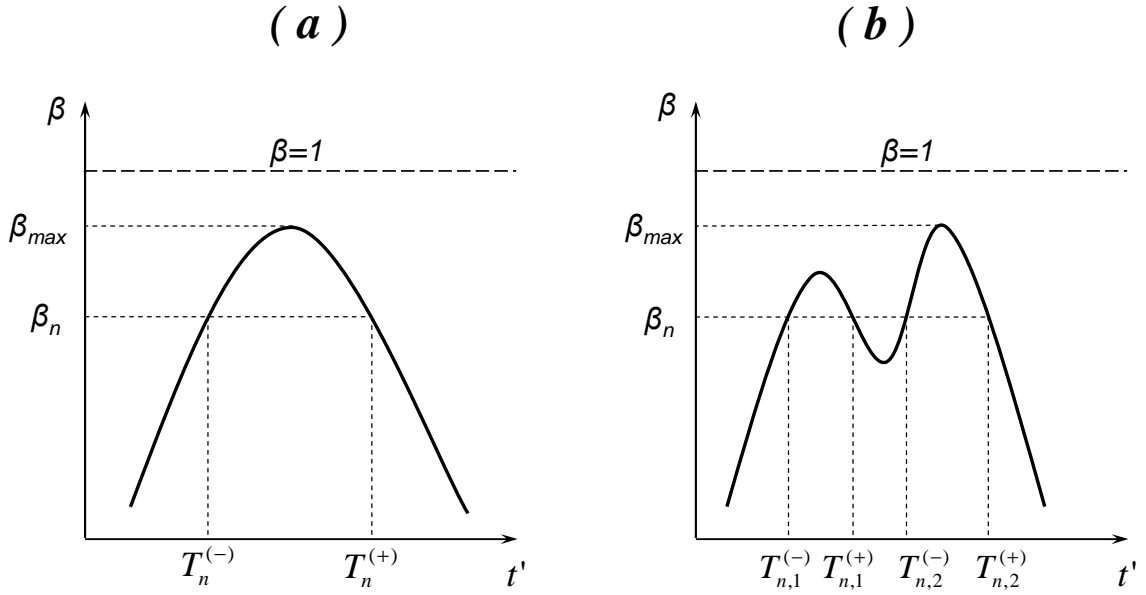


Figure 4.1: Function $\beta(t')$ for possible motions of the plasma surface. Frame (a) demonstrates the simplest case - single “hump” per half-laser period: two saddle points are responsible for the generation of n -th harmonic. Frame (b) corresponds to the complex plasma surface motion, with several local maximums of β . One can see, that the saddle points appear in pairs, two per “hump”.

finally one obtains

$$\hat{C}_n = \frac{1}{2} \sum_{t_n} \sqrt{\frac{\pi}{|d_t^2 \Phi_r(t_n)|}} \exp\left(i\Phi_1(t_n) \pm i\frac{\pi}{4}\right). \quad (4.76)$$

To calculate the spectrum we use the fact that the highest harmonics are generated around the time $t' = T_{\max}$, when the plasma surface moves towards the laser with the highest velocity β_{\max} . In its vicinity, one can approximate

$$\beta \approx \beta_{\max} \left[1 - \frac{1}{2} b^2 (t' - T_{\max})^2 \right]. \quad (4.77)$$

In other words, we approximate the function $\beta(t')$ near T_{\max} by parabola, as shown in Figure (4.1 a). Let us consider the two nearest to T_{\max} solutions of equation $\beta_n = \beta(t')$,

$$T_n^{(\pm)} : \beta(T_n^{(\pm)}) = \beta_n = 1 - \frac{2}{n}, \quad (4.78)$$

$$\Delta T_n = T_n^{(+)} - T_n^{(-)} > 0. \quad (4.79)$$

Taking into account symmetry of the parabola, we have

$$T_n^{(+)} - T_{\max} = T_{\max} - T_n^{(-)} = \frac{\Delta T_n}{2}. \quad (4.80)$$

4.3. Pulse reflection

Substituting in Eq. (4.71) the expansion from Eq. (4.77) and the expression for β from Eq. (4.71), we obtain

$$\left(1 - \frac{2}{n}\right) = \left(1 - \frac{2}{n_c}\right) \left(1 - \frac{1}{8}b^2\Delta T_n^2\right). \quad (4.81)$$

As we are considering the case $1 \ll n \ll n_c$, we obtain

$$\Delta T_n \approx \frac{4}{b} \sqrt{\frac{n_c - n}{nn_c}} \approx \frac{4}{b} n^{-1/2}. \quad (4.82)$$

One should note, that using Eq. (4.77) and Eq. (4.82), the condition $n \ll n_c$ is equivalent to

$$1 - \beta_{\max} \ll b^2\Delta T_n^2. \quad (4.83)$$

This means that we consider harmonics generation far away from the parabola peak. The simplest version of the saddle point method used above is valid if the areas that surround saddle points and define the integral do not overlap. This condition is violated for $n \rightarrow n_{cr}$ when the saddle points are close to each other. Therefore we drop out this case from our consideration.

Now let us calculate $|d_t^2\Phi_r(t_n)|$. From Eq. (4.61) we have:

$$\frac{d\Phi_r}{dt} = \frac{\omega}{c} \frac{dX(t')}{dt'} \frac{dt'}{dt} = \frac{\omega\beta}{1-\beta}, \quad (4.84)$$

$$\frac{d^2\Phi_r}{dt^2} = \frac{d}{dt'} \left(\frac{d\Phi_r}{dt} \right) \frac{dt'}{dt} = \frac{\omega}{1-\beta} \frac{d}{dt'} \left(\frac{\beta}{1-\beta} \right) = \frac{\omega}{(1-\beta)^3} \frac{d\beta}{dt'}, \quad (4.85)$$

and from Eq. (4.77)

$$\left. \frac{d\beta}{dt'} \right|_{T_n^{(\pm)}} = \pm \beta_{\max} \frac{b^2}{2} \Delta T_n, \quad (4.86)$$

$$(1-\beta)|_{T_n^{(\pm)}} = (1-\beta_{\max}) + \frac{1}{8}\beta_{\max}b^2\Delta T_n^2 \approx \frac{1}{8}\beta_{\max}b^2\Delta T_n^2. \quad (4.87)$$

Collecting Eq. (4.85), (4.86) and (4.87) together, we obtain

$$\left| \frac{d^2\Phi}{dt^2}(T_n^{(\pm)}) \right| = \frac{b\omega}{4} n^{5/2}. \quad (4.88)$$

Substitution into Eq. (4.76) gives the spectrum intensity scaling

$$\hat{C}_n^2 \propto n^{-5/2} \quad \text{for } 1 \ll n \ll n_c. \quad (4.89)$$

In that way

$$I_n \propto \begin{cases} n^{-5/2} & \text{for } n < n_c, \\ \text{exponential cut off} & \text{for } n > n_c. \end{cases} \quad (4.90)$$

4.3.3 Spectrum modulations

Let us consider the physical mechanism of high-harmonic generation in detail. All harmonics above a number n ($n < n_c$) are generated at times $T_n^{(-)} < t' < T_n^{(+)}$. Thus, the pulse duration $\Delta t = t(T_n^{(+)}) - t(T_n^{(-)})$, as it is seen by the observer can be calculated as

$$\Delta t = T_n^{(+)} - T_n^{(-)} - \frac{1}{c} (X(T_n^{(+)}) - X(T_n^{(-)})) = \int_{T_n^{(-)}}^{T_n^{(+)}} \left(1 - \frac{1}{c} \frac{dX}{dt'} \right) dt' = \quad (4.91)$$

$$= \int_{T_n^{(-)}}^{T_n^{(+)}} (1 - \beta(t')) dt' \approx \frac{1}{2} \int_{T_n^{(-)}}^{T_n^{(+)}} \beta_{\max} b^2 (t' - T_{\max})^2 dt' . \quad (4.92)$$

Finally, we have for $1 \ll n \ll n_c$

$$\Delta t_n = \frac{\beta_{\max} b^2}{24} \Delta T_n^3 \approx \frac{8}{3b} n^{-3/2} . \quad (4.93)$$

This estimation tells us that the reflected pulse can be made very short by applying a filter selecting harmonics with high numbers larger than n . We will discuss it in details below.

Now let us investigate the phase modulation of spectra. The harmonic with the number n is generated due to the saddle points, which correspond to the proper surface velocity β_n . These saddle points come into (4.76) with different phase multipliers. Figure (4.1 b) represents the case of a complicated plasma surface motion, when the surface velocity β has several maxima, ‘‘humps’’, per half-laser period. As we can see, the saddle points are grouped, i.e. there is a couple of the saddle points on every ‘‘hump’’.

Let us calculate the the phase shift for the saddle points $T_{n,i}^{(\pm)}$ belonging to the the same i -th ‘‘hump’’

$$\Delta \Phi_n = \Phi_1(T_n^{(+)}) - \Phi_1(T_n^{(-)}) . \quad (4.94)$$

Using definition from Eq. (4.59), we have

$$\Delta \Phi_n = 2(1 - m)\omega \Delta t_n + 2\frac{\omega}{c} (X(T_n^{(+)}) - X(T_n^{(-)})) . \quad (4.95)$$

The first term was calculated above (see Eq. (4.93)), and for the second term we have

$$\frac{1}{c} (X(T_n^{(+)}) - X(T_n^{(-)})) = \frac{1}{c} \int_{T_n^{(-)}}^{T_n^{(+)}} \frac{dX}{dt'} dt' = \int_{T_n^{(-)}}^{T_n^{(+)}} \beta dt' \approx \quad (4.96)$$

$$\approx \beta_{\max} \int_{T_n^{(-)}}^{T_n^{(+)}} \left(1 - \frac{1}{2} b^2 (t' - T_{\max})^2 \right) dt' = \beta_{\max} \Delta T_n \left(1 - \frac{b^2}{24} \Delta T_n^2 \right) . \quad (4.97)$$

4.4. Coherent Harmonics Focusing

Substituting in Eq. (4.95), we obtain

$$\frac{\Delta\Phi_n}{2\omega} = \beta_{\max}\Delta T_n \left(1 - m\frac{b^2}{24}\Delta T_n^2\right) = \frac{2}{3}\beta_{\max}\Delta T_n. \quad (4.98)$$

Considering $1 \ll n \ll n_c$, we finally have

$$\Delta\Phi_n = \frac{4}{3}\omega\beta_{\max}\Delta T_n \approx \frac{16}{3}\omega bn^{-1/2}. \quad (4.99)$$

As we can see, the phase shift between the contributions of the saddle points belonging to the the same ‘‘hump’’ is not very large. If we approximate the phase shift with a continuous function $\Phi(n)$

$$\Phi(n) = \Phi_n, \quad \text{for } n \in \mathbb{Z}, \quad (4.100)$$

then we can estimate the frequency modulation period

$$\hat{\Omega} \sim \frac{2\pi\omega}{|d\Phi(n)/dn|} = \frac{3\pi}{4} \frac{1}{b} n^{3/2}. \quad (4.101)$$

The interference between contributions of different ‘‘humps’’ brings modulation into the spectrum only if

$$\hat{\Omega} \ll n_c, \quad (4.102)$$

i.e.

$$\sqrt{n_c} \gg \frac{1}{b}. \quad (4.103)$$

On the other side, the phase shift between the contributions from different ‘‘humps’’ can be much larger. In the case of a non-trivial surface motion, several β ‘‘hump’’ per oscillation period can exist, which in turn can cause the spectrum modulation. Interference between the different saddle points can lead to modulations of the spectrum. This can be in agreement with mechanism proposed in [139] and can explain experimental observations [139, 140].

But it is evident, that the larger number of the saddle points does not change the averaged value for $d_t^2\Phi(t_n)$ and, consequently, does not affect the overall spectrum scaling $\sim n^{-5/2}$.

Strictly speaking, the above analysis is valid for a monochromatic incident wave. However, one should note, that taking into account the finite bandwidth does not change the spectrum significantly. So the scaling $\sim n^{-5/2}$ is valid for short laser pulses as well. Detailed analysis of finite bandwidth influence we present in paper [37].

For a discussion of the spectrum modulations see also [140, 139].

4.4 Coherent Harmonics Focusing

In the preceding Section we have shown that high harmonics can be used for ultra-short pulse generation. To produce such pulses we need to diminish the contribution of ‘‘low’’ energy photons with energy somewhat less than 1 keV. It is difficult to find a

4. High harmonics generation from plasma surface

material what is able to accomplish this task, since all material are rather transparent for these high frequencies. Therefore we choose another way. Instead of decreasing the contribution of “low” energy photons, one can increase the contribution of the highest energy ones. As we can see in this Section, harmonic focusing allows reaching this goal, because the larger the harmonic number, the stronger the intensity boost at the focus. As a result, the harmonic focusing is a way to filtering out the low number harmonics. Now we will derive conditions for which this method works efficiently.

To investigate the CHF mechanism let us consider a laser wave with the vector potential

$$\mathbf{A}(t, x) = \mathbf{A}_0 \exp \left(-\frac{(x/c - t)^2}{\tau^2} + i\omega_0(x/c - t) \right) + \mathbf{c.c.} . \quad (4.104)$$

If we suppose that this wave is reflected from a sharp surface of the plasma electron fluid, the reflected radiation contains high harmonics as it was shown above. The reflected radiation can be expressed as the Fourier integral

$$\mathbf{E}_{rf}(t, \mathbf{r}) = \int_0^{+\infty} \mathbf{E}_\omega \exp(i\omega t + i\omega x/c) d\omega + \mathbf{c.c.} , \quad (4.105)$$

where $\mathbf{r} = (x, y, z)$. As it was shown in Section 4.3.2, in the range $1 \ll \omega/\omega_0 \leq n_c$ the spectrum of the reflected radiation can be wrote in form

$$\begin{cases} |\mathbf{E}_\omega|^2 &= \eta \frac{A_0^2}{c^2} \left(\frac{\omega_0}{\omega} \right)^p , \\ \arg \mathbf{E}_\omega &\approx C\omega\tau + \varphi , \end{cases} \quad (4.106)$$

where η is the conversion efficiency, φ is the initial harmonics phase, and C is a constant. One should note, that the harmonics coherence leads to the fact that C does not depend on ω . For regime which was described in Section 4.3.2, the exponent index $p = 5/2$. In [37] it was shown, that for some interaction regime (rather exotic) even $p = 3$ can be obtained.

Eq. (4.105) is written for a plane wave reflected from a plane surface. To treat reflection from a curved surface, we will re-write (4.105) using Huygens principle (see for details [146]). The reflected radiation is given by the Fourier integral

$$\mathbf{E}_{rf}(t, \mathbf{r}) = \int_0^{+\infty} \mathbf{E}(\omega, \mathbf{r}) \exp(i\omega t) d\omega + \mathbf{c.c.} , \quad (4.107)$$

where harmonics $\mathbf{E}(\omega, \mathbf{r})$ can be expanded on the spherical waves

$$\mathbf{E}(\omega, \mathbf{r}) = \frac{\omega}{2\pi ic} \int \frac{\exp(-i\omega R/c)}{R} \mathbf{E}_\omega(\mathbf{r}') dS . \quad (4.108)$$

The integral in Eq. (4.108) is taken over the wave front S , $\mathbf{E}(\omega, \mathbf{r}')$ is the Fourier component of the electric field at the point \mathbf{r}' of S , $R = |\mathbf{r} - \mathbf{r}'|$.

4.4. Coherent Harmonics Focusing

As an example we consider the simplest case when a spherical wave is reflected from a segment of a co-focal spherical surface with the radius R_0 . The segment occupies the solid angle $\Omega \ll 4\pi$. If $R_0 \gg \lambda$, then the spectrum given by Eq. (4.106) is valid at every reflection point, and the focal field is

$$\mathbf{E}_f = R_0\Omega \int \omega \mathbf{E}_\omega \exp \left\{ i\omega \left(t - \frac{R_0}{c} \right) \right\} \frac{d\omega}{2\pi c i} + \mathbf{c.c.} . \quad (4.109)$$

Substituting the power-law spectrum from Eq. (4.106) into the integral in Eq. (4.109), we find that the field reaches its maximum \mathbf{E}_f^{max} at the focus at time $t = t_f$,

$$t_f \approx \frac{R_0}{c} - C\tau . \quad (4.110)$$

Field \mathbf{E}_f^{max} is given by formula

$$\frac{|\mathbf{E}_f^{max}|^2}{|\mathbf{E}_0|^2} = \eta \left(\frac{4R_0\Omega}{\lambda} \right)^2 \left(\frac{n_c^q - 1}{4 - p} \right)^2 \sin^2 \varphi , \quad (4.111)$$

where $\mathbf{E}_0 = \omega_0 \mathbf{A}_0 / c$ and

$$q = 2 - p/2 . \quad (4.112)$$

If $q < 0$ one has $n_c^q \ll 1$. In this case, $|\mathbf{E}_f|^2$ is defined by low order harmonics. For $q > 0$ one has $n_c^q \gg 1$ and we can rewrite Eq. (4.111) as

$$\frac{|\mathbf{E}_f^{max}|^2}{|\mathbf{E}_0|^2} = \eta \left(\frac{4R_0\Omega}{\lambda} \right)^2 \frac{n_c^{2q}}{(4 - p)^2} \sin^2 \varphi . \quad (4.113)$$

As we can see from Eq. (4.113) in this case $|\mathbf{E}_f^{max}|^2$ is defined by the coherent focusing of high order harmonics and the CHF intensity boosting factor is n_c^{2q} .

So we can see, that the condition of coherent harmonic focusing is

$$p < 4 . \quad (4.114)$$

The oscillating integral in Eq. (4.109) gives the pulse duration at the focus

$$\tau_f = \frac{2\pi}{\omega_0 n_c} . \quad (4.115)$$

Let us compare this result with a general power-law spectrum of the electric field (without coherency)

$$\mathbf{E}_\omega \propto \exp(-i\Psi(\omega)) / \omega^{p/2} . \quad (4.116)$$

For such a spectrum one finds that the intensity at the focus is

$$|\mathbf{E}|^2 \propto \left| \text{Re} \int \frac{\exp[-i\Psi(\omega) + i\omega(t - R_0/c)]}{\omega^{p/2-1}} d\omega \right|^2 . \quad (4.117)$$

4. High harmonics generation from plasma surface

If the harmonics are incoherent, then the function $\Psi(\omega)$ is a fast oscillating. Using the same stationary points method we find, that at each moment t the significant contribution to the integral in Eq. (4.117) gives only the harmonic $\omega(t)$, which frequency satisfies the equation

$$d\Psi(\omega)/d\omega = t - R_0/c . \quad (4.118)$$

Thus we can see, that there is no increase in the intensity at the focus due to the incoherent harmonic focusing for $p > 2$, (compare with Eq. (4.114)).

4.4.1 Intensity scaling of plasma coherent harmonics focusing

It follows from Eq. (4.12) that the relativistic gamma-factor of the reflecting surface scales as

$$\gamma(t) = a_0 \hat{\gamma}(\omega_0 t, \omega_0 \tau, \Gamma) , \quad (4.119)$$

where $\hat{\gamma}$ is a universal function. As a result, one finds

$$\eta = \eta(\Gamma, \omega_0 \tau) , \quad (4.120)$$

$$\varphi = \varphi(\Gamma, \omega_0 \tau) , \quad (4.121)$$

and

$$\gamma_{max} = G(\Gamma, \omega_0 \tau) a_0 , \quad (4.122)$$

$$n_c = 4a_0^2 G^2(\Gamma, \omega_0 \tau) , \quad (4.123)$$

where all the functions η , G and φ are universal.

Using the similarity theory, we can find the focal intensity analytically. We choose the parameters $\omega_0 \tau$ and Γ in such a way, that the spectral slope $p = 5/2$ and the parameter $q = 3/4$. Then, the CHF amplification factor is $n_c^{3/2}$. Let us specify our results for this particular case. From Eq. (4.111) we obtain a scaling for the focal intensity I_{CHF} produced by the CHF and for the pulse duration at the focus τ_{CHF} . If one fixes the dimensionless parameter Γ and changes the laser amplitude a_0 together with the plasma density N_e in such a way that $\Gamma = a_0 N_c / N_e = \text{const}$, then

$$I_{\text{CHF}} = \mu_1 (R_0 \Omega / \lambda)^2 a_0^3 I_0 , \quad (4.124)$$

$$\tau_{\text{CHF}} = 2\pi \mu_2 / (a_0^2 \omega_0) , \quad (4.125)$$

where I_0 and a_0 are the incident pulse intensity and its dimensionless amplitude at the reflecting surface; $\mu_1 = \mu_1(\omega_0 \tau, \Gamma)$ and $\mu_2 = \mu_2(\omega_0 \tau, \Gamma)$ are universal functions with their values of the order of unity.

4.4.2 Schwinger limit

It follows from Eq. (4.125) that the Schwinger limit

$$I_{\text{QED}} = \frac{c E_{\text{QED}}^2}{4\pi} , \quad E_{\text{QED}} = \frac{m_e^2 c^3}{e \hbar} . \quad (4.126)$$

4.5. Simulations

can be reached at the coherent harmonic focus for the incident laser pulse intensity

$$I_{crit} = \left(\frac{\lambda}{R_0 \Omega \sqrt{\mu_1}} \right)^{4/5} \left(\frac{\hbar \omega_0}{m_e c^2} \right)^{6/5} I_{\text{QED}} . \quad (4.127)$$

Assuming the geometrical factor $R_0 \Omega \sqrt{\mu_1} / \lambda \approx 1$, we get $I_{crit} \approx 8.5 \cdot 10^{22} (\mu\text{m}/\lambda)^{6/5} \text{ W/cm}^2$.

As we can see, the CHF effect allows one to reach the Schwinger limit of vacuum polarization using source laser pulses with reasonable intensities. Simultaneously, the CHF works as a spectral filter and shortens the pulse duration down to the zeptosecond range.

4.5 Simulations

To check the validity of our analytical results and to demonstrate the CHF principle, we have done a series of direct 1D and 3D particle-in-cell simulations, using the code (VLPL), see for details Appendix B.

4.5.1 Power-law spectra

To verify the power-law spectra for reflected radiation, we took the laser pulse with the Gaussian temporal profile

$$a_0 \exp(-t^2/\tau_L^2) , \quad (4.128)$$

where τ_L is the pulse duration and a_0 is the pulse amplitude. This pulse was incident onto a plasma layer with a step density profile. Taking into account possible applications, we consider the plasma density $N_e = 30N_{cr}$, which roughly corresponds to the solid hydrogen or liquid helium.

Figure (4.2) shows spectra of the reflected radiation for laser pulses with the duration $\omega\tau_L = 4\pi$ and the amplitudes $a_0 = 5, 10, 20$.

4. High harmonics generation from plasma surface

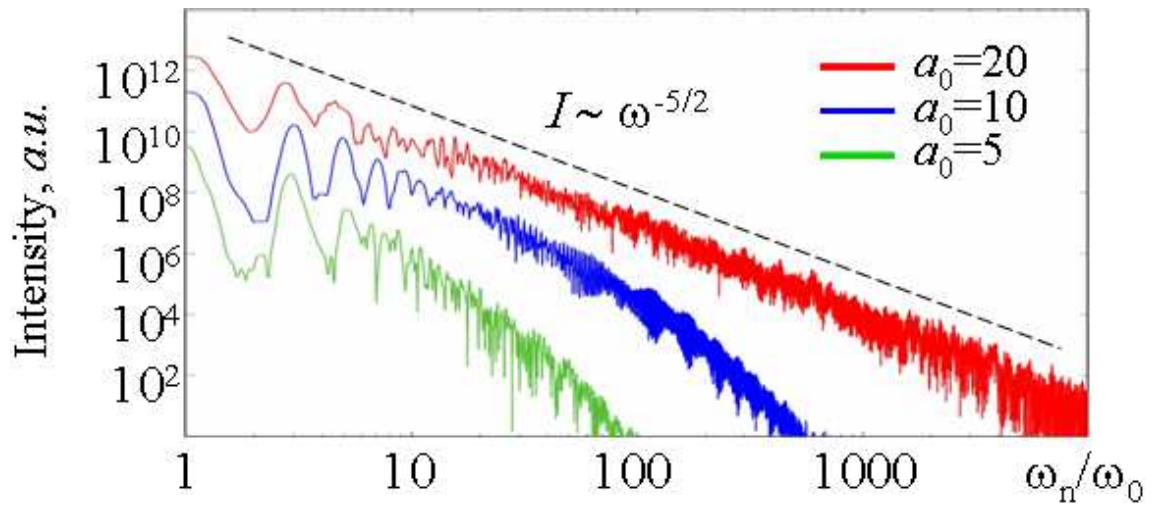


Figure 4.2: Spectra of the reflected radiation for the laser amplitudes $a_0 = 5, 10, 20$. The dashed line marks the universal scaling $I \propto \omega^{-5/2}$.

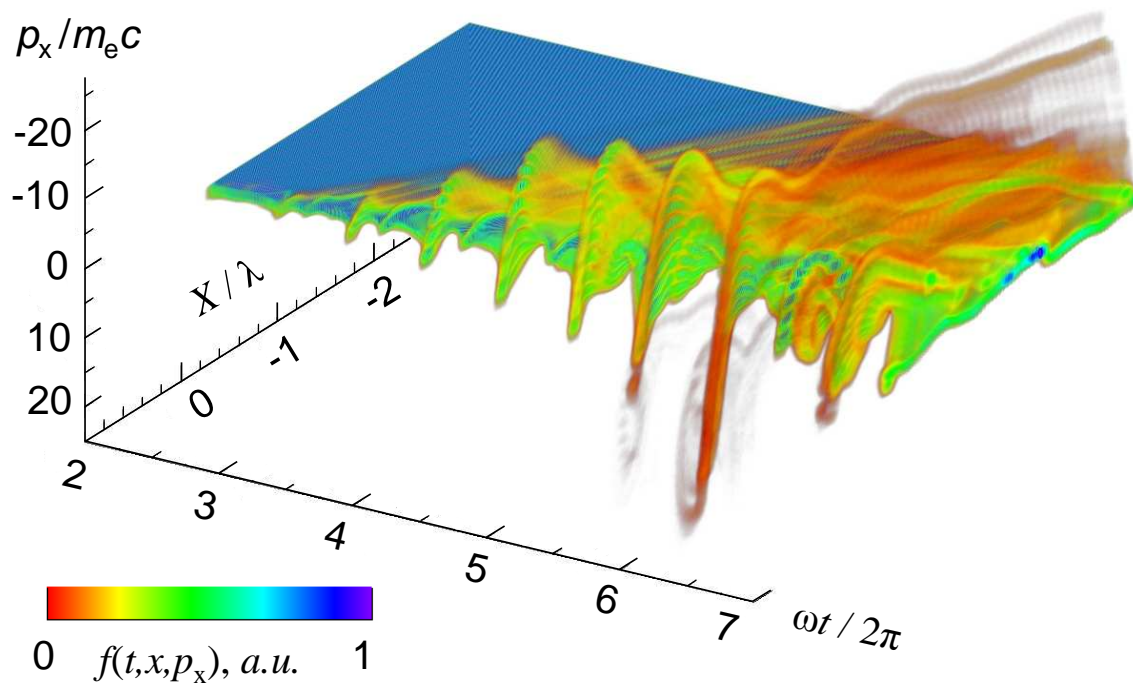


Figure 4.3: Electron distribution function. The helix represents the electron surface motion in the laser field. The reddish downward spikes stand for the surface relativistic motion towards the laser. These spikes are responsible for the zeptosecond pulse generation.

To verify the power-law scaling of the spectral intensity we use log-log scale on Figure (4.2). As one can see, the spectral intensity yields to the power-law scaling $I_\Omega \propto n^{-5/2}$, which confirms our analytical model.

In Figure (4.2) we can approximately localize the critical harmonic number n_c , where the power-law scaling changes into the exponential decay. One can observe, that the critical harmonic number n_c , increases for higher laser amplitudes.

The spectral intensity modulations discussed in previous Section can be also observed.

4.5.2 Reflected radiation structure. Ultra-short pulses

Let us consider in details the particular case $a_0 = 20$ (the red line in Figure (4.2)). As we can see, in this case, the power-law spectrum extends above the harmonic number 2000, and zeptosecond pulses can be generated.

The temporal profile of the reflected radiation is shown in Figure (4.4 a). As we can see, a train of attosecond pulses is observed in reflected radiation, (see also [141]).

To understand the reason of such structure of reflected radiation, let us investigate the evolution of distribution function of plasma electrons. In order to do this, we will introduce the function $f(t, x, p_x)$, which is the distribution function at the moment t . For considering parameters ($a = 20, N = 30N_{cr}$), this function is shown on the Figure (4.3).

At the vicinity of $x = 0$ it represents the surface motion. As we can see, after the pulse reaches the plasma boundary, it causes the surface oscillations. Each spike with $p_x > 0$ corresponds to the surface motion towards the incident laser pulse, that generates the short reflected pulse. From Figure (4.3) we can see, that plasma oscillates with period

$$T_{osc} = \frac{T_\omega}{2}, \quad (4.129)$$

where $T_\omega = 2\pi/\omega$ is the laser period. This is in agreement with Eq. (4.49). One can see from Figure (4.3), that the maximum surface gamma-factor $\gamma_{max} \approx 25$ is achieved at the time $t \approx 6T_\omega$.

Now we apply a spectral filter to select the harmonics above $n = 300$. As a result, a train of much shorter pulses is recovered, see Figure (4.4 b). Let us zoom one of these pulses, see Figure (4.4 c). This pulse width at half maximum is about 300 zs. Its intensity normalized to the laser frequency is $(eE_{zs}/mc\omega)^2 \approx 14$ that corresponds to the intensity $I_{zs} \approx 2 \times 10^{19}$ W/cm².

4.6 Numerical simulations of Coherent Harmonics Focusing

First we want to present 3D simulations, when a linearly polarized spherical laser wave is reflecting from a co-focal spherical plasma mirror. To compare the CHF and a simple geometric focusing of the laser fundamental wave we have done another 3D simulation, where the spherical laser wave was converging down to the theoretically smallest possible spot size $\lambda_0/2$.

4. High harmonics generation from plasma surface

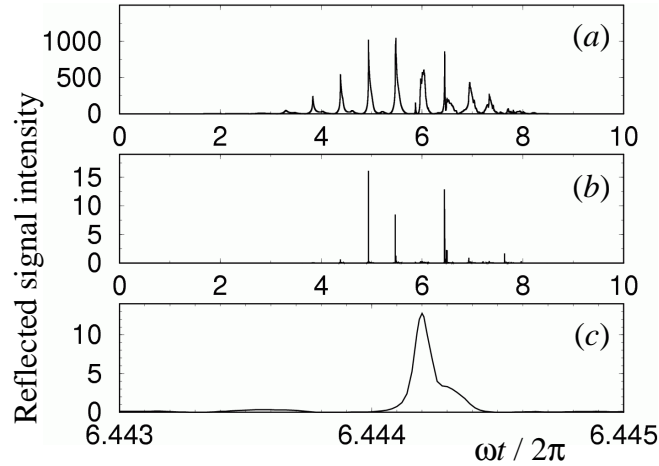


Figure 4.4: Zeptosecond pulse train: a) temporal structure of the reflected radiation; b) zeptosecond pulse train seen after spectral filtering; c) one of the zeptosecond pulses zoomed, its FWHM duration is about 300 zs.

The laser pulse has a Gaussian temporal profile:

$$a(t, R) = a_0 \left(\frac{R_0}{R} \right) \exp(-t^2/T^2) \cos(\omega_0(t - R/c)) , \quad (4.130)$$

with the amplitude $a_0 = 3$ when it arrives at the mirror surface located at $R_0 = 4\lambda$. The pulse duration was $T = 2\pi/\omega_0$. The plasma density is $N = 5N_c$ and it has step density profile.

The 3D simulation results are presented in Figure (4.5). The frame (a) in Figure (4.5) shows the intensity distribution in the focal plane of the converging fundamental laser wave (no harmonics). At the contrary, Figure (4.5 b) shows the focal plane of the CHF produced by the laser wave bounced off a concave plasma surface. The intensity in the center is boosted by more than an order of magnitude in comparison with the simple linear focusing.

Figure (4.5 c) shows the on-axis cut of the CHF reflected intensity in the polarization plane (XY) at the focusing time. Here one sees a periodic structure defined by the half-wavelength of the laser fundamental and the very sharp intensity spike at the CHF focus. The same spike is perfectly seen also in Figure (4.5 b).

4.6. Numerical simulations of Coherent Harmonics Focusing

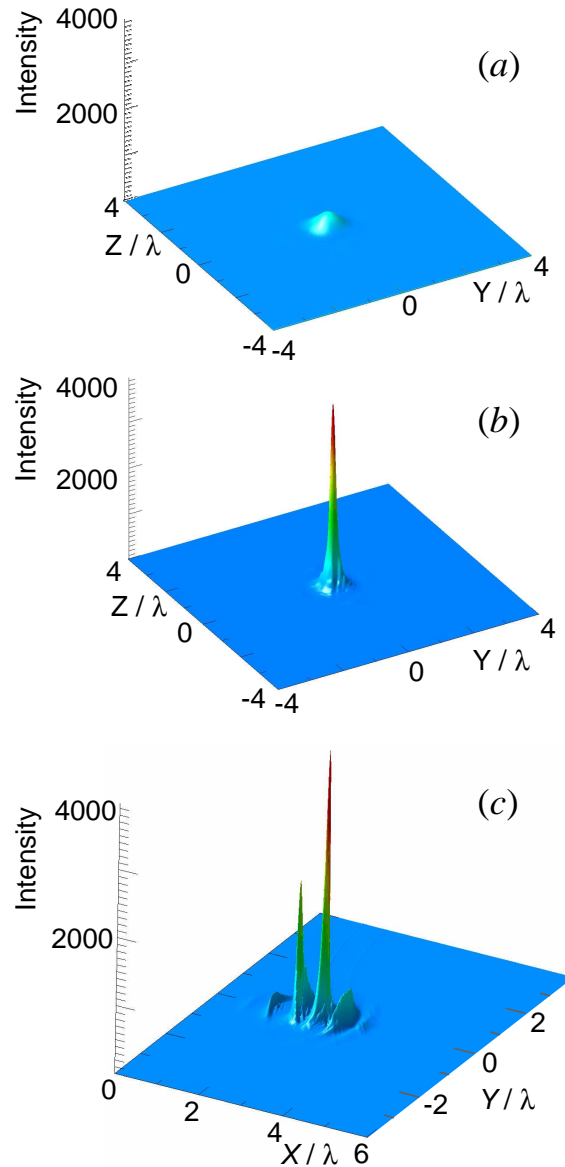


Figure 4.5: 3D PIC simulation results, distribution of the dimensionless intensity $I = (E^2 + B^2)(e^2/2mc\omega_0)^2$. (a) Intensity distribution in the focal plane (YZ) due to simple focusing of the laser fundamental; (b) intensity amplification in the focal plane (YZ) by the CHF effect; (c) on-axis CHF intensity cut in the polarization plane (XY): the periodic structure is defined by the laser fundamental. The characteristic very sharp intensity spike in the focus is due to the CHF boosting.

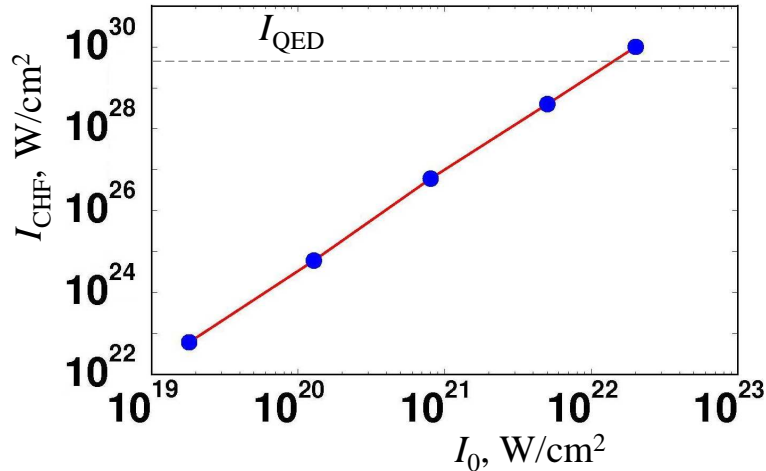


Figure 4.6: Numerically obtained scaling for the CHF focal intensity versus of the incident laser amplitude. The fundamental laser wavelength is assumed $\lambda_0 = 750$ nm, the dimensionless parameter $\Gamma = aN_c/N_e = 0.6$. The dashed line marks the vacuum breakdown intensity I_{QED} . The numerical scaling agrees with the analytical result form Eq. (4.125).

The spike tip has a width of the single grid cell $h_y = h_z = 0.0125\lambda_0$ and thus is at the very *limit of the numerical resolution*. Yet, the present 3D PIC simulation contain already 3×10^8 grid cells and 10^9 numerical particles, which is close to the limit of the available computer capabilities. The further grid refining, e.g., by factor 2 in each dimension of the 3D geometry would require 16 times more computational time and 8 times more computer memory, which is not feasible presently.

To fit the problem into the available computational resources, we have to use 1D PIC simulations. We take the fundamental laser wavelength $\lambda_0 = 750$ nm. We made a series of simulations for different a_0 fixing the dimensionless parameter $\Gamma = aN_c/N_e = 0.6$.

We assume that the 1D harmonics are reflected by a spherically focusing mirror. Then, we applied the operator from Eq. (4.109) to the harmonics \mathbf{E}_ω taken from the 1D PIC results. The mirror radius is $R_0 = 4\lambda_0$ and the solid angle $\Omega = 1$. On this way we are able to obtain numerically the scaling for the CHF focal intensity I_{CHF} over a wide range of the incident laser intensities I_0 .

The numerical results are shown in Figure (4.6). They are in a good agreement with the analytical scaling given by Eq. (4.125). The broken line in Figure (4.6) marks the vacuum breakdown intensity I_{QED} . The scaling in Figure (4.6) shows that the intensity I_{QED} can be achieved in the CHF focus by using an incident laser pulse with $I_0 \approx 10^{22}$ W/cm².

The highest incident laser pulse intensity we have simulated in 1D is $I_0 = 2.4 \times 10^{22}$ W/cm² which corresponds to the relativistic amplitude $a_0 = 100$ (the rightmost upper point in Figure (4.6)). The reflected radiation spectrum for this simulation $|E_\omega|^2$ is presented in Figure (4.7). One can see that the power-law spectrum $|E_\omega|^2 \propto (\omega_0/\omega)^{5/2}$

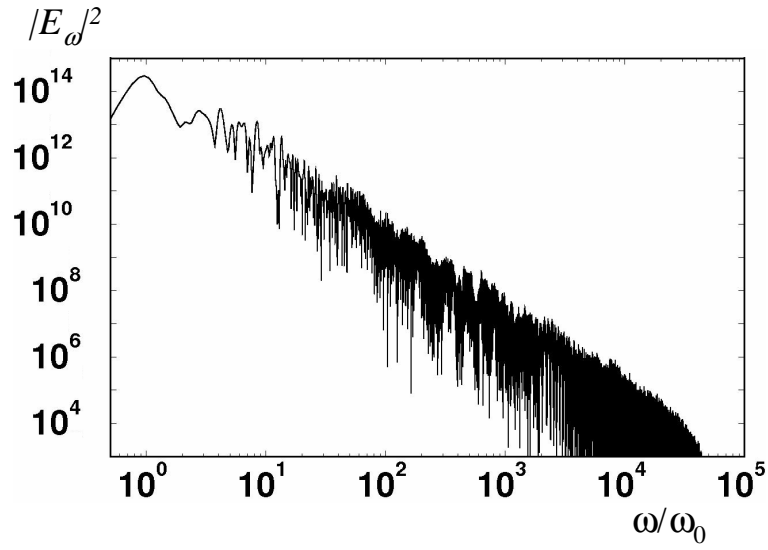


Figure 4.7: Harmonics spectrum $|E_\omega|^2$ of the reflected radiation for the incident laser intensity $2.4 \times 10^{22} \text{ W/cm}^2$ and the relativistic amplitude $a_0 = 100$. The power-law spectrum $|E_\omega|^2 \propto (\omega_0/\omega)^{5/2}$ reaches up to the frequency $\omega \approx 5 \times 10^4 \omega_0$.

reaches up to the frequency $\omega \approx 5 \times 10^4 \omega_0$. We want to note, that we can achieve the extremely high intensity via the CHF boosting because of slow-decaying harmonics spectrum.

5 Summary

5.1 Main results

The principal results presented in the thesis are the following:

1. The new efficient mechanism of proton acceleration in targets, consisted of ions mixture was proposed. To describe this mechanism, the analytical model of “ion wakefield acceleration” was developed. It was shown, that under certain conditions ions relativistic threshold amplitude is scaling as $\propto \sqrt{m_i/m_e}$.
2. The relativistic long living solitons in plasma were observed numerically in direct particle-in-cell simulation. A one-dimensional analytical theory based on the non-linear Schrödinger equation was constructed. The possibility of an effective three-dimensional laser pulse self-compression in plasma was shown numerically.
3. The theory of high harmonic generation from sharp overdense plasma surfaces is developed. The universal power-law spectrum of reflected radiation $\omega^{-5/2}$ was obtained. The possibility of zeptosecond pulses production using present laser technologies was shown.
4. The Coherent Harmonic Focusing model for the high harmonics generated off concave overdense plasma boundaries was proposed. The possibility to achieve the Schwinger limit of vacuum breakdown for a reasonable laser pulse energy was shown.

Appendix

A Particle-in-cell codes

The modern theoretical laser plasma physics is interested in intensities, at which the electrons motion (and in some cases even ions motion) is essentially relativistic (the particles gamma-factor $\gamma \gg 1$). The relativistic motion of electrons in laser plasma interaction is highly non-linear. Because of that the number of analytical methods application is limited and numerical techniques should be used.

From physical point of view all plasma processes can be divided in two classes. The first class corresponds to the case, when collisional effects succeed to relax particles to a local thermodynamic equilibrium (LTE), so that one can postulate that in each infinitesimal plasma volume the particle distribution is Maxwellian. The second class includes the physical processes, where the thermodynamic equilibrium is not achieved and the local particle distribution is essentially non-Maxwellian.

According to this, there are two basic methods of plasma description

- *(Magneto-)hydrodynamic description.* In this description, the plasma is treated as a conducting fluid (or a set of fluids). It is based on equations for moments of the distribution function and the Maxwell equations.
- *Kinetic description.* In this case one has to describe a detailed dynamics of the distribution function in the phase space. One distinguishes “Vlasov” and particle-in-cell (PIC) methods. The first method is to integrate the Vlasov equation numerically on an Eulerian grid in the phase space. The second method introduces a collection of numerical macro-particles and follows their motion on a spatial grid.

The MHD description is good for large scale simulations, such as fusion plasmas, space and solar plasmas, electric propulsion. However, if the problem is essentially kinetic, i.e., the particle distribution functions differ significantly from the Maxwellian one, then a kinetic description should be used. Examples of significantly kinetic problems are: Landau damping, wave-particle resonance, etc.

We want to note, that some problems can have several levels of description. For example, the slow ion component motion can be described as a fluid, while the electrons motion may require a kinetic description. In such cases so-called “hybrid” codes may be needed, (see for example [147]). Even more, in many situations plasma can be considered as collisionless, so its dynamics is defined mainly by kinetic effects.

In relativistic laser plasma interactions kinetic effects dominate, so that we are going to consider the kinetic approach.

The first kinetic numerical method is based on the system of Vlasov-Maxwell (or Vlasov-Poisson) equations. The physical meaning of this approach is very clear: interactions between point-like charged particles are replaced by mean electromagnetic

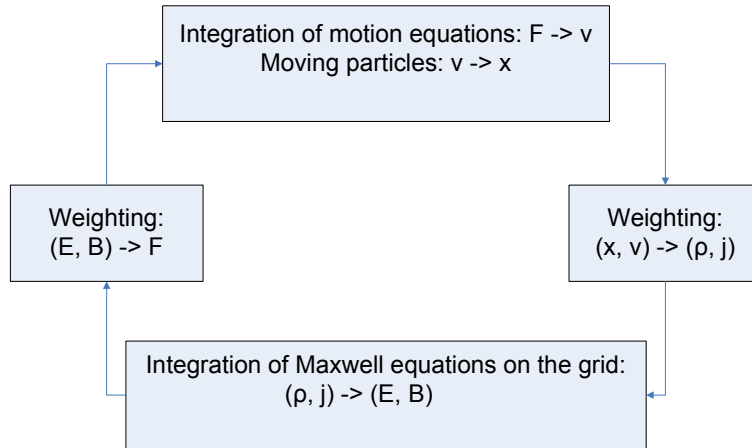


Figure A.1: One time step of particle-in-cell simulation.

fields. These fields satisfy the Maxwell equations, in which charge and current densities are determined by the particle distribution functions. However, for the most interesting cases, the system of Vlasov-Maxwell equations can not be solved analytically. A numerical solution of 3D problems with Vlasov-Maxwell description requires solution of the Vlasov equation, which is a partial differential equation for the distribution function depending on six coordinates and time. This is far beyond the possibilities of nowadays computers.

The alternative approach is the particle-in-cell (PIC) method [148, 149]. It is one of the most successful numerical technique for plasma kinetic simulations [149, 150, 148, 151].

PIC considers a motion of “macro-particles”, with the same charge to mass ratio as the physical plasma particles of a particular species q_α/m_α . As we can see, macro-particles can be treated as a large number of real particles, i.e., clusters (or “clouds”). From the hydrodynamical point of view, these macro-particles can be considered in the framework of “Lagrangian” fluid description.

The macro-particles motion is calculated according to the equations of motion in electromagnetic fields. The electromagnetic fields are calculated self-consistently solving the Maxwell equations on a spatial grid across the plasma. The charge density at each grid position is determined by assigning particles to the grid according to their positions and the weighting scheme. The scheme of a PIC computational cycle is shown on Figure (A.1), see [148] for details.

PIC codes can include binary collisions between charged particles using Monte-Carlo techniques. A particle-in-cell method merged with Monte Carlo collision (MCC) calculations was described in [152].

B Virtual Laser Plasma Laboratory

For kinetic simulations described in this thesis we used the one-dimensional and three-dimensional versions of the code **Virtual Laser Plasma Laboratory** (VLPL), which was initially created by Alexander Pukhov [153], and nowadays is being developed by Alexander Pukhov, Sergey Kiselev and the author of this thesis.

VLPL is a relativistic electromagnetic particle-in-cell (PIC) code, where the multi-component plasma is represented by macro-particles. The electromagnetic fields E and B are calculated on the grid.

Laser pulse(-s) is introduced as a time-dependent boundary condition. Periodic and absorbent boundary conditions for fields and macro-particles can be used.

VLPL is an object-oriented code, written in C++. There are 1D (1D3V) and 3D versions. The 3D version is parallelized using MPI. For simulations presented in this thesis we use the parallel cluster of 76 Xeon-Processors/154 GByte RAM.

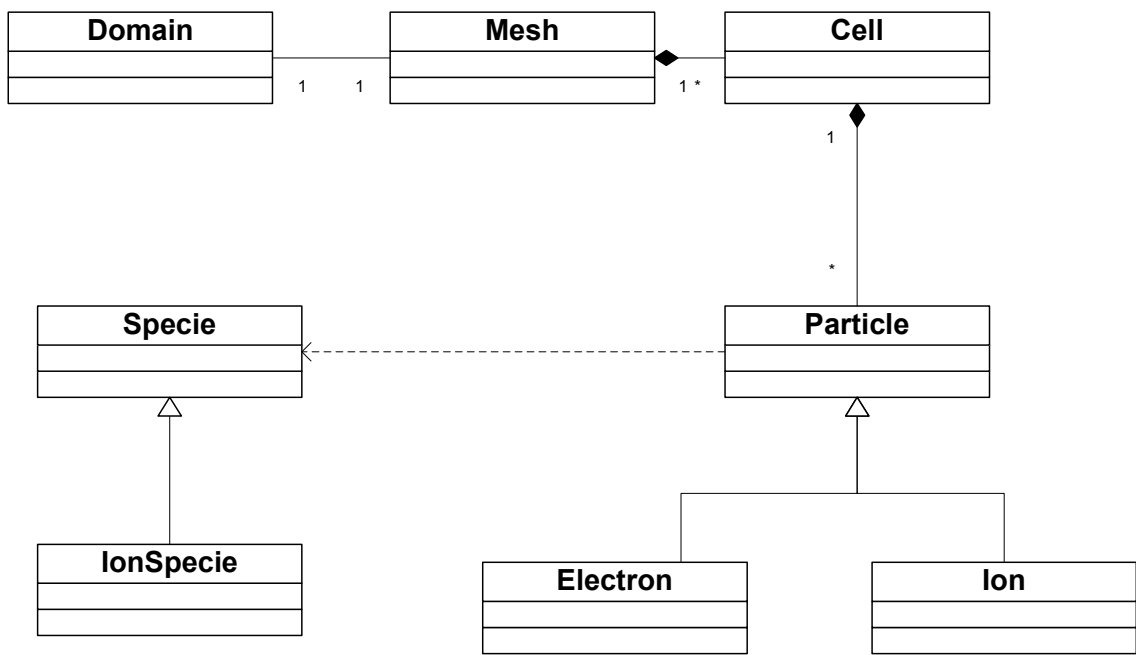


Figure B.1: VLPL class diagram.

Bibliography

- [1] D. Strickland and G. Mourou, "Compression of amplified chirped optical pulses," *Opt. Commun.*, vol. 56, p. 219, 1985.
- [2] G. Mourou and D. Umstadter, "Development and applications of compact high-intensity lasers," *Phys. Fluids B*, vol. 4, p. 2315, 1992.
- [3] M. D. Perry and G. Mourou, "Terawatt to petawatt subpicosecond lasers," *Science*, vol. 64, p. 917, 1994.
- [4] G. A. Mourou, C. P. J. Barty, and M. D. Perry, "Ultrahigh-intensity lasers: Physics of the extreme on a tabletop," *Phys. Today*, vol. 51, p. 22, 1998.
- [5] M. H. Key, M. D. Cable, T. E. Cowan, K. G. Estabrook, B. A. Hammel, S. P. Hatchett, E. A. Henry, D. E. Hinkel, J. D. Kilkenny, J. A. Koch, W. L. Kruer, A. B. Langdon, B. F. Lasinski, R. W. Lee, B. J. MacGowan, A. MacKinnon, J. D. Moody, M. J. Moran, A. A. Offenberger, D. M. Pennington, M. D. Perry, T. J. Phillips, T. C. Sangster, M. S. Singh, M. A. Stoyer, M. Tabak, G. L. Tietbohl, M. Tsukamoto, K. Wharton, and S. C. Wilks, "Hot electron production and heating by hot electrons in fast ignitor research," *Phys. of Plasmas*, vol. 5, p. 1966, 1998.
- [6] P. Sprangle, E. Esarey, and J. Krall, "Laser driven electron acceleration in vacuum, gases, and plasmas," *Phys. Plasmas*, vol. 3, p. 2183, 1996.
- [7] T. Tajima and J. M. Dawson, "Laser electron accelerator," *Phys. Rev. Lett.*, vol. 43, p. 267, 1979.
- [8] A. I. Akhiezer and R. V. Polovin, "Theory of wave motion of an electron plasma," *Sov. Phys. JETP*, vol. 3, p. 696, 1956.
- [9] J. M. Dawson, "Nonlinear electron oscillations in a cold plasma," *Phys. Rev.*, vol. 113, p. 383, 1959.
- [10] E. Esarey, P. Sprangle, J. Krall, and A. Ting, "Overview of plasma-based accelerator concepts," *IEEE Trans. Plasma Sci.*, vol. 24, p. 252, 1996.
- [11] A. Pukhov and J. Meyer-ter-Vehn, "Laser wake field acceleration: the highly nonlinear broken-wave regime," *Appl. Phys. B*, vol. 74, p. 355, 2002.

Bibliography

- [12] C. Joshi, T. Tajima, J. M. Dawson, H. A. Baldis, and N. A. Ebrahim, "Forward raman instability and electron acceleration," *Phys. Rev. Lett.*, vol. 47, p. 1285, 1981.
- [13] J. B. Rosenzweig, D. B. Cline, B. Cole, H. Figueroa, W. Gai, R. Konecny, J. Norem, P. Schoessow, and J. Simpson, "Experimental observation of plasma wake-field acceleration," *Phys. Rev. Lett.*, vol. 61, p. 98, 1988.
- [14] A. K. Berezin, Y. B. Fainberg, V. A. Kiselev, A. F. Linnik, V. V. Uskov, V. A. Balakirev, I. N. Onishchenko, G. L. Sidel'nikov, and G. V. Sotnikov, "Wake field excitation in plasma by a relativistic electron pulse with a controlled number of short bunches," *Plasma Phys. Rep.*, vol. 20, p. 596, 1994.
- [15] M. Everett, A. Lal, D. Gordon, C. E. Clayton, K. A. Marsh, and C. Joshi, "Trapped electron acceleration by a laser-driven relativistic plasma wave," *Nature*, vol. 368, p. 527, 1994.
- [16] K. Nakajima, D. Fisher, T. Kawakubo, H. Nakanishi, A. Ogata, Y. Kato, Y. Kitagawa, R. Kodama, K. Mima, H. Shiraga, K. Suzuki, K. Yamakawa, T. Zhang, Y. Sakawa, T. Shoji, Y. Nishida, N. Yugami, M. Downer, and T. Tajima, "Observation of ultrahigh gradient electron acceleration by a self-modulated intense short laser pulse," *Phys. Rev. Lett.*, vol. 74, p. 4428, 1995.
- [17] A. Modena, Z. Najmudin, A. E. Dangor, C. E. Clayton, K. A. Marsh, C. Joshi, V. Malka, C. B. Darrow, C. Danson, D. Neely, and F. N. Walsh, "Electron acceleration from the breaking of relativistic plasma waves," *Nature*, vol. 377, p. 606, 1995.
- [18] L. M. Gorbunov and V. I. Kirsanov, "The excitation of plasma waves by an electromagnetic wave packet," *Sov. Phys. JETP*, vol. 66, p. 290, 1987.
- [19] P. Sprangle, E. Esarey, A. Ting, and G. Joyce, "Laser wakefield acceleration and relativistic optical guiding," *Appl. Phys. Lett.*, vol. 53, p. 2146, 1988.
- [20] J. R. Marquès, J. P. Geindre, F. Amiranoff, P. Audebert, J. C. Gauthier, A. Antonetti, and G. Grillon, "Temporal and spatial measurements of the electron density perturbation produced in the wake of an ultrashort laser pulse," *Phys. Rev. Lett.*, vol. 76, p. 3566, 1996.
- [21] C. W. Siders, S. P. L. Blanc, D. Fisher, T. Tajima, M. C. Downer, A. Babine, A. Stepanov, and A. Sergeev, "Laser wakefield excitation and measurement by femtosecond longitudinal interferometry," *Phys. Rev. Lett.*, vol. 76, p. 3570, 1996.
- [22] K. Nakajima, T. Kawakubo, H. Nakanishi, A. Ogata, Y. Kato, Y. Kitagawa, R. Kodama, K. Mima, H. Shiraga, K. Suzuki, T. Zhang, Y. Sakawa, T. Shoji, Y. Nishida, N. Yugami, M. Downer, D. Fisher, B. Newberger, and T. Tajima, "A proof-of-principle experiment of laser wakefield acceleration," *Phys. Scripta*, vol. T52, p. 61, 1994.

Bibliography

- [23] C. E. Clayton, C. Joshi, C. Darrow, and D. Umstadter, "Relativistic plasma-wave excitation by collinear optical mixing," *Phys. Rev. Lett.*, vol. 54, p. 2343, 1985.
- [24] C. E. Clayton, K. A. Marsh, A. Dyson, M. Everett, A. Lal, W. P. Leemans, R. Williams, and C. Joshi, "Ultrahigh-gradient acceleration of injected electrons by laser-excited relativistic electron plasma waves," *Phys. Rev. Lett.*, vol. 70, p. 37, 1993.
- [25] Y. Kitagawa, T. Matsumoto, T. Minamihata, K. Sawai, K. Matsuo, K. Mima, K. Nishihara, H. Azechi, K. A. Tanaka, H. Takabe, and S. Nakai, "Beat-wave excitation of plasma wave and observation of accelerated electrons," *Phys. Rev. Lett.*, vol. 68, p. 48, 1992.
- [26] P. Sprangle, E. Esarey, J. Krall, and G. Joyce, "Propagation and guiding of intense laser pulses in plasmas," *Phys. Rev. Lett.*, vol. 69, p. 2200, 1992.
- [27] N. E. Andreev, L. M. Gorbunov, V. I. Kirsanov, A. A. Pogosova, and R. R. Ramazashvili, "Resonant excitation of wakefields by a laser pulse in a plasma," *JETP Lett.*, vol. 55, p. 571, 1992.
- [28] T. M. Antonsen Jr. and P. Mora, "Self-focusing and raman scattering of laser pulses in tenuous plasmas," *Phys. Rev. Lett.*, vol. 69, p. 2204, 1992.
- [29] E. Esarey, J. Krall, and P. Sprangle, "Envelope analysis of intense laser pulse self-modulation in plasmas," *Phys. Rev. Lett.*, vol. 72, p. 2887, 1994.
- [30] C. A. Coverdale, C. B. Darrow, C. D. Decker, W. B. Mori, K.-C. Tzeng, K. A. Marsh, C. E. Clayton, and C. Joshi, "Propagation of intense subpicosecond laser pulses through underdense plasmas," *Phys. Rev. Lett.*, vol. 74, p. 4659, 1995.
- [31] D. Gordon, "Observation of electron energies beyond the linear dephasing limit from a laser-excited relativistic plasma wave," *Phys. Rev. Lett.*, vol. 80, p. 2133, 1998.
- [32] C. Ren, B. J. Duda, R. G. Hemker, W. B. Mori, T. Katsouleas, T. M. Antonsen, Jr., and P. Mora, "Compressing and focusing a short laser pulse by a thin plasma lens," *Phys. Rev. E*, vol. 63, p. 026411, 2001.
- [33] O. Shorokhov, A. Pukhov, and I. Kostyukov, "Self-compression of laser pulses in plasma," *Phys. Rev. Lett.*, vol. 91, p. 265002, 2003.
- [34] S. Bulanov, N. Naumova, and F. Pegoraro, "Interaction of an ultrashort, relativistically strong laser pulse with an overdense plasma," *Phys. Plasmas*, vol. 1, p. 745, 1994.
- [35] R. Lichters, J. Meyer-Ter-Vehn, and A. Pukhov, "Short-pulse laser harmonics from oscillating plasma surfaces driven at relativistic intensity," *Phys. Plasmas*, vol. 3, p. 3425, 1996.

Bibliography

- [36] D. von der Linde and K. Rzazewski, "High-order optical harmonic generation from solid surfaces," *Appl. Phys. B: Lasers Opt.*, vol. 63, p. 499, 1996.
- [37] S. Gordienko, A. Pukhov, O. Shorokhov, and T. Baeva, "Relativistic doppler effect: Universal spectra and zeptosecond pulses," *Phys. Rev. Lett.*, vol. 93, p. 115002, 2004.
- [38] L. V. Keldysh, "Ionization in the field of a strong electromagnetic wave," *Sov. Phys. JETP*, vol. 20, p. 1307, 1965.
- [39] S. Augst, D. D. Meyerhofer, D. Strickland, and S. L. Chin, "Laser ionization of noble gases by coulomb-barrier suppression," *J. Opt. Soc. Am. B*, vol. 8, p. 858, 1991.
- [40] M. V. Ammosov, N. B. Delone, and V. P. Krainov, "Tunnel ionization of complex atoms and of atomic ions in an alternating electromagnetic field," *Sov. Phys. JETP*, vol. 64, p. 1191, 1986.
- [41] E. S. Sarachik and G. T. Schappet, "Classical theory of the scattering of intense laser radiation by free electrons," *Phys. Rev. D*, vol. 1, p. 2738, 1970.
- [42] P. B. Corkum, N. H. Burnett, and F. Brunel, *Atoms in Intense Laser Fields*, ed. M. Gavrilu. Academic, New York, 1992.
- [43] P. Woodward, *J. IEEE*, vol. 93, p. 1554, 1947.
- [44] J. D. Lawson, "Lasers and accelerators. (talk)," *IEEE Trans. Nucl. Sci.*, vol. NS-26, p. 4217, 1979.
- [45] C. I. Moore, J. P. Knauer, and D. D. Meyerhofer, "Observation of the transition from thomson to compton scattering in multiphoton interactions with low-energy electrons," *Phys. Rev. Lett.*, vol. 74, p. 2439, 1995.
- [46] W. L. Kruer, *The Physics of Laser-Plasma Interactions*. Reading, MA: Addison-Wesley, New York, 1988.
- [47] D. Bauer, P. Mulser, and W.-H. Steeb, "Relativistic ponderomotive force, uphill acceleration, and transition to chaos," *Phys. Rev. Lett.*, vol. 75, p. 4622, 1995.
- [48] B. Quesnel and P. Mora, "Theory and simulation of the interaction of ultraintense laser pulses with electrons in vacuum," *Phys. Rev. E*, vol. 58, p. 3719, 1998.
- [49] Y. L. Klimontovich, *The Statistical Theory of Non-Equilibrium Processes in Plasma*. M.I.T. Press, Cambridge, Mass., 1967.
- [50] A. Vlasov, "Kinetic theory of an assembly of particles with collective interaction," *J. Phys. U.S.S.R.*, vol. 9, p. 25, 1945.

Bibliography

- [51] C. D. Decker and W. B. Mori, "Group velocity of large amplitude electromagnetic waves in a plasma," *Phys. Rev. Lett.*, vol. 72, p. 490, 1994.
- [52] J. F. Drake, P. K. Kaw, Y. C. Lee, G. Schmid, C. S. Liu, and M. N. Rosenbluth, "Parametric instabilities of electromagnetic waves in plasmas," *Phys. Fluids*, vol. 17, p. 778, 1974.
- [53] C. E. Max, J. Arons, and A. B. Langdon, "Self-modulation and self-focusing of electromagnetic waves in plasmas," *Phys. Rev. Lett.*, vol. 33, p. 209, 1974.
- [54] D. W. Forslund, J. M. Kindel, and E. L. Lindman, "Plasma simulation studies of stimulated scattering processes in laser-irradiated plasmas," *Phys. Fluids*, vol. 18, p. 1017, 1975.
- [55] P. Kaw, G. Schmidt, and T. Wilcox, "Filamentation and trapping of electromagnetic radiation in plasmas," *Phys. Fluids*, vol. 16, p. 1522, 1973.
- [56] C. E. Max, "Strong self-focusing due to the ponderomotive force in plasmas," *Phys. Fluids*, vol. 19, p. 74, 1976.
- [57] R. Bingham and C. N. Lashmore-Davies, "Self-modulation and filamentation of electromagnetic waves in a plasma," *Nuclear Fusion*, vol. 16, p. 67, 1976.
- [58] S. C. Wilks, J. M. Dawson, W. B. Mori, T. Katsouleas, and M. E. Jones, "Photon accelerator," *Phys. Rev. Lett.*, vol. 62, p. 2600, 1989.
- [59] E. Esarey, A. Ting, and P. Sprangle, "Frequency shifts induced in laser pulses by plasma waves," *Phys. Rev. A*, vol. 42, p. 3526, 1990.
- [60] W. B. Mori, "The physics of the nonlinear optics of plasmas at relativistic intensities," *IEEE J. Quantum Electron.*, vol. 33, p. 1942, 1997.
- [61] C. D. Decker and W. B. Mori, "Group velocity of large-amplitude electromagnetic waves in a plasma," *Phys. Rev. E*, vol. 51, p. 1364, 1995.
- [62] G.-Z. Sun, E. Ott, Y. C. Lee, and P. Guzdar, "Self-focusing of short intense pulses in plasmas," *Phys. Fluids*, vol. 30, p. 526, 1987.
- [63] P. Sprangle, C.-M. Tang, and E. Esarey, "Relativistic self-focusing of short-pulse radiation beams in plasmas," *IEEE Trans. Plasma Sci.*, vol. 15, p. 145, 1983.
- [64] A. B. Borisov, A. V. Borovskiy, O. B. Shiryayev, V. V. Korobkin, A. M. Prokhorov, J. C. Solem, T. S. Luk, K. Boyer, and C. K. Rhodes, "Relativistic and charge-displacement self-channeling of intense ultrashort laser pulses in plasmas," *Phys. Rev. A*, vol. 45, p. 5830, 1992.

Bibliography

- [65] A. B. Borisov, A. V. Borovskiy, V. V. Korobkin, A. M. Prokhorov, O. B. Shiryayev, X. M. Shi, T. S. Luk, A. McPherson, J. C. Solem, K. Boyer, and C. K. Rhodes, "Observation of relativistic and charge-displacement self-channeling of intense sub-picosecond ultraviolet (248 nm) radiation in plasmas," *Phys. Rev. Lett.*, vol. 68, p. 2309, 1992.
- [66] P. Monot, T. Auguste, P. Gibbon, F. Jakober, G. Mainfray, A. Dulieu, M. Louis-Jacquet, G. Malka, and J. L. Miquel, "Experimental demonstration of relativistic self-channeling of a multiterawatt laser pulse in an underdense plasma," *Phys. Rev. Lett.*, vol. 74, p. 2953, 1995.
- [67] A. B. Borisov, O. B. Shiryayev, A. McPherson, K. Boyer, and C. K. Rhodes, "Stability analysis of relativistic and charge-displacement self-channelling of intense laser pulses in underdense plasmas," *Plasma Physics and Controlled Fusion*, vol. 37, p. 569, 1995.
- [68] G. A. Askar'yan, S. V. Bulanov, F. Pegoraro, and A. M. Pukhov, "Magnetic interaction of self-focusing channels and fluxes of electromagnetic radiation: their coalescence, the accumulation of energy, and the effect of external magnetic fields on them," *JETP Lett.*, vol. 60, p. 251, 1994.
- [69] A. Pukhov and J. Meyer-ter-Vehn, "Relativistic magnetic self-channeling of light in near-critical plasma: Three-dimensional particle-in-cell simulation," *Phys. Rev. Lett.*, vol. 76, p. 3975, 1996.
- [70] M. Tabak, J. Hammer, M. E. Glinsky, W. L. Kruer, S. C. Wilks, J. Woodworth, E. M. Campbell, M. D. Perry, and R. J. Mason, "Ignition and high gain with ultrapowerful lasers," *Phys. Plasmas*, vol. 1, p. 1626, 1994.
- [71] A. Pukhov and J. Meyer-ter-Vehn, "Laser hole boring into overdense plasma and relativistic electron currents for fast ignition of icf targets," *Phys. Rev. Lett.*, vol. 79, p. 2686, 1997.
- [72] A. Pukhov and J. Meyer-Ter-Vehn, "Relativistic laser-plasma interaction by multi-dimensional particle-in-cell simulations," *Phys. Plasmas*, vol. 5, p. 1880, 1998.
- [73] J. Meyer-ter-Vehn, "Fast ignition of icf targets: an overview," *Plasma Physics and Controlled Fusion*, vol. 43, p. 113, 2001.
- [74] S. Atzeni and J. Meyer-ter-Vehn, *The Physics of Inertial Fusion*. Oxford University Press, 2004.
- [75] W. P. Leemans, C. W. Siders, E. Esarey, N. Andreev, G. Shvets, and W. B. Mori, "Plasma guiding and wakefield generation for second generation experiments," *IEEE Trans. Plasma Sci.*, vol. 24, p. 331, 1996.
- [76] J. B. Rosenzweig, "Trapping, thermal effects, and wave breaking in the nonlinear plasma wake-field accelerator," *Phys. Rev. A*, vol. 38, p. 3634, 1988.

Bibliography

- [77] T. Katsouleas and W. B. Mori, "Wave-breaking amplitude of relativistic oscillations in a thermal plasma," *Phys. Rev. Lett.*, vol. 61, p. 90, 1988.
- [78] S. Gordienko and A. Pukhov, "Scalings for ultra-relativistic laser plasmas and monoenergetic electrons," <http://arxiv.org/abs/physics/0410268>, 2004.
- [79] J. B. Rosenzweig, "Nonlinear plasma dynamics in the plasma wake-field accelerator," *Phys. Rev. Lett.*, vol. 58, p. 555, 1987.
- [80] S. V. Bulanov, V. I. Kirsanov, and A. S. Sakharov, "Excitation of ultrarelativistic plasma waves by pulse of electromagnetic radiation," *JETP Lett.*, vol. 50, p. 198, 1989.
- [81] A. Ting, E. Esarey, and P. Sprangle, "Nonlinear wake-field generation and relativistic focusing of intense laser pulses in plasmas," *Phys. Fluids B*, vol. 2, p. 1390, 1990.
- [82] A. Pukhov, Z. Sheng, and J. Meyer-Ter-Vehn, "Particle acceleration in relativistic laser channels," *Phys. Plasmas*, vol. 6, p. 2847, 1999.
- [83] G. D. Tsakiris, C. Gahn, and V. K. Tripathi, "Laser induced electron acceleration in the presence of static electric and magnetic fields in a plasma," *Phys. Plasmas*, vol. 7, p. 3017, 2000.
- [84] J. Faure, Y. Glinec, A. Pukhov, S. Kiselev, S. Gordienko, E. Lefebvre, J. Rousseau, F. Burgy, and V. Malka, "A laser-plasma accelerator producing monoenergetic electron beams," *Nature*, vol. 431, p. 541, 2004.
- [85] M. Borghesi, S. Bulanov, D. H. Campbell, R. J. Clarke, T. Z. Esirkepov, M. Galimberti, L. A. Gizzi, A. J. MacKinnon, N. M. Naumova, F. Pegoraro, H. Ruhl, A. Schiavi, and O. Willi, "Macroscopic evidence of soliton formation in multiterawatt laser-plasma interaction," *Phys. Rev. Lett.*, vol. 88, p. 135002, 2002.
- [86] M. Roth, T. E. Cowan, M. H. Key, S. P. Hatchett, C. Brown, W. Fountain, J. Johnson, D. M. Pennington, R. A. Snavely, S. C. Wilks, K. Yasuike, H. Ruhl, F. Pegoraro, S. V. Bulanov, E. M. Campbell, M. D. Perry, and H. Powell, "Fast ignition by intense laser-accelerated proton beams," *Phys. Rev. Lett.*, vol. 86, p. 436, 2001.
- [87] G. Kraft, "What we can learn from heavy ion therapy for radioprotection in space," *Physica Medica*, vol. XVII, p. 13, 2001.
- [88] T. Z. Esirkepov, S. V. Bulanov, K. Nishihara, T. Tajima, F. Pegoraro, V. S. Khoroshkov, K. Mima, H. Daido, Y. Kato, Y. Kitagawa, K. Nagai, and S. Sakabe, "Proposed double-layer target for the generation of high-quality laser-accelerated ion beams," *Phys. Rev. Lett.*, vol. 89, p. 175003, 2002.

Bibliography

- [89] K. Krushelnick, E. L. Clark, M. Zepf, J. R. Davies, F. N. Beg, A. Machacek, M. I. K. Santala, M. Tatarakis, I. Watts, P. A. Norreys, and A. E. Dangor, "Energetic proton production from relativistic laser interaction with high density plasmas," *Phys. Plasmas*, vol. 7, p. 2055, 2000.
- [90] A. Maksimchuk, S. Gu, K. Flippo, D. Umstadter, and V. Y. Bychenkov, "Forward ion acceleration in thin films driven by a high-intensity laser," *Phys. Rev. Lett.*, vol. 84, p. 4108, 2000.
- [91] E. L. Clark, K. Krushelnick, J. R. Davies, M. Zepf, M. Tatarakis, F. N. Beg, A. Machacek, P. A. Norreys, M. I. K. Santala, I. Watts, and A. E. Dangor, "Measurements of energetic proton transport through magnetized plasma from intense laser interactions with solids," *Phys. Rev. Lett.*, vol. 84, p. 670, 2000.
- [92] M. Zepf, E. L. Clark, F. N. Beg, R. J. Clarke, A. E. Dangor, A. Gopal, K. Krushelnick, P. A. Norreys, M. Tatarakis, U. Wagner, and M. S. Wei, "Proton acceleration from high-intensity laser interactions with thin foil targets," *Phys. Rev. Lett.*, vol. 90, p. 064801, 2003.
- [93] M. I. K. Santala, Z. Najmudin, E. L. Clark, M. Tatarakis, K. Krushelnick, A. E. Dangor, V. Malka, J. Faure, R. Allott, and R. J. Clarke, "Observation of a hot high-current electron beam from a self-modulated laser wakefield accelerator," *Phys. Rev. Lett.*, vol. 86, p. 1227, 2001.
- [94] R. A. Snavely, M. H. Key, S. P. Hatchett, T. E. Cowan, M. Roth, T. W. Phillips, M. A. Stoyer, E. A. Henry, T. C. Sangster, M. S. Singh, S. C. Wilks, A. MacKinnon, A. Offenberger, D. M. Pennington, K. Yasuike, A. B. Langdon, B. F. Lasinski, J. Johnson, M. D. Perry, and E. M. Campbell, "Intense high-energy proton beams from petawatt-laser irradiation of solids," *Phys. Rev. Lett.*, vol. 85, p. 2945, 2000.
- [95] M. Roth, A. Blazevic, M. Geissel, T. Schlegel, T. E. Cowan, M. Allen, J.-C. Gauthier, P. Audebert, J. Fuchs, J. Meyer-ter-Vehn, M. Hegelich, S. Karsch, and A. Pukhov, "Energetic ions generated by laser pulses: A detailed study on target properties," *Phys. Rev. STAB*, vol. 5, p. 061301, 2002.
- [96] M. Borghesi, D. H. Campbell, A. Schiavi, M. G. Haines, O. Willi, A. J. MacKinnon, P. Patel, L. A. Gizzi, M. Galimberti, R. J. Clarke, F. Pegoraro, H. Ruhl, and S. Bulanov, "Electric field detection in laser-plasma interaction experiments via the proton imaging technique," *Phys. Plasmas*, vol. 9, p. 2214, 2002.
- [97] M. Hegelich, S. Karsch, G. Pretzler, D. Habs, K. Witte, W. Guenther, M. Allen, A. Blazevic, J. Fuchs, J. C. Gauthier, M. Geissel, P. Audebert, T. Cowan, and M. Roth, "MeV ion jets from short-pulse-laser interaction with thin foils," *Phys. Rev. Lett.*, vol. 89, p. 085002, 2002.
- [98] E. L. Clark, K. Krushelnick, M. Zepf, F. N. Beg, M. Tatarakis, A. Machacek, M. I. K. Santala, I. Watts, P. A. Norreys, and A. E. Dangor, "Energetic heavy-ion

Bibliography

- and proton generation from ultraintense laser-plasma interactions with solids,” *Phys. Rev. Lett.*, vol. 85, p. 1654, 2000.
- [99] A. J. MacKinnon, M. Borghesi, S. Hatchett, M. H. Key, P. K. Patel, H. Campbell, A. Schiavi, R. Snavely, S. C. Wilks, and O. Willi, “Effect of plasma scale length on multi-mev proton production by intense laser pulses,” *Phys. Rev. Lett.*, vol. 86, p. 1769, 2002.
- [100] S. C. Wilks, A. B. Langdon, T. E. Cowan, M. Roth, M. Singh, S. Hatchett, M. H. Key, D. Pennington, A. MacKinnon, and R. A. Snavely, “Energetic proton generation in ultra-intense laser-solid interactions,” *Phys. Plasmas*, vol. 8, p. 542, 2001.
- [101] A. Pukhov, “Three-dimensional simulations of ion acceleration from a foil irradiated by a short-pulse laser,” *Phys. Rev. Lett.*, vol. 86, p. 3562, 2001.
- [102] S. Karsch, S. Dusterer, H. Schwoerer, F. Ewald, D. Habs, M. Hegelich, G. Pretzler, A. Pukhov, K. Witte, and R. Sauerbrey, “High-intensity laser induced ion acceleration from heavy-water droplets,” *Phys. Rev. Lett.*, vol. 91, p. 015001, 2003.
- [103] M. Kaluza, J. Schreiber, M. I. Santala, G. D. Tsakiris, K. Eidmann, and K. J. W. J. Meyer-ter-Vehn, “Influence of the laser prepulse on proton acceleration in thin-foil experiments,” *Phys. Rev. Lett.*, vol. 93, p. 045003, 2004.
- [104] I. N. Ross, P. Matousek, M. Towrie, A. J. Langley, and J. L. Collier, “The prospects for ultrashort pulse duration and ultrahigh intensity using optical parametric chirped pulse amplifiers,” *Opt. Comm.*, vol. 144, p. 125, 1997.
- [105] S. G. Wilks, W. L. Kruer, M. Tabak, and A. Langdon, “Absorption of ultra-intense laser pulses,” *Phys. Rev. Lett.*, vol. 69, p. 1383, 1992.
- [106] E. Esarey and M. Pilloff, “Trapping and acceleration in nonlinear plasma waves,” *Phys. Plasmas*, vol. 2, p. 1432, 1995.
- [107] L. D. Landau and E. M. Lifschitz, *Mechanics*. Oxford, England: Pergamon Press, 1976.
- [108] M. Ashour-Abdalla, J. N. Leboeuf, T. Tajima, J. M. Dawson, and C. F. Kennel, “Ultrarelativistic electromagnetic pulses in plasmas,” *Phys. Rev A*, vol. 23, p. 1906, 1981.
- [109] P. Mulser and D. Bauer, “Fast ignition of fusion pellets with superintense lasers: Concepts, problems, and prospectives,” *Laser and Particle Beams*, vol. 22, p. 5, 2004.
- [110] V. E. Zakharov and A. B. Shabat, “Exact theory of two-dimensional self-focusing and one-dimensional self-modulation of waves in nonlinear media,” *Sov. Phys. JETP*, vol. 34, p. 62, 1972.

Bibliography

- [111] J. I. Gersten and N. Tzoar, "Propagation of localized electromagnetic pulses in plasmas," *Phys. Rev. Lett.*, vol. 35, p. 934, 1975.
- [112] V. A. Kozlov, A. G. Litvak, and E. Suvorov, "Solitons of envelopes of intense relativistic electromagnetic waves," *Sov. Phys. JETP*, vol. 49, p. 75, 1979.
- [113] P. K. Kaw, A. Sen, and T. Katsouleas, "Nonlinear 1d laser pulse solitons in a plasma," *Phys. Rev. Lett.*, vol. 68, p. 3172, 1992.
- [114] M. Lontano and I. Murusidze, "Dynamics of space-time self-focusing of a femtosecond relativistic laser pulse in an underdense plasma," *Opt. Express*, vol. 11, p. 248, 2003.
- [115] W. B. Mori, C. D. Decker, D. E. Hinkel, and T. Katsouleas, "Raman forward scattering of short-pulse high-intensity lasers," *Phys. Rev. Lett.*, vol. 72, p. 1482, 1994.
- [116] P. Sprangle and E. Esarey, "Stimulated backscattered harmonic generation from intense laser interactions with beams and plasmas," *Phys. Rev. Lett.*, vol. 67, p. 2021, 1991.
- [117] G. Shvets and X. Li, "Raman forward scattering in plasma channels," *Phys. Plasmas*, vol. 8, p. 8, 2001.
- [118] J. R. Peñano, B. Hafizi, P. Sprangle, R. F. Hubbard, and A. Ting, "Raman forward scattering and self-modulation of laser pulses in tapered plasma channels," *Phys. Rev. E*, vol. 66, p. 036402, 2002.
- [119] L. D. Landau and E. M. Lifschitz, *The Classical Theory of Fields*. Oxford, England: Pergamon Press, 1984.
- [120] E. Esarey, P. Sprangle, J. Krall, and A. Ting, "Self-focusing and guiding of short laser pulses in ionizing gases and plasmas," *IEEE J. Quantum Electron.*, vol. 33, p. 1879, 1997.
- [121] A. Pukhov and J. Meyer-ter-Vehn, "Relativistic magnetic self-channeling of light in near-critical plasma: Three-dimensional particle-in-cell simulation," *Phys. Rev. Lett.*, vol. 76, p. 3975, 1996.
- [122] T. Brabec and F. Krausz, "Intense few-cycle laser fields: Frontiers of nonlinear optics," *Rev. Mod. Phys.*, vol. 72, p. 545, 2000.
- [123] V. Malka, S. Fritzler, E. Lefebvre, M.-M. Aleonard, F. Burgy, J.-P. Chambaret, J.-F. Chemin, K. Krushelnick, G. Malka, S. P. D. Mangles, Z. Najmudin, M. Pittman, J.-P. Rousseau, J.-N. Scheurer, B. Walton, and A. E. Dangor, "Electron acceleration by a wake field forced by an intense ultrashort laser pulse," *Science*, vol. 298, p. 1596, 2002.

Bibliography

- [124] N. A. Papadogiannis, B. Witzel, C. Kalpouzos, and D. Charalambidis, "Observation of attosecond light localization in higher order harmonic generation," *Phys. Rev. Lett.*, vol. 83, p. 4289, 1999.
- [125] F. Krausz, "From femtochemistry to attophysics," *Physics World*, vol. 14, p. 41, 2001.
- [126] M. Lewenstein, "Resolving processes on the attosecond time scale," *Science*, vol. 297, p. 1131, 2002.
- [127] P. Bucksbaum, "Ultrafast control," *Nature*, vol. 421, p. 593, 2003.
- [128] B. Bezzerides, R. D. Jones, and D. W. Forslund, "Plasma mechanism for ultraviolet harmonic radiation due to intense co2 light," *Phys. Rev. Lett.*, vol. 49, p. 202, 1982.
- [129] Z. Chang, A. Rundquist, H. Wang, M. M. Murnane, and H. C. Kapteyn, "Generation of coherent soft x rays at 2.7 nm using high harmonics," *Phys. Rev. Lett.*, vol. 79, p. 2967, 1997.
- [130] S. Chen, A. Maksimchuk, and D. Umstadter, "Experimental observation of relativistic nonlinear thomson scattering," *Nature*, vol. 396, p. 653, 1998.
- [131] S. Banerjee, A. R. Valenzuela, R. C. Shah, A. Maksimchuk, and D. Umstadter, "High harmonic generation in relativistic laser-plasma interaction," *Phys. Plasmas*, vol. 9, p. 2393, 2002.
- [132] A. E. Kaplan and P. L. Shkolnikov, "Lasetron: A proposed source of powerful nuclear-time-scale electromagnetic bursts," *Phys. Rev. Lett.*, vol. 88, p. 074801, 2002.
- [133] S. Kohlweyer, G. D. Tsakiris, C.-G. Wahlström, C. Tillman, and I. Mercer, "Harmonic generation from solid-vacuum interface irradiated at high laser intensities," *Optics Commun.*, vol. 117, p. 431, 1995.
- [134] D. von der Linde, T. Engers, G. Jenke, P. Agostini, G. Grillon, E. Nibbering, A. Mysyrowicz, and A. Antonetti, "Generation of high-order harmonics from solid surfaces by intense femtosecond laser pulses," *Phys. Rev. A*, vol. 52, p. R25, 1995.
- [135] P. A. Norreys, M. Zepf, S. Moustazis, A. P. Fewes, J. Zhang, P. Lee, M. Bakarezos, C. N. Danson, A. Dyson, P. Gibbon, P. Loukakos, D. Neely, F. N. Walsh, J. S. Wark, and A. E. Dangor, "Efficient extreme uv harmonics generated from picosecond laser pulse interactions with solid targets," *Phys. Rev. Lett.*, vol. 76, p. 1832, 1996.
- [136] P. Gibbon and A. R. Bell, "Collisionless absorption in sharp-edged plasmas," *Phys. Rev. Lett.*, vol. 68, p. 1535, 1992.

Bibliography

- [137] H. Ruhl and P. Mulser, “Relativistic vlasov simulation of intense fs laser pulse-matter interaction,” *Phys. Lett. A*, vol. 205, p. 388, 1995.
- [138] P. Gibbon, “Harmonic generation by femtosecond laser-solid interaction: A coherent “water-window” light source?” *Phys. Rev. Lett.*, vol. 76, p. 50, 1996.
- [139] I. Watts, M. Zepf, E. L. Clark, M. Tatarakis, K. Krushelnick, A. E. Dangor, R. M. Allott, R. J. Clarke, D. Neely, and P. A. Norreys, “Dynamics of the critical surface in high-intensity laser-solid interactions: Modulation of the xuv harmonic spectra,” *Phys. Rev. Lett.*, vol. 88, p. 155001, 2002.
- [140] U. Teubner, G. Pretzler, T. Schlegel, K. Eidmann, E. Forster, and K. Witte, “Anomalies in high-order harmonic generation at relativistic intensities,” *Phys. Rev. A*, vol. 67, p. 013816, 2003.
- [141] L. Plaja, L. Roso, K. Rzazewski, and M. Lewenstein, “Generation of attosecond pulse trains during the reflection of a very intense laser on a solid surface,” *J. Opt. Soc. Am. B*, vol. 7, p. 1904, 1998.
- [142] N. M. Naumova, J. A. Nees, I. V. Sokolov, B. Hou, and G. A. Mourou, “Relativistic generation of isolated attosecond pulses in a λ^3 focal volume,” *Phys. Rev. Lett.*, vol. 92, p. 063902, 2004.
- [143] S. Gordienko, A. Pukhov, O. Shorokhov, and T. Baeva, “Coherent harmonic focusing and the light extreme,” <http://arXiv.org/abs/physics/0406019>, 2004.
- [144] L. I. Sedov, *Similarity and Dimensional Methods in Mechanics*. Academic Press, New York, 1959.
- [145] L. D. Landau and E. M. Lifschitz, *Electrodynamics of Continuous Media*. Oxford, England: Pergamon Press, 1984.
- [146] J. D. Jackson, *Classical Electrodynamics*. J. Wiley & Sons Inc., New York, 1999.
- [147] D. S. Harned, “Quasineutral hybrid simulation of macroscopic plasma phenomena,” *J. Comput. Phys.*, vol. 47, p. 452, 1982.
- [148] C. K. Birdsall and A. B. Langdon, *Plasma Physics via Computer Simulation*. Adam Hilger, New York, 1991.
- [149] R. W. Hockney and J. W. Eastwood, *Computer Simulation Using Particles*. Adam Hilger, New York, 1988.
- [150] J. Dawson, “Particle simulation of plasmas,” *Rev. Mod. Phys.*, vol. 55, p. 403, 1983.
- [151] J. Villasenor and O. Buneman, “Rigorous charge conservation for local electromagnetic field solvers,” *Comp. Phys. Comm.*, vol. 69, p. 306, 1992.

Bibliography

- [152] C. K. Birdsall, "Particle-in-cell charged-particle simulations, plus monte carlo collisions with neutral atoms, pic-mcc," *IEEE Trans. Plasma Sci.*, vol. 19, p. 65, 1991.
- [153] A. Pukhov, "Three-dimensional electromagnetic relativistic particle-in-cell code vlpl (virtual laser plasma lab)," *J. Plasma Phys.*, vol. 61, p. 425, 1999.

Acknowledgements

I would like to thank in first place my supervisor Prof. Dr. Alexander Pukhov, who supported and advised me during this scientific work. This work would be impossible without his help and very wide knowledge in physics and computational methods.

I thank Dr. Serguei Gordienko for help in theoretical techniques. His advices in choice of mathematical methods and his comments were very useful for me. I thank Dr. Igor Kostyukov, whose erudition in plasma physics helps me so much. A large part of my work during PhD-study has be done in collaboration with Prof. Dr. Alexander Pukhov, Dr. S. Gordienko and Dr. I. Kostyukov.

I am grateful to Prof. Dr. Karl-Heinz Spatschek for providing support to my work during last three years.

My special thanks goes to Teodora Baeva for interesting discussions and Serguei Kiselev for help with programming techniques and software.

I would like to thank my colleagues from the Institut für Theoretische Physik I of Duesseldorf University: Akad. Direktor Dr. Herbert Wenk for help with computer network, Eckhard Zügge for technical support and help with hardware problems, Rosemarie Gerardi and Elvira Gröters for help with organizational problems, Dr. Ernst Wolfgang Laedke, Dr. Jan Alexander Posth, Dr. Sylvie Rijkers Defrasne, Christoph Karle, Götz Lehmann, Marcus Neuer, Andreas Wingen for interesting discussions and friendly work atmosphere.

I would like to thank my wife, Dr. Yulia Artemova, who is not also the first reader of all my papers (including this), but also support me during this three years.

Erklärung

Mit meiner Unterschrift versichere ich an Eidesstatt, dass ich die vorgelegte Dissertation selbst und ohne unerlaubte Hilfe angefertigt habe und dass ich diese in der jetzigen oder einer ähnlichen Form noch keiner anderen Fakultät eingereicht habe.

Ich erkläre ferner, dass die Dissertation noch nicht veröffentlicht wurde (Veröffentlichungen nach §4(3) der Promotionsordnung bleiben hiervon ausgenommen).

Die Promotionsordnung ist mir bekannt.

Düsseldorf, im Januar 2005